# THE SYTHESIS, CHARACTERIZATION, AND STABILITY OF YUKONITE: IMPLICATIONS IN ARSENIC MOBILITY

Department of Mining and Materials Engineering
McGill University, Montréal
August 2014

A thesis submitted to McGill University in partial fulfillment of the requirements of the degree of Master of Engineering.

© Matthew Bohan, 2014

#### **Abstract**

The focus of this thesis is to investigate the stability of the mineral phase yukonite—a calcium ferric arsenate—which may be important in controlling arsenic pore water concentrations in mineral processing-derived tailings. Yukonite has been found in association with gold mine tailings in Nova Scotia and the Yukon Territory in Canada, and laboratory accelerated ageing experiments suggest yukonite may form ferric arsenate phases in the presence of gypsum. Hence, this work fills a void in knowledge regarding the solubility/stability of yukonite.

The results of this thesis are presented in the form of two manuscripts. The first study describes the synthesis and characterization of yukonite as well as its stability under oxic conditions. An atmospheric precipitation method was used to produce material identified as yukonite (Ca<sub>2</sub>Fe<sub>3</sub>(AsO<sub>4</sub>)<sub>3</sub>(OH)<sub>4</sub>·(3+x)H<sub>2</sub>O) by XRD and chemical analysis. Long-term stability experiments indicated yukonite possesses low arsenic solubility under mildly acidic, neutral, and mildly alkaline conditions. The presence of gypsum was found to have a stabilizing effect, with As(V) solubility of 0.6-0.9 mg·L<sup>-1</sup> at pH 7 and 0.6-2.4 mg·L<sup>-1</sup> at pH 8.

The second study investigates the stability of yukonite by reaction with  $CO_2$  and chemical-reducing agents. Sparging of  $CO_2$  as well as equilibration with various concentrations of NaHCO<sub>3</sub> both caused destabilization of yukonite resulting in release of arsenate and pointed to the precipitation of calcite. Yukonite showed resilience to the mild reducing potential (ca. 200 mV) achieved by reaction with sulfite  $(SO_3^{2-})$  but underwent reductive dissolution in the presence of strong reducing conditions (ca. -200 mV) due to reaction with sulfide  $(S^{2-})$ . The results indicate yukonite may play a role in arsenic immobilization where abundant  $CO_2$  and strong reducing conditions are not present.

## Résumé

L'objet de cette thèse est l'étude de la stabilité du yukonite—un minérau d'arséniate ferrique de calcium—qui peut être important pour le contrôle des teneurs en arsenic de l'eau interstitielle dans les résidus issu des traitements des minéraux. Le yukonite a été trouvé dans les résidus issus des mines d'or dans la Nouvelle Écosse et le territoire de Yukon au Canada, et des expériences de vieillissement accéléré en laboratoire suggèrent que le yukonite pourrait former des phases d'arséniate ferrique en présence de gypse. Cette recherche comble ainsi un vide au niveau des connaissances sur la solubilité et stabilité du yukonite.

Les résultats dans cette thèse sont présentés sous forme de deux manuscrits. Le premier étude décrit la synthèse et la caractérisation du yukonite ainsi que la stabilité sous conditions oxiques. Un méthode de précipitations atmosphériques a été utilisé pour produire un matériau identifié comme yukonite  $(Ca_2Fe_3(AsO_4)_3(OH)_4\cdot(3+x)H_2O)$  par des analyses chimiques et de XRD. Des expériences de stabilité à long terme ont indiqué que le yukonite possède une solubilité faible d'arsénique sous conditions d'acidité modérée, neutre, et d'alcalinité modérée. Il a été observé un effet stabilisateur en présence du gypse, une solubilité du As(V) de 0.6-0.9 mg·L<sup>-1</sup> avec un pH 7, et de 0.6-2.4 mg·L<sup>-1</sup> avec un pH 8.

Le deuxième étude examine la stabilité de yukonite en réaction avec du CO<sub>2</sub> et des agents chimiques de réduction. Le barbotage de CO<sub>2</sub> ainsi que l'établissement de l'equilibre avec différents concentrations de NaHCO<sub>3</sub> ont engendré une déstabilisation du yukonite, ce qui a eu pour résultat le dégagement d'arséniate et la précipitation de calcite. Le yukonite a montré une résistance au potentiel réducteur (ca. 200 mV) atteint lors d'une réaction avec du sulfite (SO<sub>3</sub><sup>2-</sup>) mais il a subie une dissolution réductrice en présence de fortes conditions réductrices (ca. -200 mV) en raison d'une réaction avec du sulfite (S<sup>2-</sup>). Les résultats ont indiquée que le yukonite pourrait jouer un rôle dans l'immobilization de l'arsénique dans l'absence du CO<sub>2</sub> abondant et des conditions réductrices fortes.

## **Contributions of Authors**

As an alternative to the traditional thesis format, McGill University offers the options to M.Eng. candidates to use a manuscript-based thesis format. The two results chapters of this thesis are intended for publication in Geochimica et Cosmochimica Acta and Hydrometallurgy, respectively.

Matthew Bohan, Levente Becze, John Mahoney, and George P. Demopoulos, "The Synthesis, Characterization, and Stability of Yukonite Under Oxic Conditions," *Geochimica et Cosmochimica Acta*, to be submitted.

Matthew Bohan, Thomas Feldmann, and George P. Demopoulos, "The Stability of Yukonite in CO<sub>2</sub>-Rich and Oxygen-Depleted Conditions." *Hydrometallurgy*, to be submitted.

In all works presented, the first author produced the primary materials and conducted necessary analysis and characterization of those materials. In the case of the first publication (Chapter 3), additional supporting data was included that was previously acquired by co-author Levente Becze. Also for this paper, co-author John Mahoney provided guidance related to solubility measurement and analysis part of the work. For the second publication (Chapter 4), co-author Thomas Feldmann assisted with the CO<sub>2</sub> sparging tests. Prof. Demopoulos provided guidance and filled the comprehensive supervisory role for the whole research project.

Mengule

The accuracy of the above statements is attested by the student's supervisor:

George Demopoulos

# Acknowledgements

Foremost I must express my wholehearted gratitude to Prof. Demopoulos for providing me with an excellent opportunity and a shoulder-top perspective of the field of hydrometallurgy. Time and again, his feedback served to reward my strengths and bolster my weaknesses as a student. But his guidance has impacted me well beyond the walls of the classroom and lab; he is an expert of not only engineering particle growth, but also personal growth. In many ways he was the perfect influence at a critical time in my life, something I feel I am only just beginning to appreciate. For his countless hours of assistance, I am grateful.

Of course, no one has lifted me up more than my family, for which I am thankful. My parents have graciously supported my education from day one, the ultimate gift. There's no one I look up to more than my dad, whose wisdom and values have guided me well. The one exception is my mom, who has been equally inspirational and who has filled many crucial roles over the years: editor-in-chief, college advisor, and life coach. I'm thankful for Mike, whose generosity and advice has far exceeded the duties of a big brother.

This appreciation extends to many others who have been my family away from home in Montréal over the years. I'm thankful for having been enriched by the many faces of the HydroMET Group, who have one time or another lent a helping hand: Nathan, Liying, Jay, Nima, Marie-Christine, Micah, Amrita, and Ravi. I must single out Christoph for being an outstanding friend, chemistry wizard, and fruitful partner on the arsenic project. Likewise to Ivonne, for the many adventures, cups of coffee, and for help in translation. I'm also grateful for Thomas' friendship and mentorship in the lab. To Jess and Renaud, thank you for getting me on my feet in the lab, and thanks to Levente Becze, Mario Gomez, and Yongfeng Jia for setting the foundation for my project. Also, thanks to Mert Celikin for his discussions regarding TEM.

In a very pragmatic way, many others have been crucial in completing this thesis. I must recognize two people for their frequent help with ICP measurements: Andrew Golsztajn and Ranjan Roy. Thank you to Monique Riendeau for her kind expertise on a variety of techniques ranging from XRD to particle size analysis, and also Dr. Sriraman Rajagopalan for his help with XRD. Thanks to Dr. John Mahoney for providing his affability and expertise with PHREEQC. Last, but certainly not least, thank you to Barbara Hanley, Leslie Selway, and Terry Zatylny for always handling administrative matters with grace and facilitating my life as a graduate student.

# **Thesis Contents**

LIST OF FIGURES	VII
LIST OF TABLES	X
CHAPTER 1. INTRODUCTION	X
CHAPTER 2. LITERATURE REVIEW	4
2.1. As-H <sub>2</sub> O System	4
2.2. FE-AS-H <sub>2</sub> O SYSTEM.	
2.3. CA-AS-H <sub>2</sub> O SYSTEM	
2.4. CA-FE-AS-H <sub>2</sub> O SYSTEM	
2.5. Yukonite	9
2.5.1. Historical developments	10
2.5.2. Chemical Composition	13
2.5.3. Crystallographic, Molecular, and Atomic Structure	
2.5.4. Physical Description and Morphology	
2.5.5. Natural occurrences	
2.5.6. Synthesis of yukonite	
2.5.7. Stability of yukonite	
2.6. CONCLUSION	
References	
CHAPTER 3. THE SYNTHESIS, CHARACTERIZATION, AND STABILITY O	OF YUKONITE UNDER
OXIC CONDITIONS	
ABSTRACT	41
3.1. Introduction.	
3.2. Experimental	
3.2.1. Synthesis procedure	
3.2.2. Characterization methods	
3.2.3. Stability experiments	
3.3. RESULTS AND DISCUSSION	
3.3.1. Synthesis and Characterization	
3.3.1.1. Phase identification and structure	
3.3.1.2. Synthesis Reactions	
3.3.1.4. Effect of neutralization temperature	
3.3.1.5. Chemical Composition	
3.3.2. Stability	
3.3.2.1. Pre-treatment of synthetic yukonite	
3.3.2.2. Solubility	
3.3.2.3. Effect of gypsum-saturation	
3.3.3. Implications	
3.4. CONCLUSIONS	
ACKNOWLEDGEMENTS	
CHAPTER 4. THE STABILITY OF YUKONITE-A CALCIUM FERRIC ARSE RICH AND REDUCING CONDITIONS	
ABSTRACT	
4.1. INTRODUCTION	
4.3. EXPERIMENTAL	
4.3.1. Synthesis and characterization	8 <i>1</i>
4 3 / N(I) III)	X I

4.4. RESULTS AND DISCUSSION	83
4.4.1. Reaction with CO <sub>2</sub>	84
4.4.2. Reaction with NaHCO <sub>3</sub>	
4.4.3. Stability in Sub-Oxic Conditions: Reaction with Na <sub>2</sub> SO <sub>3</sub>	
4.4.4. Stability in Anoxic Conditions: Reaction with NaHS	
4.4.5. Implications	
4.5. CONCLUSIONS	94
ACKNOWLEDGEMENTS	9:
References	95
CHAPTER 5. GLOBAL CONCLUSIONS	98
APPENDIX	100

# **List of Figures**

<b>Fig. 2.1.</b> Pourbaix diagram for As-O-H system at 25°C, 1 bar, and [As] = 10 <sup>-6</sup> M [16]	4
<b>Fig. 2.2.</b> (a) The removal of As(V) from solution adsorption with various Fe(III)/As(V) ratios (1.5x to 10x) from 300 mg/L As(V) solution [19] and (b) equilibrium As solubility of amorphous FeAsO <sub>4</sub> ·2H <sub>2</sub> O (i.e. pcFA) and crystalline FeAsO <sub>4</sub> ·2H <sub>2</sub> O (i.e. scorodite) [20]	5
<b>Fig. 2.3.</b> Phase diagrams by Robins and Tozawa delineating the stability regions of calcium arsenate, $Ca_3(AsO_4)_2$ as a function of pH and the logarithmic As/Ca ratio, in the case of <b>(a)</b> a closed system and <b>(b)</b> an open system, $P_{CO_2} = 10^{-3.52} atm [23]$	6
<b>Fig. 2.4.</b> Powder X-Ray diffractograms of yukonite from (a) Tagish Lake, Yukon Territory, Canada, and (b) Saalfield, Thuringen, Germany, compared with PDF 35-553, from Ross & Post, 1997 [40]. The Saalfield sample contains a trace of erythrite, Er, (Co <sub>3</sub> (AsO <sub>4</sub> ) <sub>2</sub> ·8H <sub>2</sub> O)	10
<b>Fig. 2.5.</b> Scatter plot of yukonite compositions for all known occurrences. Chemical formulae have been renormalized and presented as molar ratios of Ca: As and Fe: As	15
<b>Fig. 2.6.</b> Thermogravimetric analysis (TGA) curves of: (a) Yukonite aggregates from Tagish Lake, Yukon Territory, Canada (21.8 wt.% H <sub>2</sub> O) [37]; (b) Yukonite from Nalychevski hot springs, Kamchatka, Russia (17.8 wt.% H <sub>2</sub> O) [37]	16
<b>Fig. 2.7.</b> Substitution of up to 15.9 at.% SiO <sub>4</sub> <sup>4-</sup> for AsO <sub>4</sub> <sup>3-</sup> and a strong inverse correlation between As and Si suggest direct substitution in the crystal structure [37]	16
<b>Fig. 2.8.</b> Scatter plot of yukonite compositions for 11 analyses. Formulae have been renormalized and presented as molar ratios of Ca: As and Fe: As	19
<b>Fig. 2.9.</b> Powder X-Ray diffractograms of type yukonite (top to bottom) at room temperature, and after heating to 50°C, 100°C, and 150°C. From Ross and Post, 1997 [40]	24
<b>Fig. 2.10.</b> Powder X-Ray diffractogram of type yukonite overlaid with arseniosiderite reference pattern (top) in comparison to that of arseniosiderite, kolfanite, and mitridatite. From Ross and Post, 1997 [40]	24
<b>Fig. 2.11.</b> Graphical representation of the [001] incident Fe <sub>9</sub> O <sub>6</sub> (PO <sub>4</sub> ) <sub>9</sub> ) <sup>-12</sup> sheet in mitridatite (Ca <sub>6</sub> Fe <sub>9</sub> (PO <sub>4</sub> ) <sub>9</sub> O <sub>2</sub> ·9H <sub>2</sub> O). The shaded grey are Fe <sup>3+</sup> -O octahedra and the white are AsO <sub>4</sub> <sup>3-</sup> tetrahedra. Parallel to the page are sheets of CaO <sub>5</sub> (H <sub>2</sub> O) <sub>2</sub> polyhedra with additional hydrogen bonded water. Mitridatite is isomorphous with arseniosiderite Ca <sub>6</sub> Fe <sub>9</sub> (AsO <sub>4</sub> ) <sub>9</sub> O <sub>2</sub> ·9H <sub>2</sub> O, which shows structural similarities with yukonite by XRD. From Moore and Araki, 1977 [60]	25
Fig. 2.12. HR-TEM images of Nalychevski yukonite (a,b) and type yukonite (c) [37]	27
<b>Fig. 2.13.</b> Scatter plot of Ca,As-ferrihydrite, yukonite, and arseniosiderite found in the Ketza River gold mine tailings in the Yukon Territory, Canada. From Paktunc et al [42]	29
<b>Fig. 2.14.</b> Secondary electron scanning electron micrograph of synthetic yukonite taken at 10 kV. From Gomez et al [49]	30

<b>Fig. 3.1:</b> Overview of general synthesis scheme. Variables in the synthesis include: initial As concentration (1.4-12.8 gL-1), neutralization temperature (20°C vs. 95°C), and reaction (ageing) time (1-96 h) at 95°C. Material used in solubility studies: Study A (1.4 g·L <sup>-1</sup> , 95°C, 24 h), and Study B (9.0 g·L <sup>-1</sup> , 20°C, 24 h).
<b>Fig. 3.2.</b> ICCD diffraction data files compared with X-ray diffraction pattern obtained for synthetic yukonite. Synthesis conditions: Type 2-9.0 ([As]=9.0 g·L <sup>-1</sup> , 20°C neutralization, 24 h at 95°C ageing).
<b>Fig. 3.3.</b> Scanning electron micrographs of synthetic yukonite. Synthesis conditions: Type 2-9.0 ([As]=9.0 g·L <sup>-1</sup> , 20°C neutralization, 24 h at 95°C ageing).
<b>Fig. 3.4.</b> Structural evolution of synthetic yukonite. Synthesis conditions: Type 1-9.0 ([As]=9.0 g·L <sup>-1</sup> , 95°C neutralization, 1 h (top) and 24 h (bottom) at 95°C ageing)
<b>Fig. 3.5. (a)</b> Overlay of XRD diffractograms taken at 24 h, 48 h, and 72 h, which show increasing peak height and decreasing FWHM suggesting greater "crystal quality" as a result of longer ageing. <b>(b)</b> A magnification of the dotted area of XRD pattern in (a) showing increased peak height with ageing time.
<b>Fig. 3.6.</b> Comparison of XRD diffractograms of Type 1 (neutralization T=95°C) and Type 2 (neutralization T=20°C) yukonite (with smoothing).
<b>Fig. 3.7.</b> Particle size distributions of Type 1 and Type 2 yukonite.
<b>Fig. 3.8.</b> Scatterplot of Ca/As and Fe/As molar ratios of all known natural yukonite analyses
<b>Fig. 3.9.</b> Raw and corrected Ca/As and Fe/As molar ratios of select natural and synthetic yukonite analyses.
<b>Fig. 3.10.</b> Washing procedures for (a) Study A and (b) Study B show As concentration after each step. Solid black bars indicate As in filtrate in mg·L <sup>-1</sup> after repulp. Gray bars (Study A only) indicate As concentration in wash water.
<b>Fig. 3.11.</b> Results of Study A ("Synthetic 1"). (a) Arsenic solubility measurements over time of samples at various pH. (b) pH measurements over time.
<b>Fig. 3.12.</b> Results of Study B ("Type 2"). (a) Arsenic solubility measurements over time of samples at various pH. (b) pH measurements over time.
<b>Fig. 3.13.</b> Plot of equilibrium As concentrations for Study A and Study B in gypsum-free solution (see Table 3.3.) and natural sample yukonite sample equilibrated for 197 days
<b>Fig. 3.14.</b> Results of Study A-g ("Synthetic 1") with gypsum-saturated solution. (a) Arsenic solubility measurements over time of samples at various pH. (b) pH measurements over time
<b>Fig. 3.15.</b> Results of Study A-g ("Synthetic 1") with gypsum-saturated solution. (a) Arsenic solubility measurements over time of samples at various pH. (b) pH measurements over time
<b>Fig. 3.16.</b> Results of Study B and Study B-g. Equilibrium As concentrations after 132 ageing in gypsum-free (triangles) and gypsum-saturated (circles) solutions

<b>Fig. 4.1.</b> Yukonite stability experiment conducted at 70°C by sparging (99.8%) CO <sub>2</sub> (circles) in comparison to no sparging (triangles) in an Applikon reactor for 48 h with pH controlled at 8 with NaOH and HNO <sub>3</sub> . Plots show (a) dissolved inorganic carbon concentration and (b) As concentration with respect to time.	84
<b>Fig. 4.2.</b> Calcium concentration with respect to time for yukonite stability study with sparging of 99.8% CO <sub>2</sub> gas shows a LaMer-like trend. Initial increase in calcium concentration eventually peaks, suggesting nucleation of a calcium phase, and declines, indicating growth of that phase. This is seen as indirect evidence of formation of calcite.	85
<b>Fig. 4.3.</b> Results of equilibrium study with variable NaHCO <sub>3</sub> concentrations showing (a) pH and (b) As concentration over time.	
<b>Fig. 4.4.</b> (a) Determination of initial reaction rates from various concentration NaHCO <sub>3</sub> solutions at 20°C (b) ln-ln plot of Rate vs. [DIC] to determine the reaction order (slope)	88
<b>Fig. 4.5.</b> Reaction of yukonite with 0.125 M NaHCO <sub>3</sub> at T = 20°C, 40°C, 70°C show (a) As concentration and (b) pH over time	90
<b>Fig. 4.6.</b> Arrhenius plot for reaction of yukonite in $0.125$ M NaHCO <sub>3</sub> at T = $20^{\circ}$ C, $40^{\circ}$ C, $70^{\circ}$ C	90
<b>Fig. 4.7.</b> Sub-oxic stability study of yukonite by reaction with $0.012M\ Na_2SO_3$ under a $N_2$ atmosphere. As concentration is plotted along with (a) $E_h$ and (b) pH	91
<b>Fig. 4.8</b> . Anoxic stability study of yukonite by reaction of $0.001$ NaHS under a $N_2$ atmosphere. As concentration is plotted along with (a) $E_h$ and (b) pH	92
Appendix	
<b>Fig. A-1</b> . Thermogravimetric analysis performed with a TA Instruments Q500 instrument at a heating rate of 10°C·min <sup>-1</sup> show nearly identical mass loss over the temperature range (50-800°C) investigated for Type 1-9.0 and Type 2-9.0 synthetic yukonite samples. This mass is assumed to be crystallization water. As measured as mass loss at 600°C, the two samples had 14.67% and 14.65% crystallization water, respectively.	100

# **List of Tables**

Table 2.1. Overview of proposed chemical formulae of yukonite.	14
Table 2.2. Summary of X-ray diffraction data from literature for yukonite.	23
Table 2.3. Composition and phase identification of synthesis products after 19 days. Recreated from [47].	32
Table 2.4. Solubility data of natural yukonite and natural arseniosiderite. Recreated from [20]	34
<b>Table 2.5.</b> Solubility data of synthetic yukonite equilibrated in gypsum-free and gypsum-saturated solutions. Synthesis conditions: 1.4 g/L initial As(V) conc., Ca : Fe : As = $0.5 : 0.75 : 1$ , $t = 24$ h, T = $95$ °C. Recreated from [48]	34
Chapter 3	
Table 3.1. Chemical composition of synthetic and natural yukonite samples	58
<b>Table 3.2.</b> Ca/Fe/As molar ratios of synthetic yukonite samples in comparison to the theoretical ratios of arseniosiderite, raw and corrected	62
Table 3.3. Solubility data for synthetic yukonite under oxic conditions in gypsum-free solution	63
Table 3.4. Solubility data for synthetic yukonite under oxic conditions in gypsum-saturated solution.	64
Table 3.5. Effect of synthesis conditions on material properties and solubility	68

# **Chapter 1. Introduction**

Arsenic (As) is an element that affects the health of millions of people globally. In Bangladesh alone, 77 million people consume water daily from tube-wells naturally contaminated with arsenic, a circumstance the World Health Organized dubbed "the largest poisoning of a population in history," considering its magnitude "beyond the accidents at Bhopal, India, in 1984, and Chernobyl, Ukraine, in 1986 [1]." In contrast, the source of arsenic in drinking water (0.860 mg/L between 1958 and 1970, now 0.040 mg/L) shown to cause lung cancer in northern Chileans has been of anthropogenic origin, a consequence of negligent mining activity [2]. Unlike other water contaminants (e.g. bacteria, organic materials), being an element, arsenic cannot be destroyed; only its form can be altered to prevent human ingestion.

Thus, technologies to remove arsenic from water employ physiochemical processes such as adsorption and precipitation. Adsorption of arsenic on hydrous ferric oxide (HFO) is the method used by the more than 225,000 SONO water filters that have been deployed in Bangladesh, India, and Nepal to remove arsenic from contaminated tube-wells [3]. Precipitation of arsenic is preferred for large-scale treatment, especially in industrial settings. In the mining and metallurgical industry, arsenic commonly enters process effluents during the milling and refining of metals. For instance, some uranium ores contain arsenic-bearing minerals that dissolve during acid leach uranium recovery, releasing soluble arsenic into solution. Such process liquors contain up to 700 mg/L arsenic [4], while U.S. EPA drinking water standards permit just 0.010 mg/L [5].

The U.S. EPA Best Demonstrated Available Technology (BDAT) for removing arsenic from metallurgical effluents is coprecipitation with ferric iron (Fe(III)/As(V) molar ratio > 3) and subsequent lime (CaO) neutralization [6]. The process leaves the effluent nearly free of arsenic, permitting effluent release while respecting the Canadian Metal Mining Effluent Regulation 0.5 mg/L monthly average (1.0 mg/L for a grab sample) [7]. The mechanism by which arsenic was removed was traditionally understood as purely adsorption on ferrihydrite (FeOOH) (i.e. arsenical ferrihydrite), with the "coprecipitated solids" also containing significant gypsum (CaSO<sub>4</sub>·2H<sub>2</sub>O). However, recent evidence has shown an additional phase, poorly-crystalline ferric arsenate (pcFA), which resembles the natural crystalline mineral scorodite, also plays a role [8,9]. Scorodite, for example, is known to pass the U.S. EPA Toxicity Characteristic

Leaching Procedure (TCLP) by leaching less than 5.0 mg/L during the 24-hour test and is therefore classified as non-hazardous. In the case of a scorodite-gypsum mixture, 1.5 mg/L arsenic was leached by this test [10].

However, the TCLP test does not indicate long-term stability (i.e. solubility, pore water concentrations) of the disposed solids (i.e. tailings). Regulatory agencies put the burden of proof of stability on the prospective mining companies. For instance, processing of uranium ores at the McClean Lake Operation in northern Saskatchewan fell under the jurisdiction of the Canadian Nuclear Safety Commission. In this case, regulators required evidence that pore waters in the JEB Tailings Management Facility, which will contain the precipitated solids indefinitely, will not exceed 5 mg/L arsenic for 10,000 years [11]. Long-term ageing of coprecipitated solids have shown low-levels of arsenic release under acidic conditions (for instance, < 0.01 mg/L As(V) after for Fe(III)/As(V) = 4), evidence that the arsenic-controlling phases are thermodynamically stable [12]. However, it has been suggested that over time and under alkaline conditions, high surface area ferrihydrite is metastable with respect to low surface area hematite and goethite [13], which raises the concern that decreased sorption capacity may release soluble arsenic.

The dissolution of coprecpitated solids and release of arsenic in alkaline conditions begs the question of what new insoluble arsenic-bearing phase, if any, might form to control arsenic pore water concentrations. Owing to the presence of the calcium sulfate-saturated water in the gypsum-enriched tailings, the possible formation of calcium iron arsenate phases has been suggested. Accelerated ageing studies of simulated coprecpitated tailings were conducted at McGill University by raising slurry temperatures to 75°C to improve the kinetics of phase transformation. After several weeks, a phase transformation from pcFA to a calcium iron arsenate phase resembling the natural mineral "yukonite" was observed [12].

The purpose of this master's thesis is to investigate the potential of yukonite to serve as an arsenic-stable phase. The solubility of yukonite is not well understood and its stability with respect to various disposal conditions has not been investigated. In this work, yukonite is synthesized in the laboratory so that its solubility can be studied under possible conditions that may develop in disposal conditions; namely, variable: pH (acid vs. alkaline), E<sub>H</sub> (oxidizing vs. reducing redox potential), and P<sub>CO2</sub> (partial pressure CO<sub>2</sub> or dissolved inorganic carbon concentration). Therefore, it will commence with a literature review of yukonite and related chemical systems in the context of arsenic immobilization. Subsequent to that the results

generated from this study are presented in Chapters 3 and 4 in the form of manuscripts. Finally, Chapter 5 summarized the major global findings of the current research.

# **Chapter 2. Literature Review**

## 2.1. As-H<sub>2</sub>O System

Arsenic is a highly toxic metalloid abundant in natural geochemical systems, averaging 3 ppm in the earth's crust. Primarily found in association with sulfidic ore bodies, perhaps as much as 60 percent of atmospheric arsenic is anthropogenic in origin [14]. Arsenic exists in four oxidation states: As(5), As(3), As(0), and As(-3) [15]. While organic arsenic compounds exist, only inorganic compounds – without arsenic-carbon bonds – will be considered in this work. In aqueous systems (Fig. 2.1.) [16], dissolved As(V) takes the form of arsenic acid, the arsenate oxvanion (AsO<sub>4</sub><sup>3-</sup>) being the prevalent form under oxygen-rich conditions. The presence of oxygen-depleted (sub-oxic or anoxic) environments as indicated by low E<sub>h</sub> could lead to its reduction to the As(III) oxidation state to arsenious acid, the arsenite oxyanion (AsO<sub>3</sub><sup>3-</sup>). In both oxidation states, the protonation of these anions is pH dependent. Its oxidation state and speciation has implications in the mobility, bioavailability, and biotoxicity of arsenic, where As(III) is generally considered the more mobile and toxic form [14]. As a solid, arsenic is found naturally in all four oxidation states (as arsenates, arsenites, metallics, and arsenides), and thus forms a variety of compounds. The mineral-water equilibria of these compounds are responsible for controlling As concentrations in aqueous systems, which is highly dependent upon the particular mineral form. For this reason, there is great interest in understanding the solubility and stability of arsenic compounds under a variety of environmental conditions.

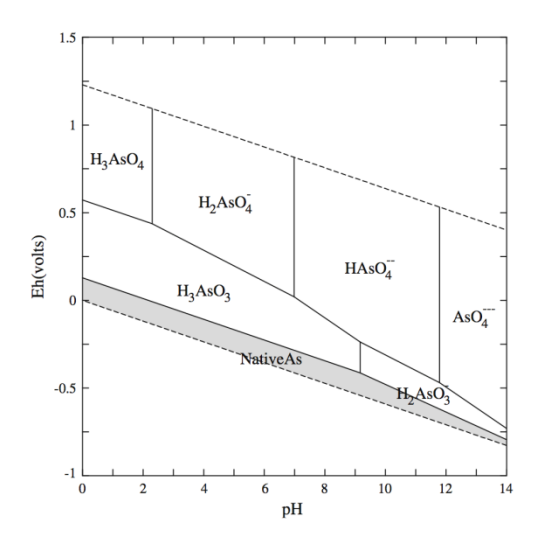
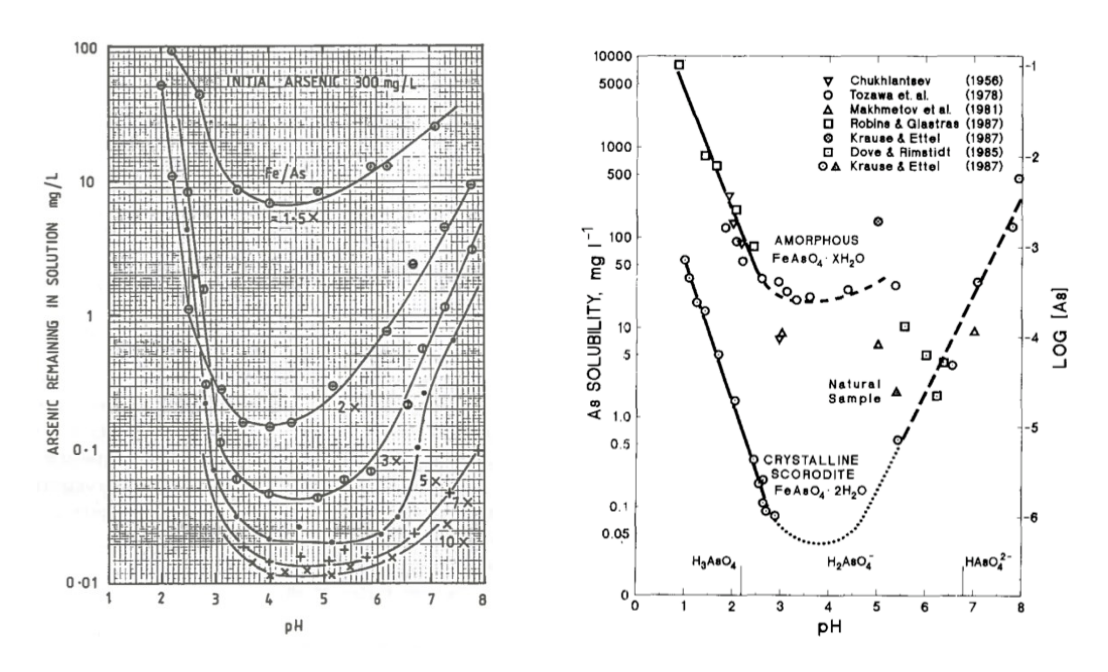


Fig. 2.1. Pourbaix diagram for As-O-H system at  $25^{\circ}$ C, 1 bar, and [As] =  $10^{-6}$  M [16].

### 2.2. Fe-As-H<sub>2</sub>O System

Iron may be present in aqueous systems as either ferric, Fe(III), or ferrous, Fe(II). Ferric forms strong inner-sphere complexes with As [17], resulting in highly stable surface-complexes or compounds that can contribute to the long-term fixation of As. For instance, under neutral and alkaline conditions, AsO<sub>4</sub><sup>3-</sup> is strongly retained by ferric hydroxide (Fe(OH)<sub>3</sub>, i.e. ferrihydrite) via surface complexation as unprotonated and protonated species (i.e. FeO<sub>2</sub>As(O)<sub>2</sub><sup>2-</sup> and FeO<sub>2</sub>As(O)(OH)<sup>-</sup>, where Fe is the ferrihydrite surface) [18]. This chemistry is fundamental to the immobilization of arsenic by iron. The traditional view of arsenic retention in coprecipitated solids was attributed to adsorption of As(V) on ferrihydrite formed by hydrolysis during neutralization. Consistent with this view, increase in Fe(III)/As ratio results in a greater extent of removal of As(V) from solution due to greater availability of sorption sites. For instance, increasing the Fe/As ratio from 1.5x to 10x in one case (Fig. 2.2a.) resulted in ca. 3 orders of magnitude lower residual As. Under certain conditions, amorphous (also called poorly-crystalline) ferric arsenate or even crystalline ferric arsenate (i.e. scorodite) may form and control As concentrations [19]. These phases possess low As solubility (Fig. 2.2b.), with the solubility of crystalline material being 100 times less than the amorphous [20]. Both of these



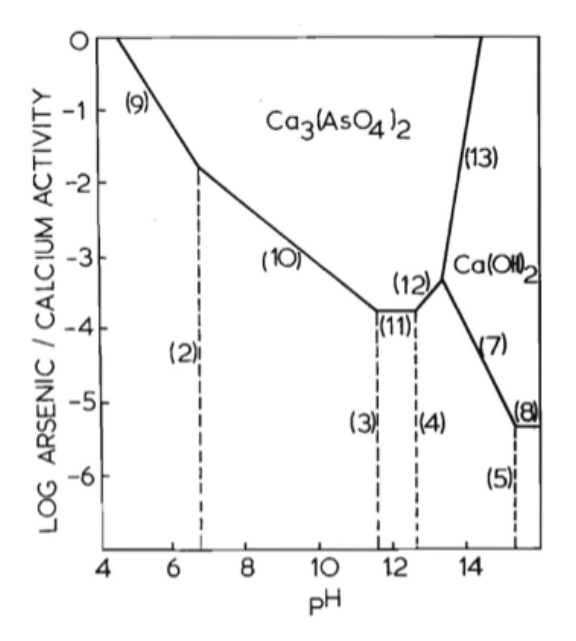
**Fig. 2.2.** (a) The removal of As(V) from solution adsorption with various Fe(III)/As(V) ratios (1.5x to 10x) from 300 mg/L As(V) solution [19] and (b) equilibrium As solubility of amorphous FeAsO<sub>4</sub>·2H<sub>2</sub>O (i.e. pcFA) and crystalline FeAsO<sub>4</sub>·2H<sub>2</sub>O (i.e. scorodite) [20].

mechanisms of arsenic immobilization are thought to play a role in mineral-water interactions of coprecipitated solids, where both ferrihydrite and ferric arsenate exist in equilibrium. For instance, for 3 < pH < 7, the equilibrium can be explained by **Eqn. 2.1** [21].

$$FeAsO_4 \cdot (2+x)H_2O + OH^- \leftrightarrow FeOOH \cdot (1+x)H_2O + H_2AsO_{4(aq)}^-$$
 (2.1)

The stability of coprecipitated solids is also influenced by the choice of base in neutralization; Jia and Demopoulos found the use of CaO instead of NaOH decreased As solubility by 25 times, indicating a stabilizing effect by the presence of Ca<sup>2+</sup> ions [12].

While the stability of iron-arsenic phases in their oxidized Fe(III) and As(V) forms is adequate, it is not indicative of stability of compounds formed from reduced species (e.g. Fe(II) and/or As(III)). For this reason, recent attention has been given to the stability of ferric arsenates under oxygen-depleted conditions that may form in metallurgical tailings, for instance, due to bacterially mediated reduction reactions. For example, at the tailings impoundment at the Campbell Mine in Balmertown, ON, Canada, reductive dissolution by heterotrophic bacteria was responsible for dissolution of As-rich hematite and maghemite, elevating As porewater concentrations as high as 100 mg/L [22].



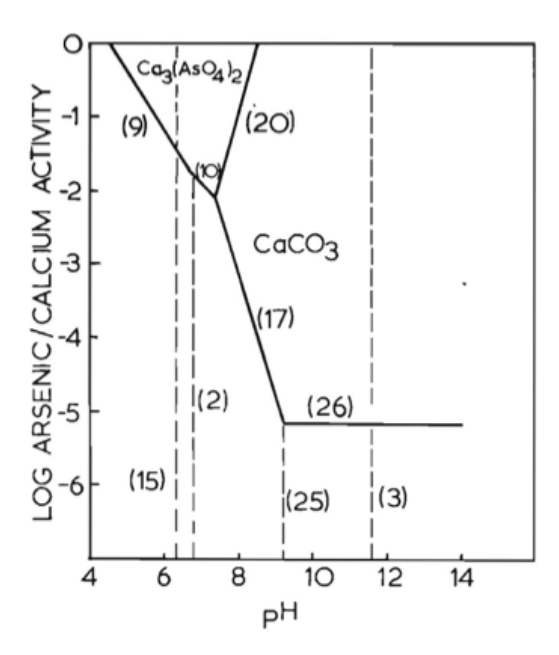


**Fig. 2.3.** Phase diagrams by Robins and Tozawa delineating the stability regions of calcium arsenate,  $Ca_3(AsO_4)_2$  as a function of pH and the logarithmic As/Ca ratio, in the case of **(a)** a closed system and **(b)** an open system,  $P_{CO_3} = 10^{-3.52} atm [23]$ .

# 2.3. Ca-As-H<sub>2</sub>O System

Precipitation of arsenic by neutralization with lime leads to the formation of either calcium arsenate or calcium arsenite phases. Many phases have been identified possessing a variety of Ca/As ratios, hydration states, and solubilities. Of the many As(V) phases, weilite (CaHAsO<sub>4</sub>) and pharmacolite (CaHAsO<sub>4</sub>·2H<sub>2</sub>O) both have a Ca/As = 1 but differ in hydration state. In practice, the Ca/As molar ratio and crystal structure of the precipitated phase(s) depends upon solution pH [24]. In terms of stability in the context of metallurgical tailings, Donahue and Hendry suggested Ca<sub>4</sub>(OH)<sub>2</sub>(AsO<sub>4</sub>)<sub>2</sub>·4H<sub>2</sub>O would likely precipitate at the Rabbit Lake Uranium mine TMF, resulting in long term dissolved As concentrations between 13 and 126 mg·L<sup>-1</sup> under alkaline disposal conditions [25]. In addition to simple calcium arsenates, calcium apatite phases such as Johnbaumite (Ca<sub>5</sub>(AsO<sub>4</sub>)<sub>3</sub>OH) – arsenate analog to hydroxylapatite of human bone – have attracted considerable attention as a potential arsenic sink. With a Ca/As ratio of 1.67, As solubility of 10.5 and 19.5 mg·L<sup>-1</sup> and pH 9.87 and 9.77, respectively [26].

In contrast to the findings of Donahue and Hendry, As concentrations ca. 3 orders of magnitude lower  $(0.1 \text{ mg} \cdot \text{L}^{-1})$  were reported of  $\text{Ca}_4(\text{OH})_2(\text{AsO}_4)_2 \cdot 4\text{H}_2\text{O}$  in equilibrium with pH 12.23 solution for a closed system [26]. The exclusion of air from system was responsible for the discrepancy, as initially pointed out by Robins and Tozawa [27]. These authors noticed the dissolution of calcium arsenate as studied by Tozawa, Utmetsu, and Nishimura to be incongruent, with stoichiometric arsenic concentrations 16-times higher than calcium in solution. This led to the conclusion based on thermodynamic arguments that calcium arsenates are unstable with respect to calcite at pH > 8, and therefore, in the long-term, will dissolve releasing arsenic into the environment. This reaction is represented by the following equation (Eqn. 2.):

$$Ca_3(AsO_4)_{2(s)} + 3CO_3^{2-}_{(aq)} + 2H_2O \rightarrow 3CaCO_{3(s)} + 2HAsO_4^{2-}_{(aq)} + 2OH^-$$
 (2.2)

Thus, introduction of carbon dioxide, bicarbonate, or carbonate will lead to increased dissolution of calcium arsenates. Based on thermodynamic calculations, Robins and Tozawa were able to produce diagrams that show how the delineation of the calcium arsenate stability change between closed systems (**Fig. 2.3a.**) and systems open to the atmosphere with  $P_{CO_2} = 10^{-3.52}$  atm (**Fig. 2.3b.**) [27].

### 2.4. Ca-Fe-As-H<sub>2</sub>O System

Calcium iron arsenic phases have attracted recent attention due to several findings in modern metallurgical tailings. Unlike iron or calcium arsenates, these phases were not strategically precipitated for the purposes of arsenic immobilization but have evolved through natural geochemical processes. At the Mokrsko-west gold deposit in the Czech Republic, arseniosiderite (Ca<sub>2</sub>Fe<sub>3</sub>(AsO<sub>4</sub>)<sub>3</sub>O<sub>2</sub>·3H<sub>2</sub>O), pharmacosiderite (KFe<sub>4</sub>(AsO<sub>4</sub>)<sub>3</sub>(OH)<sub>4</sub>·6-7H<sub>2</sub>O) with ca. 2 wt.% Ca, and possibly yukonite (Ca<sub>3</sub>Fe<sub>7</sub>(AsO<sub>4</sub>)<sub>6</sub>(OH)<sub>9</sub>·18H<sub>2</sub>O, PDF 35-553) were found in soils surrounding past mining activity [28], likely the result of oxidative weathering of primary minerals. At the Ketza River mine in the Yukon Territory, Canada, ca. 10 year old tailings from a gold operation were found to contain arseniosiderite, yukonite, and iron oxyhydroxides containing Ca among calcium arsenates, iron arsenates, and calcite [29]. In Nova Scotia, widespread gold mining activity at the turn of the 20<sup>th</sup> century has left uncontained As-rich tailings containing yukonite and an amorphous Ca-Fe arsenate, the stability of which is unclear [30]. Recently, amorphous Ca-Fe arsenates resembling yukonite were discovered at the Bi'r Tawilah gold prospect in Saudi Arabia [31].

While the stability of Ca-Fe-As phases is not well understood, many authors have suggested they are highly soluble. For instance, Paktunc et al. concluded the tailings at Ketza River are susceptible to leaching of arsenic based on a column flow-through (pH 7-8) and solubility (pH 6.5-7) study [32] of air-exposed tailings that released up to 34.7 mg/L and 3.9 mg/L, respectively. Ca-Fe-As phases were speculated to be the source of solubilized As, but the samples contained a mixture of many As-rich phases. These authors and many others (e.g. [33],[34]) cite a conference paper by Swash and Monhemius that systematically investigated the Ca-Fe-AsO<sub>4</sub> system. Here, a total of 135 TCLP tests were performed on Ca-Fe-As phases synthesized at various temperature (20-225°C), Ca/Fe/As ratio, and pH. While interesting, there are many shortcomings of this study that prevent its conclusions from being definitive. For instance, no details are provided about the washing procedure necessary to remove entrained/interstitial arsenic in pore water left over from synthesis. The TCLP itself only reveals solubility at pH 5. Most significantly, the authors note the phases formed were very different from arseniosiderite and yukonite, which are apparently stable enough to persist in the environment [35]. Therefore, a greater understanding of Ca-Fe-As phase stability is needed.

#### 2.5. Yukonite

Yukonite is a hydrated basic calcium ferric arsenate [Ca(II)-Fe(III)-As(V)-H<sub>2</sub>O] mineral first reported in 1913 and grandfathered in by the International Mineralogical Association (IMA) as a mineral discovered prior to 1959 [36], [37]. However, in similar vein to Pluto as a planet, its classification of a mineral is controversial according to modern definitions. This is immediately evident upon examining its two powder diffraction files (PDF) available from the International Center for Diffraction Data (ICDD): PDF 51-1416 and PDF 35-553. In addition to minor differences in the diffraction patterns (e.g. peak shifts and peak absences), the two listed chemical formulae are patently different: Ca<sub>6.5</sub>Fe<sub>15</sub>(AsO<sub>4</sub>)<sub>9</sub>O<sub>16</sub>·25.5H<sub>2</sub>O and Ca<sub>3</sub>Fe<sub>7</sub>(AsO<sub>4</sub>)<sub>6</sub>(OH)<sub>9</sub>·18H<sub>2</sub>O, respectively.

According to the International Mineralogical Association (IMA), in general terms, a mineral is "an element or chemical compound that is normally crystalline and which has been formed as a result of geological processes." A mineral must be a naturally formed homogenous phase of definite composition (or range of compositions) and possess a single crystal structure (long-range order of atomic lattice) [38].

In this section, the mineralogy of yukonite is discussed following a thorough literature search. As it would be, the mineralogy of yukonite is highly complex and its nature is subject to debate. For instance, being poorly-crystalline (short-range order of atomic lattice) and having variable composition, it is unclear whether yukonite is a single phase, a solid-solution, or an admixture of multiple phases. Of importance for its synthesis in the laboratory and studying its environmental stability, which is the purpose of this work, is that the intricacies of yukonite be fully acknowledged and understood.

First, a historical overview of the literature (2.5.1.) provides context for a critical analysis and discussion of yukonite in terms of chemical composition (2.5.2.), atomic, molecular, crystallographic stricture (2.5.3.), and physical characteristics and morphology (2.5.4.). Subsequently, a synopsis of natural occurrences (2.5.5.) is given to understand the geological conditions that have proven hospitable for yukonite formation and persistence and to prime a discussion of its synthesis (2.5.6.) and environmental stability (2.5.7.).

#### 2.5.1. Historical developments

In spite of its relative scarcity, occurrences of yukonite have been documented around the globe. In total, there are 12 scientific papers that describe occurrences of natural yukonite at 8 different localities.

In 1913, Tyrrell and Graham reported the 1906 discovery of yukonite at Windy Arm on Tagish Lake in the Yukon Territory, Canada, where it was found at the site of the Daulton Mine, an operational silver mine. (Later, the Daulton mine site would be rebranded as the Venus Mine. In the literature, yukonite referred to as either "Yukon," "Tagish Lake," "Daulton Mine," or "Venus Mine" all comes from this geographic location. Tagish Lake will be used in this work). Chemical analysis of the mineral, which appeared amorphous under an optical microscope, produced the first chemical formula:  $(Ca_3Fe_2)_2(AsO_4)_2(OH)_6.5H_2O$  [36]. Jambor reinvestigated type yukonite in 1966, confirming the chemical analysis of Tyrrell and Graham but reimagining the chemical formula as  $Ca_6Fe_{16}(AsO_4)_{10}(OH)_{30}.23H_2O$ . Significantly, Jambor [39] produced the first X-ray diffraction data. While the data was of poor quality and did not allow for the determination of crystallographic parameters, it showed that structure of yukonite was not entirely amorphous. Furthermore, a characteristic diffraction pattern for comparison opened the door for identification of new occurrences of material with similar chemical composition.

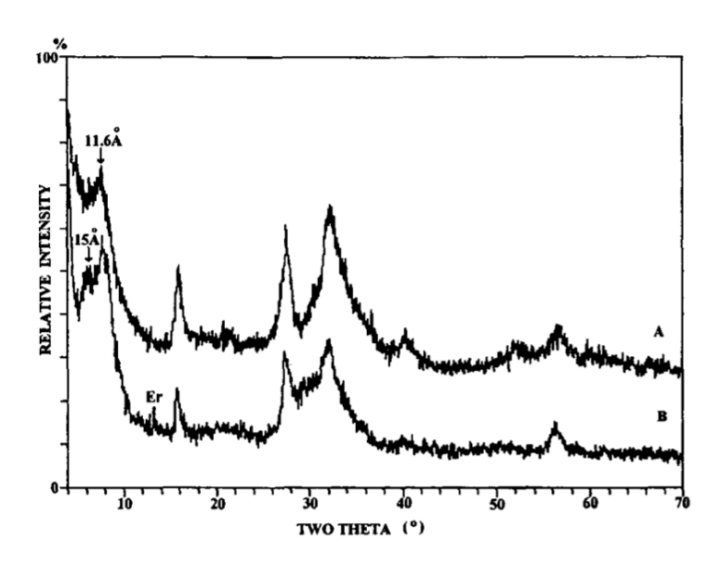


**Fig. 2.4.** Powder X-Ray diffractograms of yukonite from (a) Tagish Lake, Yukon Territory, Canada, and (b) Saalfield, Thuringen, Germany, compared with PDF 35-553, from Ross & Post, 1997 [40]. The Saalfield sample contains a trace of erythrite, Er,  $(Co_3(AsO_4)_2 \cdot 8H_2O)$ .

This was the case in 1982, when Dunn reported a second occurrence at the Sterling Hill Mine in New Jersey, citing excellent agreement of the X-ray diffraction pattern and consistency of chemical composition [39]. However, Dunn's electron microprobe analysis did show small but significant deviation of composition from type yukonite and revealed, for the first time, incorporation of minor elements such as Al, Mg, Mn, P, S, Si, and Zn [39]. In 1997, researchers Ross and Post of the Smithsonian Institution discovered a third occurrence when analyzing samples indigenous to Germany formerly identified as "asbolite" from a collection at the U.S. National Museum of Natural History. X-ray diffraction (Fig. 2.4.) and electron microprobe analysis revealed asbolite to be the same phase as yukonite, constituting the first occurrence of yukonite outside of North America [40]. A year later, Pieczka et al. of the University of Mining and Metallurgy in Kraków discovered a fourth occurrence near the abandoned Czarnów mine in Rędziny, Sudetes, Poland [41].

To this point, yukonite was almost exclusively found in association with mining activity, but with the exception of a simple solubility study by Krause and Ettel in 1989, study of yukonite was reserved for mineralogists [20]. However, its fifth discovery at the Ketza River Mine, Yukon Territory, Canada, was the first time yukonite was found in process tailings of a modern metallurgical operation (mine closure in 1990), which brought to the forefront the possible role of yukonite in the geochemical control of arsenic in arsenical waste. Reported by Paktunc et al. of CANMET (Canada Centre for Mineral and Energy Technology), a pair of publications in 2003 and 2004 investigated the mineralogy of the gold mine tailings using, among other techniques, X-ray absorption spectroscopy [29], [42]. Soprovich from Environment Canada conducted a column leaching experiment on the Ketza River Tailings, which concluded the tails had a potential to leach arsenic, but by its nature could not conclusively indict a specific arsenic-bearing mineral phase [32].

More new discoveries of yukonite followed in quick succession. Nishikawa et al. in 2006 reported the sixth discovery of yukonite in hot springs belonging to the Nalychevskie geothermal system, near an active volcano in Kamchatka, Russia. A unique find, the phase identified as yukonite that formed from thermal waters (64°C) contained an occasional particle that produced single crystal electron diffraction patterns. The Nalychevskie material contained up to 8.7 wt.% Si and showed an inverse correlation in the stoichiometry of As and Si, implying yukonite permits direct substitution in its structure, at least in the case of silicate and arsenate [37]. In

2007, Filippi et al. reported a possible occurrence of yukonite at the Mokrsko-west gold deposit in the Czech Republic in samples definitively containing arseniosiderite and scorodite [28]. Then in 2009, at the Grotta Della Monaca Cave, Sant'Agata Di Esaro, Italy, yukonite was discovered again. Despite contamination with scorodite, the study by Garavelli et al. used a collaborative approach of X-ray diffraction, electron microscopy, and infrared spectroscopy to gain new insight to the nature of yukonite [43].

Between 2009 and 2011, a series of abandoned gold mines (closure between 1860-1940) became the subject of intense study due to presence of arsenic-bearing minerals in uncontained tailings. Walker et al. in 2009 identified yukonite that was very closely associated with pharmacosiderite [KFe<sub>4</sub>(AsO<sub>4</sub>)<sub>3</sub>(OH)<sub>4</sub>·6-7H<sub>2</sub>O], noting that the similar diffraction patterns complicated characterization [30]. This finding was corroborated by Corriveau et al. in 2011 [44], also noting a Ca-Fe arsenate likely to be yukonite. Both studies acknowledge a lack of understanding of the solubility of yukonite yet assume it to be relatively soluble. This assumption was further promoted by Meunier et al., 2011, who found an uncharacterized sample apparently rich in yukonite to be highly soluble under "gastric conditions," using a physiologically based extraction test (PBET) that features a 60-minute acid digestion (pH 1.8) [45].

Finally, extensive study of yukonite has been conducted in recent times by the HydroMET Group at McGill University. As previously mentioned, both poorly-crystalline ferric arsenate and scorodite were found to transform to yukonite in the presence of gypsum saturation upon accelerated ageing at 75°C [12], [46]. This led to the development of a synthesis method for yukonite, first reported by Becze and Demopoulos in 2007 [47]. In this study, variable synthesis conditions produced either yukonite or kolfanite (Ca<sub>2</sub>Fe<sub>3</sub>O<sub>2</sub>(AsO<sub>4</sub>)<sub>3</sub>·2H<sub>2</sub>O) after 19 days ageing at 95°C. Subsequently, in 2010, Becze et al. reported a 24-hour yukonite synthesis procedure and, for the first time, solubility data in neutral to alkaline conditions, noting decreased solubility in gypsum-saturated solution [48]. In conjunction, Gomez et al. published in 2009 extensive work on the characterization of both natural and synthetic yukonite, also comparing yukonite to arseniosiderite using vibrational and X-ray absorption spectroscopy [49].

#### 2.5.2. Chemical Composition

The chemical composition of yukonite has been found to be variable; however, the source of variability is not clear. As will be discussed, variability in reported chemical composition likely arises from some combination of the following factors: (1) error associated with analytical technique, (2) presence of impurity phases, (3) substitution of minor elements, and (4) resolution of analytical method due to mixture of phases. Since the first chemical formula of  $(Ca_3Fe_2)_2(AsO_4)_2(OH)_6.5H_2O$  by Tyrrell and Graham in 1913, many new distinct formulae have been proposed: Jambor, 1966; Ross and Post, 1997; Pieczka et al., 1998; Nishikawa et al., 2006; Garavelli et al., 2009; Gomez et al., 2009 [37], [39]–[41], [43], [49]. Still more provided chemical analyses of natural yukonite without calculating a formula: Dunn, 1982; Paktunc et. al., Walker et al., 2009 [30], [39], [42]. All known chemical formulae for yukonite are tabulated in Table 2.1.

As evident from the multitude of proposed formulae in the literature, there is no consensus on the chemical formula of yukonite. This uncertainty in composition arises from the absence of crystallographic parameters (i.e. crystal system, space group, and unit cell dimensions) that would isolate a discrete crystallochemical formula (a chemical formula derived from a knowledge of the arrangement of atoms in space) [41]. Such information remains elusive. X-ray crystallographic data of adequate quality to determine crystal structure has not been obtained, a consequence of the poor crystallinity of the material and not of poor methods of characterization [37], [40]. Rather, the composition is understood only by empirical analyses that themselves do not necessarily point to a single theoretical end-member chemical formula.

The comparison of the composition of yukonite has been complicated by the use of different strategies used to normalize formula coefficients. In the absence of crystallographic information, the number of atoms that compose a single undefined unit cell of yukonite is arbitrary. To ease comparison, the data of all known analyses have been recalculated in this review. Here, the number of As atoms is normalized to unity and the molar ratios of Ca to As and Fe to As are plotted in **Fig. 2.5**. The recalculated molar Ca: Fe: As ratios for known formulae can also be viewed in **Table 2.1**.

 Table 2.1. Overview of proposed chemical formulae of yukonite.

Locality	First Author, Year	Chemical Formula	Ca : Fe : As Molar Ratio
Tagish Lake	Tyrrell, 1913	$2Ca_3As_2O_8\cdot 3Fe_2As_2O_8\cdot 5Fe_2(OH)_6\cdot 23H_2O$	0.60 : 1.60 : 1
	Jambor, 1966	$Ca_6Fe_{16}(AsO_4)_{10}(OH)_{30}\cdot 23H_2O$	0.60 : 1.60 : 1
(R5783)	Ross, 1997	$(Ca_{6.44}K_{0.13}Mg_{0.23})(Fe_{14.68}Al_{0.36})(AsO_4)_9O_{15.78}\cdot 25.5H_2O$	0.72 : 1.63 : 1
	Pieczka, 1998	$*Ca_{6.10}Fe_{13.28}(AsO_4)_{9.20}(OH)_{23.16} \cdot 6.77H_2O$	0.66 : 1.44 : 1
	Garavelli, 2009	$Ca_{1.76}Fe^{2^{+}}{}_{0.10}Fe^{3^{+}}{}_{3.56}[(As_{0.89}Si_{0.08}P_{0.03})O_{4}]_{3}(OH)_{5.16}\cdot 3H_{2}O$	0.66:1.37:1
	Gomez, 2009	$Ca_2Fe_5(AsO_4)_3(OH)_{10}\cdot 2H_2O$	0.54 : 1.67 : 1
Sterling Hill Mine	Pieczka, 1998	$Ca_{5.62}Fe_{10.94}(AsO_4)_{8.47}(OH)_{20.34} \cdot 22.99H_2O$	0.66 : 1.29 : 1
		$Ca_{5.12}Fe_{9.96}(AsO_4)_{9.59}(OH)_{16.86} \cdot 10.73H_2O$	0.53 : 1.04 : 1
Saalfield (103710-1)	Ross, 1997	$(Ca_{5.80}K_{0.11}Mg_{0.27})(Fe_{10.61}Al_{0.52})(AsO_4)_9O_{9.34}\cdot 24.3H_2O$	0.64 : 1.18 : 1
	Pieczka, 1998	$Ca_{6.44}Fe_{11.78}(AsO_4)_{10.00}(OH)_{20.56} \cdot 17.06H_2O$	0.64:1.18:1
Rędziny	Pieczka, 1998	$Ca_{6.46}Fe_{10.70}(AsO_4)_{9.75}(OH)_{16.37}\cdot 15.72H_2O$	0.66 : 1.10 : 1
Nalychevski hot springs	Nishikawa, 2006	$Ca_{2}Fe_{3}(AsO_{4})_{3}(OH)_{4}\cdot 4H_{2}O$	0.67:1.00:1
Grotta della Monaca cave	Garavelli, 2009	$Ca_{1.76}Fe^{2^{+}}{}_{0.09}Fe^{3^{+}}{}_{3.12}[(As_{0.81}Si_{0.10}P_{0.09})O_{4}]_{3}(OH)_{3.76}\cdot 4H_{2}O$	0.72:1.32:1
	Gomez, 2009	$Ca_2Fe_3(AsO_4)_3(OH)_4\cdot 5H_2O$	0.62:1.13:1
Synthetic	Gomez, 2009	$Ca_2Fe_5(AsO_4)_3(OH)_{10}\cdot 5H_2O$	0.75 : 1.65 : 1
		$Ca_2Fe_3(AsO_4)_3(OH)_4\cdot 11H_2O$	0.57:1.22:1
		$Ca_2Fe_5(AsO_4)_3(OH)_{10}\cdot 2H_2O$	0.71 : 1.61 : 1
ICDD	PDF 35-553	$Ca_3Fe_7(AsO_4)_6(OH)_9\cdot 18H_2O$	0.50:1.17:1
	PDF 51-1416	$Ca_{6.5}Fe_{15}(AsO_4)_9O_{16}\cdot 25.5H_2O$	0.72 : 1.67 : 1

<sup>\*</sup>Reformulated from prior chemical analysis

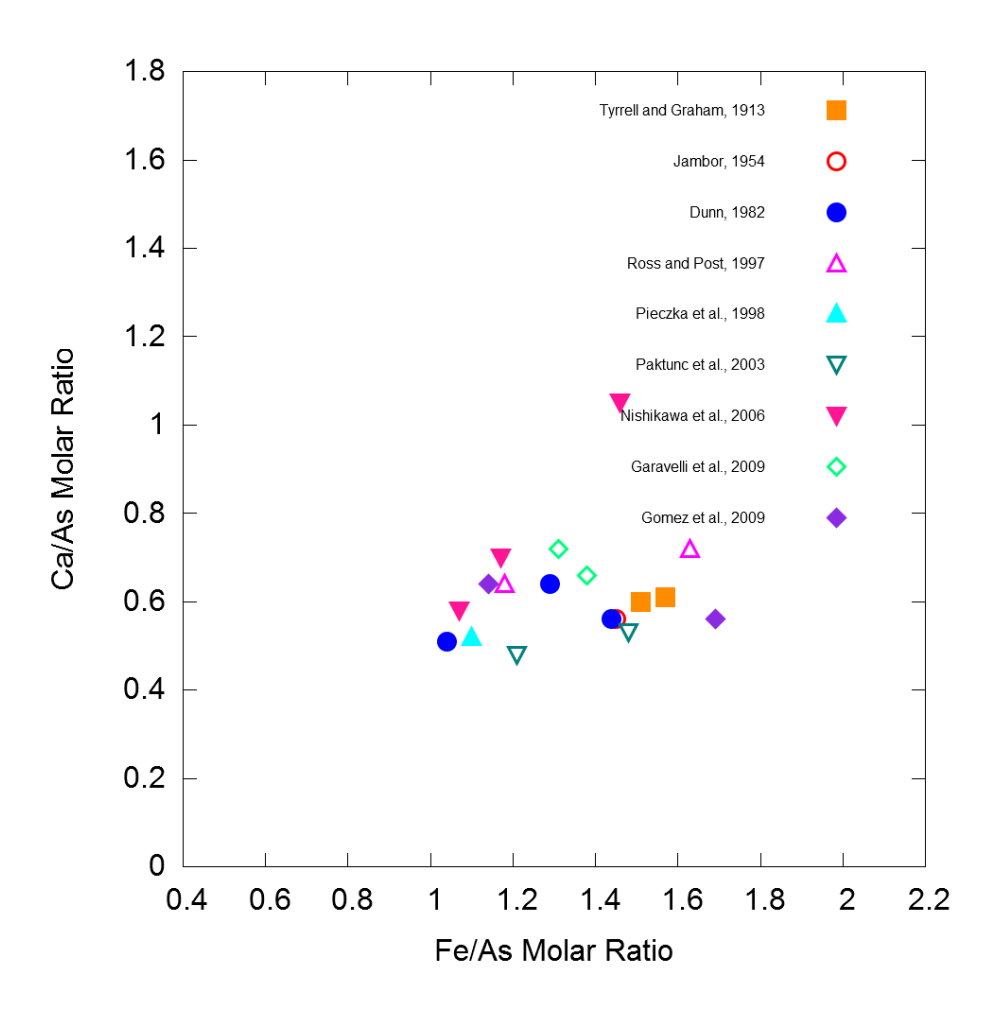


**Fig. 2.5.** Scatter plot of yukonite compositions for all known occurrences. Chemical formulae have been renormalized and presented as molar ratios of Ca: As and Fe: As.

Direct comparison reveals a wide range of compositions in terms of the major elements of yukonite. In general, the trend is obeyed that the Ca: As ratio is less than 1 and the Fe: As ratio is greater than 1, where the mean (std. dev.) ratios are 0.63 (0.12) and 1.34 (0.21), respectively. In other words, for each arsenic atom there are about 0.63 Ca atoms and about 1.34 Fe atoms. It is noted that there is more deviation in Fe than in Ca. In addition, it's important to note that significant composition variation occurs even within specimens from the same locality.

In addition to variation in major elements, reports of the water content of yukonite have similarly varied. The uncertainty started with Tyrrell and Graham's initial report, indicating two possible values for type yukonite: 17.57 wt.% by Penfield's method and 20.28 wt.% by the adsorption method, the latter of which was viewed as more accurate. But Jambor's analysis of type yukonite by DTA-TGA suggested the opposite, finding 17.9 wt.%. Nishikawa et al. (**Fig. 2.6.**) used TGA to determined 21.8 wt.% for Tagish Lake yukonite and 17.8 wt.% for Nalychevski hot springs yukonite, and Garavelli et al. reported a range of 16.4-17.8 wt.% by

DTA-TGA for different samples from Grotta della Monaca, in agreement with 17.2 wt.% by Gomez et al. for this type by TGA. Gomez et al. also analyzed Tagish Lake yukonite, finding 19.9 wt.% and for the synthetic samples: 14.8, 13.7, and 14.7 wt.% [49]. Thus, natural yukonite samples were found to range from 16.8 wt.% to 21.8 wt.%. Dunn [39], Ross and Post [40], and Pieczka et al. [41] also reported values that ranged from 11.5 to 19.7 wt.%; however, these were calculated by difference from chemical analysis and therefore are not considered accurate. From this information, the origin of variability is not immediately clear and will be further discussed in 2.5.3.

Such a wide range of composition of major elements and molecular water is harmful to the view of yukonite as a single phase. How can this be justified?

One explanation of the discrepancies in composition is error associated with chemical analysis, exacerbated by the use of different analytical methods. Studies have used an array of different techniques: wet chemical analysis [36], Electron Microprobe Analysis (EMPA) [39]–[41], [49], Electron Microprobe Wavelength Dispersive Spectroscopy (EM-WDS) [42] and Energy-Dispersive Spectroscopy tethered to (1) Scanning Electron Microscopy (SEM-EDS) and (2) Transmission Electron Microscopy, TEM-EDS [43]. For instance, many authors have cited

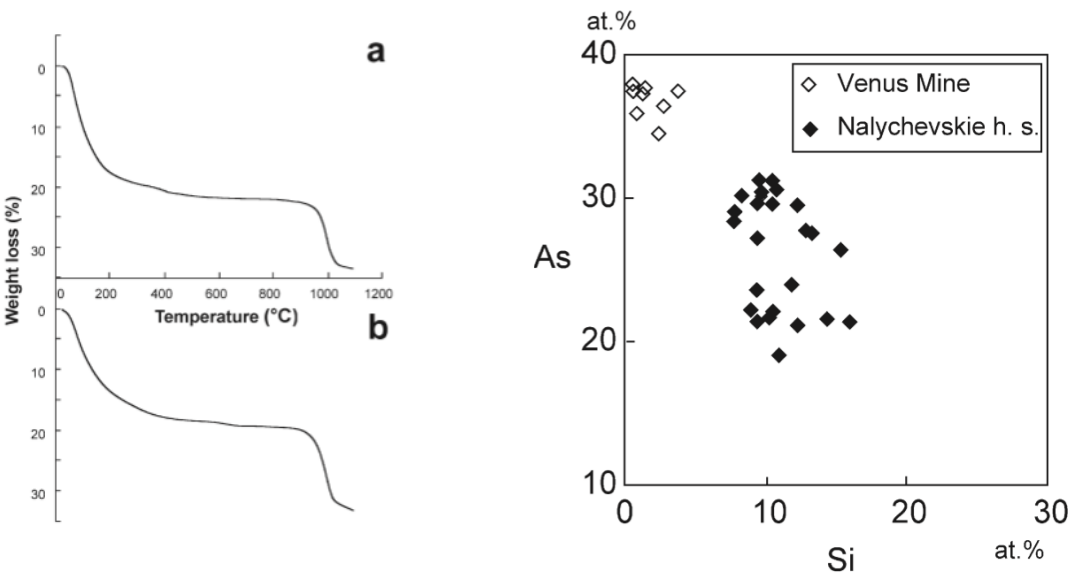


**Fig. 2.6.** (left) Thermogravimetric analysis (TGA) curves of: (a) Yukonite aggregates from Tagish Lake, Yukon Territory, Canada (21.8 wt.% H<sub>2</sub>O) [37]; (b) Yukonite from Nalychevski hot springs, Kamchatka, Russia (17.8 wt.% H<sub>2</sub>O) [37].

**Fig. 2.7.** (right) Substitution of up to 15.9 at.%  $SiO_4^{4-}$  for  $AsO_4^{3-}$  and a strong inverse correlation between As and Si suggest direct substitution in the crystal structure [37].

difficulty in measuring chemical composition of yukonite with electron beam methods due to sample decomposition [39], [40]. Dunn suggested the error of the analysis with microprobe was at least 5% due to sample dehydration under the electron beam, and Ross and Post consider their analysis only approximate. It follows that difference from chemical analysis is not a suitable method of determining water content.

While analytical methods are undoubtedly a source of error, it does not explain why two different samples from the same locality measured using the same technique (let alone same instrument) would have vastly different compositions, as in the case of the two Ketza River (Ca: As, Fe: As) samples: (0.48, 1.21) and (0.53, 1.48) as measured by Paktunc et al. with EM-WDS. This could be, however, explained by the presence of impurity phases, an entirely probable scenario amidst the complex mineralogy at Ketza River. For instance, Garavelli et al. noted yukonite from Grotta della Monaca was contaminated with significant amounts of scorodite, chemically analyzed by TEM-EDS with phase identification by Selected Area Electron Diffraction, TEM-SEAD, and also noted minor amounts of calcium carbonate (e.g., calcite) and calcium sulfate (i.e. gypsum) contamination, phases which were not detected by XRD, suggesting the quantity was below the approximately 5 at.% detection limit of XRD [43]. Gomez et al. confirmed the scorodite impurity and noted that the quantity of scorodite was enough to produce adequate X-ray reflections to be visible with X-ray diffraction (XRD) [49]. Walker et al. noted yukonite found in Nova Scotia to be admixed with pharmacosiderite, which was difficult to differentiate even with micron-resolution XRD (µ-XRD) due to overlapping diffraction patterns [30].

Thus, small amounts of crystalline impurity material could be present in many samples characterized only by XRD, or could have been missed in investigation with TEM-EDS, in the case where an inadequate number of sample points were measured. The same can be said for XRD invisible amorphous phases, such as ferrihydrite, poorly-crystalline ferric arsenate, or Ca-Fe arsenate, which can only be noticed, in theory, by high resolution TEM (HR-TEM). In practice, it is debatable whether these amorphous phases can reliably be identified by electron beam methods. As previously noted, yukonite has been consistently shown to dehydrate upon electron beam analysis. The process of losing structure water is damaging to yukonite, and as noted by Garavelli et al. [43], it is possible that amorphous phases identified by electron beam methods have become amorphous during the process of analysis. This is also consistent with the

experience of this author. Thus, it is possible no analyses have yet to accurately characterize yukonite, where unique tools such as cryo-TEM might be necessary for accurate analysis.

Another explanation for the variable composition exemplified at Ketza River is substitution of minor elements into the structure of yukonite, as alluded to by several authors [37], [41], [43]. The presence of minor elements was not originally noticed by Tyrrell and Graham or Jambor, whose analyses considered only major elements (Ca, Fe, As) and crystallographic water [36], [39]. It was not until Dunn's electron microprobe analysis that it was noted both Tagish Lake and Sterling Hill yukonite had minor, but significant, incorporations of Al, Mg, Mn, P, S, Si, and Zn, up to 3.8 wt.% ZnO in the case of Sterling Hill. Later, Ross and Post also found K in both Tagish Lake and Saalfield yukonite but apparently did not analyze for Mn, S, Si, or Zn. In the chemical analysis of Rędziny yukonite, Pieczka et al. also consider Al, Mg, Mn, P, S, Si, and Zn. On the other hand, Nishikawa et al. considered only K, Mn, and Si as minor elements in the analysis of yukonite Nalychevski hot springs. Garavelli et al. looked for Al, As, Ba, Ca, Fe, Mg, Fe, P, and Si in Grotta della Monaca yukonite.

The problem then, as Goldschmidt put it, is "not all guests are equally welcome in a lattice, and the crystal in many cases makes a choice between them," [50]. Goldschmidt argued that these ionic "guests" directly substitute when they have similar ionic potential, the quotient of ionic charge and ionic radius. According to frequently alluded to "rules" of Goldschmidt's, direct substitution of ions in a crystal structure can occur so long as the atomic radii are within 15 % in size and electroneutrality of the structure is maintained. In practice, this generally means substitution of ions differing in charge by greater than  $\pm 1$  will be minimal. Later, Ahrens suggested the selective incorporation of ion into a crystal lattice was dictated by anion affinity [51]. Either way, certain minor elements are substituted into lattice positions of major elements (e.g. Ca, Fe, As) and hence influence the relative composition of the major elements in our comparison. Unfortunately, these effects also depend on the crystal field, and therefore the structure of yukonite [52]. Thus, it is impossible to predict which ions are directly substituting into the crystallographic positions of major elements and which are simply incorporated as inclusions in interstitial space. One exception is the case of As and Si, where chemical analysis of Nalychevskie hot springs yukonite revealed a strong negative correlation between Si and As (Fig. 2.7.), Si substituted for as much as 15.9 at.% of As.

Analyses by Pieczka et al., Nishikawa et al., and Garavelli et al. have accounted for substitution of minor elements by considering molar ratios of the sum of like ions, typically in terms of valance. For instance,  $Ca = \Sigma$  bivalent cations =  $Ca^{2+} + Mg^{2+} + Mn^{2+} + Zn^{2+}$ ;  $Fe = \Sigma$  trivalent cations =  $Al^{3+} + Fe^{3+}$ ; and  $As = \Sigma$  multivalent anions =  $AsO_4^{3-} + PO_4^{3-} + SO_4^{2-} + SiO_4^{3-}$ . While this is a vast simplification of even Goldschmidt's generalized rules, it is useful to consider how the composition might change in the event of substitution. In **Fig. 2.8.**, 11 yukonite composition datasets were chosen that were considered to be close to total analyses (i.e. they include most minor elements). In squares, the molar Fe: As and Ca: Fe are first plotted for the case of uncorrected data which is ratios of only major elements. In circles, the ratios of elements are represented by sums of like ions, using the aforementioned scheme of Garavelli et al.

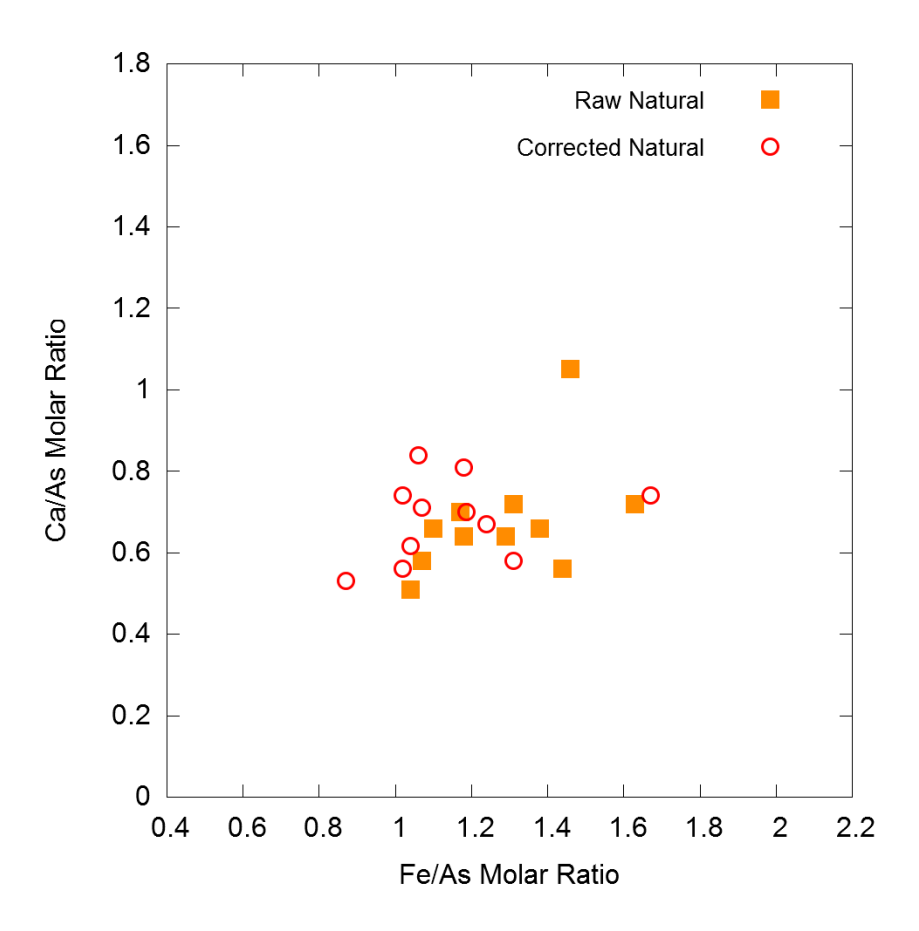


**Fig. 2.8.** Scatter plot of yukonite compositions for 11 analyses. Formulae have been renormalized and presented as molar ratios of Ca: As and Fe: As.

The mean (std. dev.) ratios for uncorrected and corrected data are 0.68 (0.14) and 1.34 (0.21) and 0.71 (0.10) and 1.22 (0.21), respectively. Thus, the rudimentary composition

corrections show better coherence in the case of Ca: As molar ratios and similar coherence in the case of Fe: As ratios. Interestingly, the corrected data suggest yukonite may have higher Ca: As and lower Fe: As ratios than evident from considering only major elements. Still, it stops well short of converging on an end-member chemical composition. It is possible minor element substitution could explain yukonite's variable composition, but it is impossible to be sure without knowledge of its crystallographic structure.

Finally, Garavelli et al. suggests variation in composition may occur due to inadequate spatial resolution of analytical methods, suggesting yukonite may not be a single phase but a mixture of small crystallites in an amorphous matrix of varying composition (more on this in **2.5.3.**) [43]. Wet chemical analysis by Tyrrell and Graham gave only an average composition of the bulk. According to Dunn [39], samples from Sterling Hill showed homogeneity at a 10 μm spot size with electron microprobe; however, the analyses were conducted with a 40 μm spot size. Pieczka's analysis averaged composition over 12 points with a 20 μm spot size [41]. Thus, they suggest only TEM-EDS, with high resolution (5 nm), can detect the true composition of cryptocrystalline (nanocrystalline) yukonite. Their analysis gives significantly less Fe and more closely resembles arseniosiderite:

$$Ca_{1.76}Fe^{2+}_{0.09}Fe^{3+}_{3.12}[(As_{0.81}Si_{0.10}P_{0.09})O_4]_3(OH)_{3.76}\cdot 4H_2O$$
 (2.3)

The basis of this theory is contested by Gomez et al. [49], who notes that their analysis with EMPA (micron resolution) of Grotta della Monaca yukonite gave the same analytical results as Garavelli et al., asserting that differences in composition arise not from variety in analytical techniques but from the ability of yukonite to incorporate various amounts of Ca, Fe, As, and H<sub>2</sub>O into its structure. While this conclusion is not specifically challenged here, the notion that the chemical analyses are the same is not the case. Specifically, Gomez et al. did not analyze for Si or P, which together make up 18.6 at.% of tetrahedrally coordinated species in the Grotta della Monaca sample according to the analysis of Garavelli et al. To recalculate ignoring these crucial quantities, the molar ratios (Ca: Fe: As) become 0.72: 1.32: 1.00, compared to 0.62: 1.13: 1.00 from Gomez et al. For this reason, analyses of Tagish Lake yukonite and Romanech arseniosiderite by Gomez et al. should also be considered incomplete.

Despite this, Gomez et al. found variable compositions for synthetic yukonite where, due to relatively pristine laboratory conditions, availability of foreign ions was minimal and

consistent, and impurities such as gypsum and calcite were not present. Barring unnoticed sample contamination with amorphous phases (ferrihydrite, calcium arsenate, etc.), this suggests variable composition may be a natural consequence of its structure. Interestingly, while the Ca: Fe: As ratios were variable (in two cases close to 0.75: 1.65: 1 and in another 0.57: 1.22: 1), the Ca: Fe ratio was found to be very close to 0.45: 1 in all instances. At least in this case, it appears the composition variation is in the anion (e.g. AsO<sub>4</sub><sup>3-</sup> and OH<sup>-</sup>).

The discussion of the variable composition of yukonite has yielded several possible explanations of merit without making any definite conclusions. It appears all play a role, but it is unclear to what extent. Thus, it is necessary now to consider the intimate connection between composition and structure in an effort to better understand yukonite's peculiar mineralogy.

#### 2.5.3. Crystallographic, Molecular, and Atomic Structure

The discussion of the chemical composition of yukonite suggested possible answers to the question of its variability, but at its end a new question was posed: Is the uncertainty of chemical composition a by-product of structural phenomena? In this section, knowledge of the structure of yukonite is reviewed and discussed. The discussion is built upon crystallographic information obtained from diffraction (X-ray and electron) data, molecular information from vibrational spectroscopy (infrared and Raman) and synchrotron-based X-ray absorption spectroscopy. In particular, the frequently alluded to relationship with arseniosiderite (Ca<sub>6</sub>Fe<sub>9</sub>(AsO<sub>4</sub>)<sub>9</sub>O<sub>2</sub>·9H<sub>2</sub>O) is evaluated and also the possible relationship with Ca and As rich ferrihydrite suggested by Paktunc et al. is examined. As previously mentioned, the crystallographic structure of yukonite has not been solved and, therefore, a black and white understanding of the way its atoms arrange in space is not known. Hence, it will be the mission of this review to use words to interpret and assemble indirect structural information to create a lucid representation.

In the discussion of the structure/order or yukonite, the word "crystalline" and its derivatives and modifiers (e.g., "crystallinity," "poorly-crystalline," etc.) are used somewhat ambiguously. However, the ambiguity is not necessarily due to carelessness but rather the grey area yukonite falls in terms of order of its atomic structure. Therefore, when working with poorresolved information, it is important to begin by sharpening the nomenclatural tools that will be used to build an accurate depiction of the structure of yukonite.

According to the IMA [53], a crystalline mineral is differentiated from an amorphous phase by "atomic ordering on a scale that produces an 'indexable' (i.e. with Miller indices) diffraction pattern" by radiation of the appropriate wavelength (e.g. X-ray, electron, neutron, etc.). To be indexable, atoms (or molecules) must be arranged periodically in three dimensions, forming distinct crystallographic planes. When incident radiation encounters these planes and, due to constructive and destructive interference, it is diffracted at specific Bragg angles [54, pp. 79–85], which are a function of the interatomic spacing between the crystallographic planes (dspacing). The result is a distinct diffraction pattern that can indexed by mathematical coordinate system to describe the orientation of the crystallographic planes in three-dimensional space. Material without sufficient order does not diffract at specific Bragg angles, and therefore an index cannot be determined, in which case it is axiomatically considered amorphous by the IMA. "Crystallinity" is defined as a ratio of fully crystalline material to amorphous material in a given sample. Practically, this can be determined by analysis of XRD diffractograms, where the area of peaks resulting from Bragg reflections from ordered atomic planes is integrated and divided by the integration of the background area, which results from the random reflections of amorphous material with no ordered lattices [55]. This is not to be confused with "poorly-crystalline," which instead describes a material with limited atomic ordering [56, pp. 23–1].

In a perfectly crystalline material, each atom is perfectly aligned for an infinite distance in every direction. Such a material is not known in the real world, owing to defects (e.g., atoms out of place and impurity particles). Grain boundaries are a special type of defect where discrete regions of crystalline material of varying sizes intersect at different orientations with respect to each other. A material of this description is also known as polycrystalline [54, p. 256]. Polycrystalline materials can also be referred to by the size of the crystalline regions. For example, regions of crystalline material that have atomic order greater than 1 µm in at least one dimension (i.e. "long range order") are called microcrystalline, whereas regions of crystalline material with atomic order of only a few nanometers (i.e. "short range order") are called nanocrystalline [57, p. 148]. Therefore, "poorly-crystalline" is a term applied to materials that fall in between these two extremes that implies some level of short range order over limited periodicity [56, pp. 23–1], [58, pp. 38–40]. Materials without grain boundaries can also be nanocrystalline; for example, a hypocrystalline material is one where nanocrystals are embedded in a glassy (amorphous) matrix [59].

**Table 2.2:** Summary of X-ray diffraction data from literature for yukonite.

1	2	3	4	5	6	7	8
d(Å)	d(Å)	d(Å)	d(Å)	d(Å)	d(Å)	d(Å)	Crystal
I	I	I	I	I	I	I	Symmetry
$(I_{corrected})$	$(I_{corrected})$	$(I_{corrected})$	$(I_{corrected})$	$(I_{corrected})$	$(I_{corrected})$	$(I_{corrected})$	(hlk)
-	15.7 100 (175)	14.10 100 (175)	-	14.20 52 (52)	15.70 100 (103)	15.69 100 (337)	001
<b>5.60</b> 80 (80)	<b>5.69</b> 33 (58)	<b>5.58</b> 37 (65)	<b>5.61</b> 82 (82)	<b>5.61</b> 72 (72)	<b>5.65</b> 90 (93)	<b>5.640</b> 34.9 (118)	110
3.25 100 (100)	3.27 57 (100)	3.25 57 (100)	3.243 100 (100)	3.26 100 (100)	<b>3.26</b> 97 (100)	3.275 29.7 (100)	300
2.79 80 (80)	<b>2.81</b> 63 (111)	2.79 60 (105)	2.778 80 (80)	2.80 85 (85)	2.80 85 (88)	2.8083 28.7 (97)	220
2.23 30 (30)	2.25 11 (19)	2.24 11 (19)	2.226 22 (22)	2.24 24 (24)	2.23 24 (25)	2.2456 8.5 (29)	320
1.76 5 (5)	1.77 11 (19)	<b>1.76</b> 9 (16)	1.767 5 (5)	1.76 20 (20)	1.75 52 (54)	1.7642 8.6 (29)	510
1.63 40 (40)	1.64 17 (30)	1.63 20 (35)	35 (35)	1.63 23 (23)	<b>1.63</b> 49 (51)	1.6417 14.9 (50)	600
1.51 20 (20)	-	1.51 20 (35)	-	-	-	<b>1.5084</b> 6.7 (23)	610

<sup>1.</sup> Dunn, 1982. Analysis by Jambor [39]. Also PDF 35-553

<sup>2.</sup> Ross and Post, 1997. Saalfield [40]. Also PDF 51-1416

Ross and Post, 1997. Tagish Lake [40].
 Pieczka et al., 1998. Rędziny [41].

Nishikawa et al., 2006. Nalychevski hot springs [37]. 5.

Nishikawa et al., 2006. Tagish Lake (Venus Mine) [37].

<sup>7.</sup> Garavelli et al., 2009. Grotta della Monaca [43].

<sup>8.</sup> Miller indices for hexagonal cell according to TEM data [37], [43].

#### Crystallographic structure

As noted, the first observations by optical microscopy indicated yukonite was amorphous [3]. However, the advent of X-ray diffraction and its subsequent re-examination revealed a characteristic X-ray diffraction pattern indicating yukonite is not entirely amorphous. The pattern (e.g. Fig. 2.4, Fig. 2.9, Fig. 2.10) shows broad, poorly resolved peaks. In the context of the previous discussion, these features indicate Bragg reflections from crystallographic planes that occur not at discrete angles but instead as broad distributions, indicating varying interatomic distances between planes resulting from a disordered crystallographic structure and/or small crystallites [13].

All known diffraction patterns for natural yukonite are tabulated in **Table 2.2.** Comparison of peak intensities is complicated as they are reported as normalized percentages, where the highest peak of the diffractogram represents 100%. In most datasets, the most intense peak occurs at 14.10-15.70 Å and represents 100% intensity. However, some diffraction experiments did not detect this peak. In these cases, intensities are instead normalized to the peak at approximately 3.25 Å. Therefore, to facilitate comparison the raw intensities have been recalculated and normalized to the 3.25 Å peak, I<sub>corrected</sub>. In general, the crystallographic patterns between localities and authors are in very good agreement. However, the inconsistent presence and variable position of the aforementioned low-angle peak is peculiar and has structural

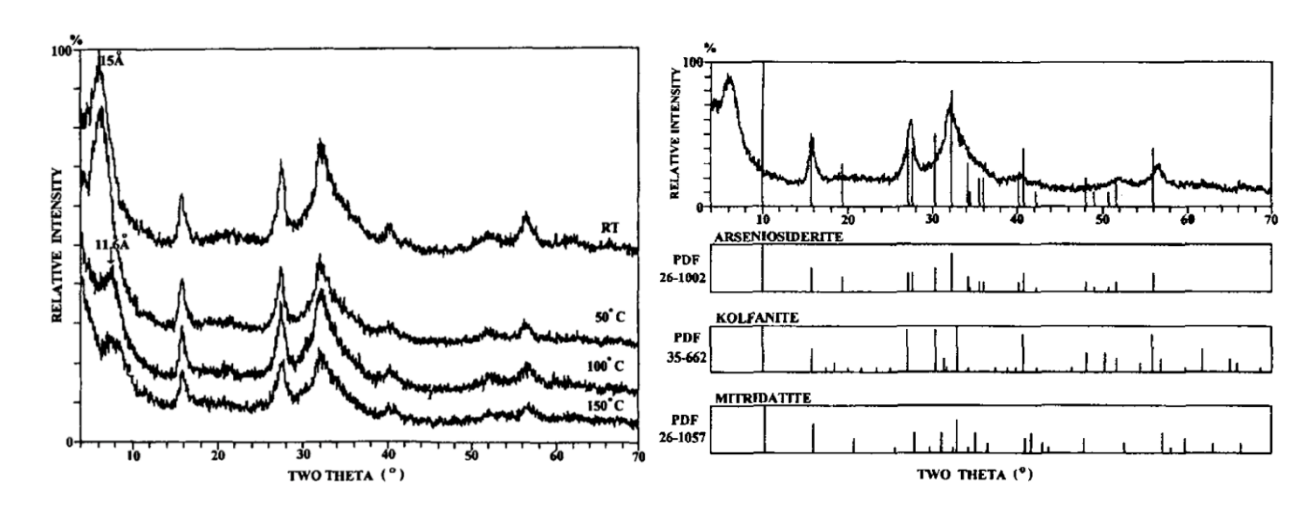


**Fig. 2.9.** Powder X-Ray diffractograms of type yukonite (top to bottom) at room temperature, and after heating to 50°C, 100°C, and 150°C. From Ross and Post, 1997 [40].

**Fig. 2.10.** Powder X-Ray diffractogram of type yukonite overlaid with arseniosiderite reference pattern (top) in comparison to that of arseniosiderite, kolfanite, and mitridatite. From Ross and Post, 1997 [40].

implications. Ross and Post were the first to identify the peak, which did not appear in Jambor's characterization. They speculated its absence could have been due to the difficulty of detecting low-angle peaks on XRD equipment of the era. In their own analysis, they found the most intense peak of Saalfield yukonite to be different from type yukonite (15.7 Å and 14.1 Å, respectively). Moreover, it changed during the course of analysis, with the 15.7 Å peak weakening and a new, broader peak occurring at 11.6 Å. Suspecting sample dehydration, they heated "type" yukonite samples to various temperatures (Fig. 2.9.) and found the peak shift occurred only at 100°C and higher, confirming the low-angle peak shifts in response to the formation of different hydration states. Thus, the structure of yukonite apparently can expand and contract to accommodate various levels of hydration. Given their new insight, Ross and Post also elaborated on Tyrrell and Graham's initial assertion that yukonite resembled arseniosiderite in its chemical composition by comparison of diffraction patterns (Fig. 2.10.). The diffraction pattern of yukonite strongly resembles that of arseniosiderite but differs in its broader peaks and in the location of the low-angle peak, 14.1 Å in the case of yukonite and 8.8 Å in the case of arseniosiderite. While the crystal structure of arseniosiderite is not rigorously known, according to Moore and Araki it is isomorphous with respect to mitriditate (Ca<sub>6</sub>Fe<sub>9</sub>(PO<sub>4</sub>)<sub>9</sub>O<sub>2</sub>·9H<sub>2</sub>O), the structure of which is shown in Fig. 2.11. Thus, arseniosiderite is likely a sheet structure,

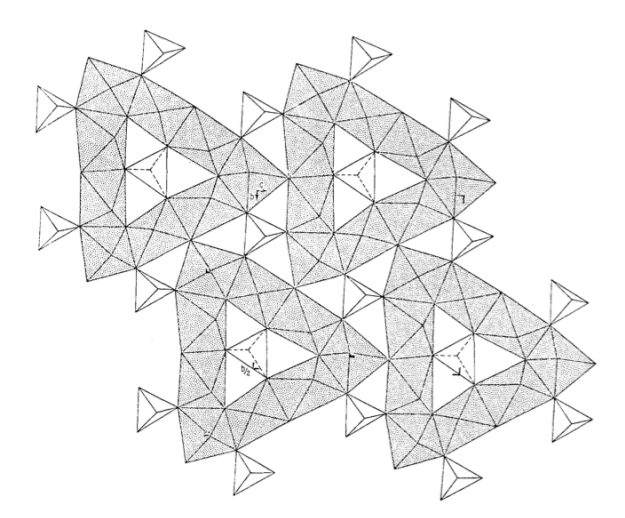


**Fig. 2.11.** Graphical representation of the [001] incident  $Fe_9O_6(PO_4)_9)^{-12}$  sheet in mitridatite  $(Ca_6Fe_9(PO_4)_9O_2\cdot 9H_2O)$ . The shaded grey are  $Fe^{3^+}$ -O octahedra and the white are  $AsO_4^{3^-}$  tetrahedra. Parallel to the page are sheets of  $CaO_5(H_2O)_2$  polyhedra with additional hydrogen bonded water. Mitridatite is isomorphous with arseniosiderite  $Ca_6Fe_9(AsO_4)_9O_2\cdot 9H_2O$ , which shows structural similarities with yukonite by XRD. From Moore and Araki, 1977 [60].

consisting of planes of trigonal edge-sharing nonamers of iron octahedra, with corner-sharing arsenate tetrahedra in, above, and below the plane. These planes are stacked in between layers of  $CaO_5(H_2O)_2$  polyhedra with additional water groups fixed by hydrogen bonding. In light of the evident similarity of yukonite to arseniosiderite, it is reasonable to suggest yukonite might have a structure similar to mitridatite and arseniosiderite. Some crystallographic evidence supporting this is gained in observing the low-angle peak, which in yukonite shifts toward lower degrees two theta with increased hydration and toward higher degrees two theta with decreased hydration [13]. In arseniosiderite, the low-angle peak is 8.8 Å, which is consistent with the fact that in contains relatively less crystallographic water than yukonite (As :  $\Sigma$  [O<sup>2-</sup>, OH<sup>-</sup>, H<sub>2</sub>O] ca. 1, As :  $\Sigma$  [O<sup>2-</sup>, OH<sup>-</sup>, H<sub>2</sub>O] ca. 3, respectively).

The story of the crystal structure of yukonite told by X-ray diffraction is corroborated by electron diffraction data. Nishikawa et al. noted that lattice spacings from electron diffraction patterns were in agreement with those of X-ray diffraction. Significantly, these authors found single crystal diffraction to occur from occasional grains from Nalychevskie hot springs, unprecedented in the study of yukonite. This allowed for yukonite to be indexed for the first time, but its thin, 5 nm thick crystal habit prevented the determination of its unit cell. As noted by Garavelli et al., the presence of these rare single-crystals, found only in small quantities in this particular locality, was likely due to the unique physiochemical conditions of the hightemperature springs (more on this in 2.5.5.). Nishikawa proposed indexes based on hexagonal crystal symmetry found in some crystals (Table 2.2.), but the majority of the crystals were of orthorhombic symmetry. Nishikawa seconded this approach [37], citing the likely similarity of the structure of arseniosiderite proposed by Moore and Araki (Fig. 2.11.) as collateral. However, Gomez et al. suggested the crystals possessing hexagonal symmetry could have actually been a small contamination of arseniosiderite, which went undetected by XRD. Nishikawa et al. were also able to capture high-resolution TEM images that clearly show the order of yukonite's crystal lattice on a scale consistent with diffraction measurements (Fig. 2.12.) [37].

TEM observations by Garavelli et al. of Grotta della Monaca yukonite similarly found either anhedral grains in aggregates > 50 nm or, alternatively, thin flakes 20-30 nm wide in aggregates > 50 nm [43]. According to TEM analysis by Gomez et al., yukonite particles had physical size greater  $\ge 100$  nm with internal order over only 1-15 nm. Thus, in comparison

to its cousin arseniosiderite, which has atomic order on a micron scale (long-range), yukonite possesses short-range atomic order of its crystal structure. However, X-ray and electron methods stop short on providing an explanation for this behavior.

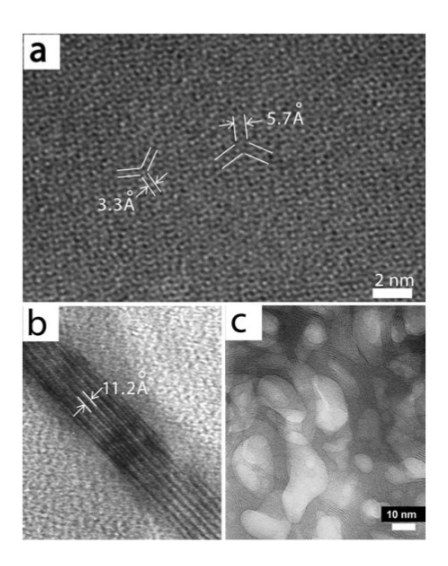


Fig. 2.12. HR-TEM images of Nalychevski yukonite (a,b) and type yukonite (c) [37].

## Molecular and atomic structure

The use of molecular-sensitive vibrational spectroscopy has provided clarity in the investigation in the structure of yukonite and its relationship to arensiosiderite. The use of FTIR in conjunction with annealing of samples at various temperatures by Garavelli et al. [43] gave the first evidence confirming the presence of hydroxyl units in the structure of yukonite. This was confirmed by Gomez et al. [49], with both ATR-IR and Raman spectroscopy. Further, these researchers argued comparison of vibrational spectra between yukonite and arseniosiderite explained the difference in long-range atomic order between the two. In the case of yukonite, a wide hydroxyl IR stretch in the 3111-3215 cm<sup>-1</sup> region is indicative of a disordered hydrogen bonding environment. Arseniosiderite, on the other hand, exhibits two distinct hydroxyl stretches at 3100 and 3576 cm<sup>-1</sup>, which can be correlated to two distinct crystallographic water bonding environments. Thus, it is concluded that the well-developed hydrogen bonding network permits the long-range atomic order of arseniosiderite's layered sheets, while the presence of a greater

amount of interlayer water in yukonite inhibits significant hydrogen bonding, leading to only short-range atomic order.

Several studies' ([29], [42], [49], [61]) use of synchrotron-based X-ray absorption fine structure spectroscopy (XAFS) have given insight to the structure of yukonite on a molecular level. XAFS is the combination of two related techniques, X-ray absorption near-edge spectroscopy (XANES) and extended X-ray absorption fine structure (EXAFS). The former gives information about speciation (oxidation state) while the latter provides information about the local bonding environment of an atom, such as coordination numbers and bond length. According to Paktunc et al. [29], [42], the local coordination environment of yukonite and arseniosiderite were identical in terms of As-O and As-Fe bond length and coordination number, the only difference being the As-Ca coordination number (4.17 and 2.44, respectively). However, as noted by Gomez et al. [49], these authors give several values of coordination numbers for arseniosiderite: 2.44, 3.60, 5.5, creating uncertainty. Significantly, Gomez et al. were able to show with Ca 2p, Fe 2p, and As-K edge XANES that the local structural environment of Ca, Fe, and As in yukonite and arseniosiderite was identical, with the only difference arising in long-range order.

Paktunc et al. also noted that, in addition to adsorbed As, up to 12.7 wt.% CaO was found in association with ferrihydrite in the Ketza River gold mine tailings. The authors stated such a high amount of calcium implies it is not adsorbed but incorporated in the structure as a coprecipitate. Noting a similar Ca/As ratio of the coprecipitate to yukonite and arseniosiderite, it was suggested that the phases may be related, visualized by plotting wt.% CaO vs wt.% As<sub>2</sub>O<sub>5</sub> (Fig. 2.13.). This finding is consistent with an arsenate-adsorbed ferrihydrite phase that is metastable with respect to yukonite, where a minor amount of yukonite nanocrystallites have formed at the expense of arsenate-adsorbed ferrihydrite. However, this relationship remains unclear due to a significant gap between Ca, As-ferrihydrite and yukonite. The authors also suggested that yukonite may be metastable with respect to arseniosiderite, evidenced by the precipitation of the latter around a Ca-Fe arsenate spheroid.

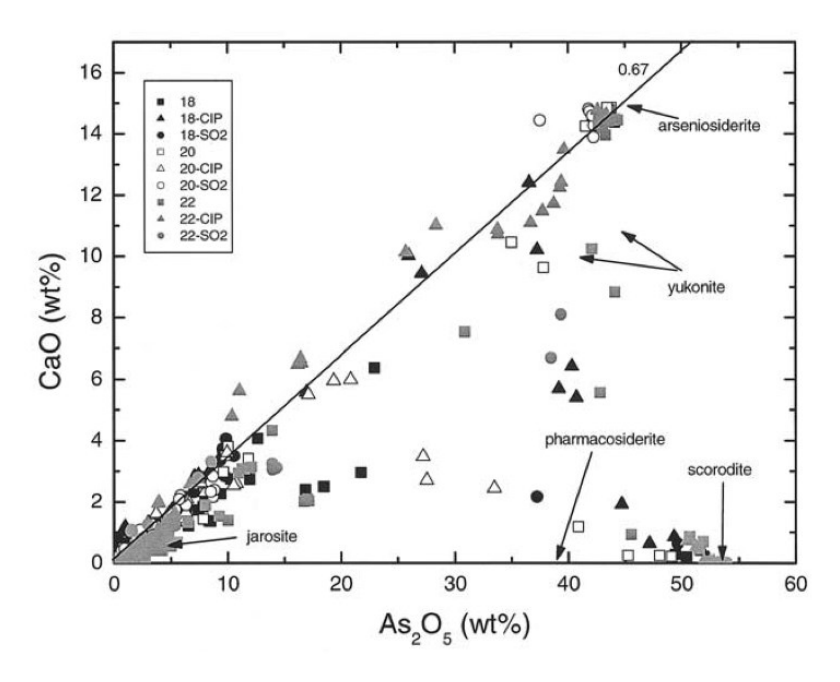


**Fig. 2.13.** Scatter plot of Ca,As-ferrihydrite, yukonite, and arseniosiderite found in the Ketza River gold mine tailings in the Yukon Territory, Canada. From Paktunc et al [42].

## 2.5.4. Physical Description and Morphology

Investigation into its structure has revealed yukonite is a hypocrystalline material, with nanocrystalline domains only 1-15 nm in size [49] embedded in an amorphous matrix. When wet, yukonite is gel-like but dries to form aggregates of small particles [39], [41].

Unsurprisingly, the morphology of yukonite is not exhibited on the macro scale. In one case, the aggregates were described as having a "lath-like" crystal habit, consistent with the proposed sheet structure of yukonite [39]. In another instance, it was found to form leaf-like aggregates with radial growth textures [42]. Much more commonly, however, yukonite has been found to occur as spheroidal aggregates, either massive or concretionary [36], [37], [39], [41]–[43]. These can be up to the size of a "walnut," as described by Tyrrell and Graham, and also fine grained, reported by Nishikawa et al. to be between 1-100 µm. Gomez et al. found all particles were ≥ 100 nm (Fig. 2.14.) [37], [41], [49]. In addition to discrete grains, yukonite is also found as a psuedomorphous replacement product of parasymplesite and kittigite [39], a replacement product of arsenopyrite and scorodite [29], and as deposits on arsenopyrite and iron-rich carbonates [30].

Yukonite particles are universally brittle, exhibiting smooth and conchoidal fracture [36], [40], [41], [43]. They are also relatively soft, with a measure of 2-3 on the Mohs scale. Attempts to measure its density, approximately 2.65-2.86, were complicated by evolving carbon dioxide when placed in solution [36]. In thin sections, yukonite is translucent, as opposed to opaque, consistent with an ionic bonded structure. This is evident to the naked eye by noticing its luster, which is vitreous or pitchy [36], [41]. The colour of yukonite is most generally described as brown. However, most authors report variation even within localities, with most occurrences described as dark brown [36], [39], [41], [43], reddish-brown [30], [39], [40], [43] or yellow-brown [36], [43]. It has also been noted, especially in small fragments, to have a violet tint [41], [43]. Its colour apparently varies with particle size. Yukonite tends to be dark brown in large masses, but its brown-yellow streak suggests smaller particles are lighter brown or yellowish in colour [36], [40]. This is also consistent with Tyrrell and Graham's initial description of "concretionary masses embedded in a pale yellowish brown earth material resembling ochre."

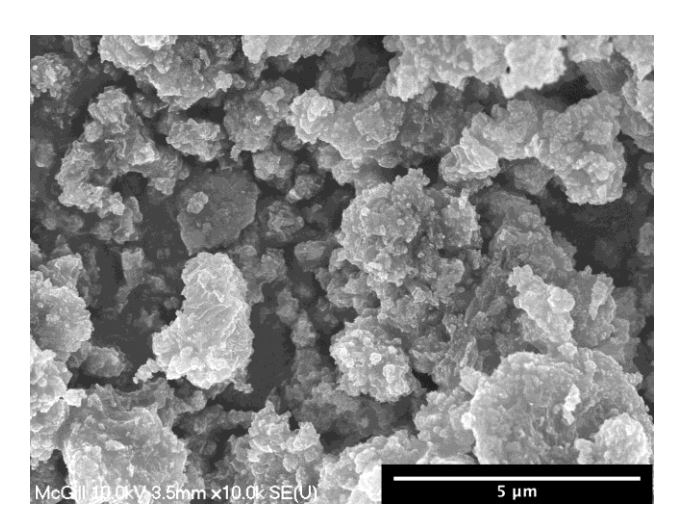


**Fig. 2.14.** Secondary electron scanning electron micrograph of synthetic yukonite taken at 10 kV. From Gomez et al [49].

#### 2.5.5. Natural occurrences

Understanding the geological conditions under which a mineral is formed provides clues both in terms of how it could be synthesized and also under which conditions it is metastable or stable. Yukonite is typically found in association with mining activity, either in land altered by mines or in mine tailings. In both cases, it tends to occur as an oxidation product of primary arsenidic or sulfidic minerals in the presence of a calcium-rich environment under neutral-to-alkaline conditions.

For instance, the Daulton Mine in the Yukon Terrirtory, Canada, consisted of quartz veins containing silver-bearing galena (PbS), in association with pyrargyrite, argentite, chalcopyrite, and arsenopyrite (FeAsS), among others. Here, yukonite was found in a zone of oxidation of sulfidic ore that contained arsenopyrite [36]. Subsequently, yukonite was found at the Sterling Hill Mine in New Jersey, United States, a zinc ore body of diverse mineralogy (e.g. willemite, Zn<sub>2</sub>SiO<sub>4</sub>; zincite, ZnO) situated in white crystalline limestone, rich in calcite [39], [62]. Yukonite found near the Czarnów mine in Rędziny, Sudetes, Poland, was found in a brown-yellow layer of oxidized iron mineralization, intergrown with pharmacosiderite and arsenopyrite. In this case, a polymetallic ore was deposited in a dolostone (i.e. dolomite stone, CaMg(CO<sub>3</sub>)<sub>2</sub>) quarry, including primary and secondary sulfides and arsenides and secondary, oxidized Fe-Cu-Zn-Pb-Mn oxides, carbonates, silicates, arsenates, and vanadates [41]. The site where yukonite was found at the Grotta della Monaca cave was a prehistoric mine site, where metallic minerals were intensively mined in the second half of the third millennium B.C. The surrounding mineralogy was primarly calcite, and also aragonite, dolomite, malachite, azurite, goethite, lepidoscrocite, limonite, gypsum, apatite-(CaOH), and asmpleite. Yukonite was found in direct association with calcium phosphate and iron oxides [43].

At the Ketza River Mine in the Yukon Territory, Canada, yukonite was found in gold mine tailings that were deposited in a sub-aqueous tailings impoundment between 1988-1990, composed primarily of iron oxyhydroxides, and also included quartz, calcite, dolomite, muscovite, scorodite, and calcium-iron arsenates. Yukonite was found as a replacement product of scorodite and arsenopyrite, the latter constituting 0.1 wt.% total tailings mass. In total, the tailings were 4 wt.% arsenic [29]. In Nova Scotia, Canada, yukonite was found in tailings of a mine that extracted and processed arsenopyrite-bearing gold ore between 1861 and 1942. In this case, the tailings, including waste rock, were not impounded but scattered along local riverbeds. The tailings consist primarily of quartz, with muscovite, chlorite, and plagioclase; in some cases but not others, calcium carbonates such as ankerite and calcite. Depending on the sample, the tailings contained between 0.7 and 7 wt.% arsenic, primarily in the form of scorodite and

hydrous ferric arsenate (HFA). Less common arsenic carriers include yukonite, and also: amorphous hydrous ferric oxyhydroxide (HFO), kankite, pharmacosiderite, amorphous Ca-Fe arsenates, and arsenopyrite [30].

An exceptional occurrence of yukonite was at the Nalychevskie hot springs in Kamchatka, Russia. Unlike other occurrences that occurred at ambient temperature, this yukonite formed at the shore in the bottom of a borehole of thermal springs. The supernatant solution from which yukonite precipitated was 64°C, pH 6.3, and slightly reducing at E<sub>H</sub> -10 mV. The thermal waters contained notable concentrations of Na<sup>+</sup> (937 mg/L), Cl<sup>-</sup> (1454 mg/L, As (6.4 mg/L), H<sub>3</sub>BO<sub>4</sub> (401 mg/L), Ca<sup>2+</sup> (232 mg/L), SO<sub>4</sub><sup>2-</sup> (456 mg/L), and dissolved inorganic carbon (498 mg/L).

**Table 2.3:** Composition and phase identification of synthesis products after 19 days. Recreated from [47].

Ca : Fe : As Initial Molar Ratio		Phase			
	Ca	Fe	As	S	Identified
0.5 : 0.75 : 1	7.68	20.95	20.29	0	Yukonite
0.5:1:1	6.276	23.87	16.70	0	Yukonite
0.5:1.5:1	4.608	25.32	10.86	0	Yukonite
1:0.75:1	10.18	17.58	21.68	0	Yukonite
1:1:1	9.37	20.21	18.08	0.32	Yukonite
1:1.5:1	6.48	21.42	12.42	0	Yukonite
2:0.75:1	11.17	13.48	17.13	1.6	Kolfanite
2:1:1	11.75	19.31	17.42	1.33	Yukonite
2:1.5:1	8.816	22.48	13.7	0.99	Yukonite

## 2.5.6. Synthesis of yukonite

The McGill HydroMET Group has reported the only synthesis method for yukonite [47], [48]. The synthesis method was inspired by previously discussed high temperature accelerating

ageing studies that showed coprecipitated solids and also scorodite transformed to yukonite at 70°C in the presence of gypsum-saturated solution. In the synthesis study, gypsum-saturated solution was equilibrated with ferric sulfate and disodium sodium arsenate in varying Ca: Fe: As ratios at pH 0.5. Subsequently, the solutions were heated to 95°C, at which point neutralization to pH 8 was performed by continuous addition of 5% NaOH over 15 minutes. The solutions were then aged for 19 days, with slurry samples taken at days 1, 13, and 19.

Two variables were identified by that study to affect the resulting composition: synthesis time and solution composition. In the case of the former, analysis of the synthesis supernatant revealed a decrease in concentration of component ions with time with Ca and As levels stabilization after approximately 13 days, while Fe concentrations were very low (< 1 mg/L) throughout the experiment. This implies the composition of the precipitated solids also changes with synthesis time. A second variable was initial solution composition (i.e. different Ca: Fe: As ratios). In this study, many different ratios were tried to empirically arrive at the best synthesis conditions (**Table 2.3**). All ratios achieved a product after 19 days determined to be yukonite by X-ray diffraction, with the exception of 2: 0.75: 1, which produced kolfanite. However, the composition of the yukonite produced by a 0.5: 0.75: 1 was closest to natural occurrences. Thus, a second report by Becze et al. in 2010 revealed a finalized synthesis method with a Ca: Fe: As ratio of 0.5: 0.75: 1 and a 24 h synthesis time.

## 2.5.7. Stability of yukonite

Knowledge of the solubility or stability of yukonite is sparse. A lone study by Krause and Ettel [20], has investigated the solubility of natural specimens of yukonite and arseniosiderite of unknown origin, though the yukonite sample is presumably type yukonite from the Yukon Territory, Canada. No chemical composition data was reported, however X-ray diffraction of the yukonite sample revealed no pattern and the arseniosiderite sample was consistent with known patterns, with the addition of some very minor unidentified peaks. The experiment (**Table 2.4**) consisted of dry-ground samples in solution (2.5 wt.%) with stirring for 48 days without pH adjustment, followed by adjustment to pH 5.0 using H<sub>2</sub>SO<sub>4</sub> or NaOH after sampling, which commenced Day 0. Both minerals behaved similarly. In both cases, there was high initial release of arsenic with decrease in the long term, to 6.3 mg/L after 197 days in the case of yukonite. Unfortunately, calcium concentrations were not measured. Interestingly, the data from Krause

and Ettel is remarkably consistent with findings by Nishikawa et al., who found yukonite at the bank of a thermal pool at Nalychevskie hot springs. Chemical analysis revealed the pH 6.3 thermal pool contained 6.4 mg/L As. This is favorable evidence of yukonite's capacity to control arsenic pore water concentrations.

The McGill HydroMET Group conducted a more thorough study of the solubility of yukonite. In this study (**Table 2.5**), synthetic yukonite was subjected to solutions of varying pH, both with and without gypsum-saturation. The results show that yukonite is in general most stable at circumneutral pH with decreasing stability with increasing alkalinity. While there was just 8.96 mg/L As at pH 7 in gypsum-free solution, the presence of gypsum-saturation significant suppresses yukonite solubility and extends its region of relative stability to pH 9.5.

**Table 2.4:** Solubility data of natural yukonite and natural arseniosiderite. Recreated from [20].

Yukonite					Arseniosiderite		
Days	рН	Fe (mg/L)	As (mg/L)	рН	Fe (mg/L)	As (mg/L)	
0	6.9	-	-	8.1	-	-	
9	-	0.2	61	-	< 0.2	28	
27	5.55	< 0.2	51	8.15	< 0.2	27	
48	5.5	< 0.2	37	7.85	< 0.2	16	
93	-	< 0.2	28	-	< 0.2	3.1	
197	6.15	< 0.2	6.3	6.85	< 0.2	6.7	

**Table 2.5:** Solubility data of synthetic yukonite equilibrated in gypsum-free and gypsum-saturated solutions. Synthesis conditions: 1.4 g/L initial As(V) conc., Ca : Fe : As = 0.5 : 0.75 : 1, t = 24 h, T = 95°C. Recreated from [48].

	Gyps	Gypsum-free solution		Gypsum-saturated solution		
pH Duration (days)	7 458	8 456	9.5 455	7 623	8 623	9.5 623
As (mg/L)	8.96	47.8	276.4	0.75	2.05	6.3
Ca (mg/L)	1.12	0.02	0.03	599	579	423
Fe (mg/L)	< 0.1	< 0.1	0.57	< 0.1	< 0.1	< 0.1

It should be noted that supposed high solubility of Ca-Fe-As phases, including yukonite, has been alluded to by many (Paktunc et al., etc) based on a conference proceedings of Swash and Monhemius detailing a study of the synthesis and solubility of Ca-Fe-As phases. What is misleading here is the suggestion that the solubility of these phases is representative of the solubility of yukonite, which is not the case. Moreover, the solubility data in general is questionable given that the samples were not washed prior to synthesis to remove both arsenic trapped in pore water and adsorbed arsenic.

## 2.6. Conclusion

Yukonite is a calcium iron arsenate phase that may play a role in geochemical control of arsenic in the environment, including in mining and metallurgical tailings. In reviewing available literature, it is the view of this author that yukonite is a hypocrystalline material composed of nanocrystallites embedded in an amorphous matrix. The nanocrystallites are similar in composition and structure to arseniosiderite, but differ in crystallite size (compared to micro domains of arseniosiderite) and degree of hydration, where yukonite has a greater percentage of molecular water that inhibits its growth beyond a few nanometers. The amorphous matrix is variable in composition, in part explaining inconsistencies in reported chemical composition of yukonite. However, the variation in reported composition also arises from selective incorporation, in some cases direct substitution, of minor elements, and also analytical error.

Little is known about the stability of yukonite. As recently noted by Walker et al., a thermodynamic basis for the relationships among the Fe Arsenates and Ca-Fe arsenates remains to be established [30]. In the first step of attaining this knowledge, a study by the HydroMET Group at McGill University has investigated the solubility and long-term stability of yukonite in oxic (i.e. oxidizing) conditions of neutral-to-alkaline pH, finding yukonite to be generally stable and significantly less soluble in the presence of gypsum-saturated solution. However, there is still much to uncover in terms of its stability.

The purpose of this thesis is to further investigate the stability of yukonite to evaluate its potential as a stable arsenic-bearing phase. In particular, it will probe its (1) solubility under oxic conditions in acidic solution, (2) stability with respect to CO<sub>2</sub> or dissolved inorganic carbon, and (3) stability under sub-oxic and anoxic (i.e. oxygen-depleted) conditions.

## References

- [1] A. H. Smith, E. O. Lingas, and M. Rahman, "Contamination of drinking-water by arsenic in Bangladesh: a public health emergency," *Bull. World Health Organ.*, vol. 78, no. 9, pp. 1093–1103, 2000.
- [2] "Lung Cancer and Arsenic Concentrations in Drinking Water in...: Epidemiology."
  [Online]. Available:
  http://journals.lww.com/epidem/Fulltext/2000/11000/Lung\_Cancer\_and\_Arsenic\_Concentrations\_in\_Drinking.10.aspx. [Accessed: 24-Jun-2014].
- [3] A. Neumann, R. Kaegi, A. Voegelin, A. Hussam, A. K. M. Munir, and S. J. Hug, "Arsenic Removal with Composite Iron Matrix Filters in Bangladesh: A Field and Laboratory Study," *Environ. Sci. Technol.*, vol. 47, no. 9, pp. 4544–4554, 2013.
- [4] J. Mahoney, D. Langmuir, N. Gosselin, and J. Rowson, "Arsenic readily released to pore waters from buried mill tailings," *Appl. Geochem.*, vol. 20, no. 5, pp. 947–959, 2005.
- [5] U. S. Epa, "National Primary Drinking Water Regulations: Arsenic and Clarifications to Compliance and New Source Contaminants Monitoring," Fed. Regist., vol. 66, pp. 6975– 7066, 2001.
- [6] Anonymous, "Final Report Arsenic Removal Demonstration Project." Mine Waste Technology Project Activity III, Project 9, EPA, 1999.
- [7] L. S. Branch, "Consolidated federal laws of canada, Metal Mining Effluent Regulations," 02-Mar-2012. [Online]. Available: http://laws-lois.justice.gc.ca/eng/regulations/sor-2002-222/FullText.html. [Accessed: 24-Jun-2014].
- [8] N. Chen, D. T. Jiang, J. Cutler, T. Kotzer, Y. F. Jia, G. P. Demopoulos, and J. W. Rowson, "Structural characterization of poorly-crystalline scorodite, iron(III)—arsenate coprecipitates and uranium mill neutralized raffinate solids using X-ray absorption fine structure spectroscopy," *Geochim. Cosmochim. Acta*, vol. 73, no. 11, pp. 3260–3276, 2009.
- [9] C. Mikutta, P. N. Mandaliev, and R. Kretzschmar, "New Clues to the Local Atomic Structure of Short-Range Ordered Ferric Arsenate from Extended X-ray Absorption Fine Structure Spectroscopy," *Environ. Sci. Technol.*, vol. 47, no. 7, pp. 3122–3131, 2013.
- [10] D. Filippou and G. P. Demopoulos, "Arsenic immobilization by controlled scorodite precipitation," *JOM*, vol. 49, no. 12, pp. 52–55, 1997.
- [11] J. Mahoney, M. Slaughter, D. Langmuir, and J. Rowson, "Control of As and Ni releases from a uranium mill tailings neutralization circuit: Solution chemistry, mineralogy and geochemical modeling of laboratory study results," *Appl. Geochem.*, vol. 22, no. 12, pp. 2758–2776, 2007.
- [12] Y. Jia and G. P. Demopoulos, "Coprecipitation of arsenate with iron(III) in aqueous sulfate media: Effect of time, lime as base and co-ions on arsenic retention," *Water Res.*, vol. 42, no. 3, pp. 661–668, 2008.
- [13] U. Schwertmann and E. Murad, "Effect of pH on the formation of goethite and hematite from ferrihydrite," *Clays Clay Miner.*, vol. 31, no. 4, pp. 277–284, 1983.
- [14] W. R. Cullen and K. J. Reimer, "Arsenic speciation in the environment," *Chem. Rev.*, vol. 89, no. 4, pp. 713–764, 1989.
- [15] D. C. Lynch, "A review of the physical chemistry of arsenic as it pertains to primary metals production," *Arsen. Metall. Fundam. Appl.*, RG Reddy, JL Hendrix, PB Queneau, Eds., pp. 3–33, 1988.

- [16] P. Lu and C. Zhu, "Arsenic Eh–pH diagrams at 25°C and 1 bar," *Environ. Earth Sci.*, vol. 62, no. 8, pp. 1673–1683, 2011.
- [17] G. A. Waychunas, B. A. Rea, C. C. Fuller, and J. A. Davis, "Surface chemistry of ferrihydrite: Part 1. EXAFS studies of the geometry of coprecipitated and adsorbed arsenate," *Geochim. Cosmochim. Acta*, vol. 57, no. 10, pp. 2251–2269, 1993.
- [18] Y. Jia, L. Xu, X. Wang, and G. P. Demopoulos, "Infrared spectroscopic and X-ray diffraction characterization of the nature of adsorbed arsenate on ferrihydrite," *Geochim. Cosmochim. Acta*, vol. 71, no. 7, pp. 1643–1654, 2007.
- [19] R. G. Robins, J. C. Y. Huang, and G. Khoe, "The adsorption of arsenate ion by ferric hydroxide," *Arsen. Metall. Fundam. Appl.*, RG Reddy, JL Hendrix, PB Queneau, Eds.,, 1987, vol. 39, pp. A2–A2.
- [20] E. Krause and V. A. Ettel, "Solubilities and stabilities of ferric arsenate compounds," *Hydrometallurgy*, vol. 22, no. 3, pp. 311–337, 1989.
- [21] J. F. L. Berre, R. Gauvin, and G. P. Demopoulos, "Characterization of Poorly-Crystalline Ferric Arsenate Precipitated from Equimolar Fe(III)-As(V) Solutions in the pH Range 2 to 8," *Metall. Mater. Trans. B*, vol. 38, no. 5, pp. 751–762, 2007.
- [22] H. McCreadie, D. W. Blowes, C. J. Ptacek, and J. L. Jambor, "Influence of Reduction Reactions and Solid-Phase Composition on Porewater Concentrations of Arsenic," *Environ. Sci. Technol.*, vol. 34, no. 15, pp. 3159–3166, 2000.
- [23] R. G. Robins and K. Tozawa, "Arsenic removal from gold processing waste waters: the potential ineffectiveness of lime," *Can. Min. Metall. Bull.*, vol. 75, no. 840, pp. 171–174, 1982.
- [24] T. Nishimura and R. G. Robins, "A Re-evaluation of the Solubility and Stability Regions of Calcium Arsenites and Calcium Arsenates in Aqueous Solution at 25°C," *Miner. Process. Extr. Metall. Rev.*, vol. 18, no. 3–4, pp. 283–308, 1998.
- [25] R. Donahue and M. J. Hendry, "Geochemistry of arsenic in uranium mine mill tailings, Saskatchewan, Canada," *Appl. Geochem.*, vol. 18, no. 11, pp. 1733–1750, 2003.
- [26] J. V. Bothe Jr. and P. W. Brown, "The stabilities of calcium arsenates at 23±1°C," *J. Hazard. Mater.*, vol. 69, no. 2, pp. 197–207, 1999.
- [27] R. G. Robins and K. Tozawa, "Arsenic removal from gold processing waste waters: the potential ineffectiveness of lime," *Can. Min. Metall. Bull.*, vol. 75, no. 840, pp. 171–174, 1982.
- [28] M. Filippi, B. Doušová, and V. Machovič, "Mineralogical speciation of arsenic in soils above the Mokrsko-west gold deposit, Czech Republic," *Geoderma*, vol. 139, no. 1–2, pp. 154–170, 2007.
- [29] D. Paktunc, A. Foster, and G. Laflamme, "Speciation and Characterization of Arsenic in Ketza River Mine Tailings Using X-ray Absorption Spectroscopy," *Environ. Sci. Technol.*, vol. 37, no. 10, pp. 2067–2074, 2003.
- [30] S. R. Walker, M. B. Parsons, H. E. Jamieson, and A. Lanzirotti, "Arsenic Mineralogy of Near-Surface Tailings and Soils: Influences on Arsenic Mobility and Bioaccessibility in the Nova Scotia Gold Mining Districts," *Can. Mineral.*, vol. 47, no. 3, pp. 533–556, 2009.
- [31] A. A. Surour, A. H. Ahmed, and H. M. Harbi, "Yukonite-like alteration products (Ca–Fe arsenate and As-rich Fe-oxyhydroxide) formed by in situ weathering in granodiorite, Bi'r Tawilah gold prospect, Saudi Arabia," *Eur. J. Mineral.*, vol. 25, no. 1, pp. 61–70, 2013.

- [32] E. A. Soprovich, "Arsenic release from oxide tailings containing scorodite, Fe-Ca arsenates and As-containing goethites," in *Proceedings of the Seventh International Conference on Tailings and Mine Waste'00*, A.A. Balkema, Ed., 2000, pp. 23–26.
- [33] P. A. Riveros, J. E. Dutrizac, and P. Spencer, "Arsenic disposal practices in the metallurgical industry," *Can. Metall. Q.*, vol. 40, no. 4, pp. 395–420, 2001.
- [34] P. Drahota and M. Filippi, "Secondary arsenic minerals in the environment: a review," *Environ. Int.*, vol. 35, no. 8, pp. 1243–1255, 2009.
- [35] P. M. Swash and A. J. Monhemius, "Synthesis, characterization and solubility testing of solids in the Ca-Fe-AsO4 system," *Sudbury '95—Mining Environ. CANMET*, pp. 17–28, 1995.
- [36] J. B. Tyrrell and R. P. D. Graham, "Yukonite, a New Hydrous Arsenate of Iron and Calcum, from Tagish Lake, Yukon Territory, Canada: With a Note on the Associated Symplesite," 1913.
- [37] O. Nishikawa, V. Okrugin, N. Belkova, I. Saji, K. Shiraki, and K. Tazaki, "Crystal symmetry and chemical composition of yukonite: TEM study of specimens collected from Nalychevskie hot springs, Kamchatka, Russia and from Venus Mine, Yukon Territory, Canada," *Mineral. Mag.*, vol. 70, no. 1, pp. 73–81, 2006.
- [38] V.-C. E. Nickel and C. J. Grice, "The IMA Commission on New Minerals and Mineral Names: procedures and guidelines on mineral nomenclature, 1998," *Mineral. Petrol.*, vol. 64, no. 1–4, pp. 237–263, 1998.
- [39] P. J. Dunn, "New Data for Pitticite and a Second Occurrence of Yukonite at Sterling Hill, New Jersey," *Mineral. Mag.*, vol. 46, no. 339, pp. 261–264, 1982.
- [40] D. R. Ross and J. E. Post, "New data on yukonite," *Powder Diffr.*, vol. 12, no. 02, pp. 113–116, 1997.
- [41] A. Pieczka, B. Golebiowska, and W. Franus, "Yukonite, a rare Ca-Fe arsenate, from Redziny (Sudetes, Poland)," *Eur. J. Mineral.*, vol. 10, no. 6, pp. 1367–1370, 1998.
- [42] D. Paktunc, A. Foster, S. Heald, and G. Laflamme, "Speciation and characterization of arsenic in gold ores and cyanidation tailings using X-ray absorption spectroscopy," *Geochim. Cosmochim. Acta*, vol. 68, no. 5, pp. 969–983, 2004.
- [43] A. Garavelli, D. Pinto, F. Vurro, M. Mellini, C. Viti, T. Balić-Žunić, and G. Della Ventura, "Yukonite from the Grotta Della Monaca cave, Sant'agata di Esaro, Italy: characterization and comparison with cotype material from the Daulton mine, Yukon, Canada," *Can. Mineral.*, vol. 47, no. 1, pp. 39–51, 2009.
- [44] M. C. Corriveau, H. E. Jamieson, M. B. Parsons, and G. E. M. Hall, "Mineralogical characterization of arsenic in gold mine tailings from three sites in Nova Scotia," *Geochem. Explor. Environ. Anal.*, vol. 11, no. 3, pp. 179–192, 2011.
- [45] L. Meunier, S. R. Walker, J. Wragg, M. B. Parsons, I. Koch, H. E. Jamieson, and K. J. Reimer, "Effects of Soil Composition and Mineralogy on the Bioaccessibility of Arsenic from Tailings and Soil in Gold Mine Districts of Nova Scotia," *Environ. Sci. Technol.*, vol. 44, no. 7, pp. 2667–2674, 2010.
- [46] M.-C. Bluteau, L. Becze, and G. P. Demopoulos, "The dissolution of scorodite in gypsum-saturated waters: Evidence of Ca–Fe–AsO4 mineral formation and its impact on arsenic retention," *Hydrometallurgy*, vol. 97, no. 3–4, pp. 221–227, 2009.
- [47] L. Becze and G. P. Demopoulos, "Hydrometallurgical synthesis and stability evaluation of Ca-As-AsO4 compounds," in *Extraction and Processing: Proceedings of Symposium*, 2007, p. 11.

- [48] L. Becze, M. A. Gomez, V. Petkov, J. N. Cutler, and G. P. Demopoulos, "The potential arsenic retention role of Ca-Fe(III)-AsO4 compounds in lime neutralized co-precipitation tailings," in *Uranium 2010*, EK Lam, JW Rowson, E Özberk, Eds., CIM, 2010, vol. II., pp 327-333.
- [49] M. A. Gomez, L. Becze, R. I. R. Blyth, J. N. Cutler, and G. P. Demopoulos, "Molecular and structural investigation of yukonite (synthetic & natural) and its relation to arseniosiderite," *Geochim. Cosmochim. Acta*, vol. 74, no. 20, pp. 5835–5851, 2010.
- [50] V. M. Goldschmidt, "The principles of distribution of chemical elements in minerals and rocks. The seventh Hugo Müller Lecture, delivered before the Chemical Society on March 17th, 1937," *J. Chem. Soc. Resumed*, pp. 655–673, 1937.
- [51] L. H. Ahrens, "The use of ionization potentials Part 2. Anion affinity and geochemistry," *Geochim. Cosmochim. Acta*, vol. 3, no. 1, pp. 1–29, 1953.
- [52] J. A. Tossell and D. J. Vaughan, *Theoretical geochemistry: applications of quantum mechanics in the earth and mineral sciences*. Oxford; New York: Oxford University Press, 1991
- [53] E. H. Nickel, "The definition of a mineral," *Mineral. J.*, vol. 17, no. 7, pp. 346–349, 1995.
- [54] B. D. Cullity, *Elements Of X Ray Diffraction*. Addison-Wesley Publishing Company, Inc., 1956.
- [55] W. Ruland, "X-ray determination of crystallinity and diffuse disorder scattering," *AYQ Acta Crystallogr.*, vol. 14, no. 11, pp. 1180–1185, 1961.
- [56] P. M. Huang, Y. Li, and M. E. Sumner, *Handbook of Soil Sciences: Properties and Processes, Second Edition.* CRC Press, 2011.
- [57] M. Winterer, *Nanocrystalline Ceramics Synthesis and Structure*. Berlin, Heidelberg: Springer Berlin Heidelberg, 2002.
- [58] D. R. Askeland, The science and engineering of materials. Boston: PWS Pub., 1994.
- [59] M.-H. Education, "Dictionary of Earth Science." McGraw Hill Professional, 01-Nov-2002.
- [60] P. B. Moore and T. Araki, "Mitridatite: A Remarkable Octahedral Sheet Structure," *Mineral. Mag.*, vol. 41, no. 320, pp. 527–528, 1977.
- [61] S. R. Walker, M. B. Parsons, H. E. Jamieson, and A. Lanzirotti, "Arsenic Mineralogy of Near-Surface Tailings and Soils: Influences on Arsenic Mobility and Bioaccessibility in the Nova Scotia Gold Mining Districts," *Can. Mineral.*, vol. 47, no. 3, pp. 533–556, 2009.
- [62] R. W. Metsger, C. B. Tennant, and J. L. Rodda, "Geochemistry of the Sterling Hill Zinc Deposit, Sussex County, New Jersey," *Geol. Soc. Am. Bull.*, vol. 69, no. 6, pp. 775–788, 1958.

# Chapter 3. The Synthesis, Characterization, and Stability of Yukonite Under Oxic Conditions

The results of this thesis are presented in the form of two manuscripts that together describe the stability of the arsenate-bearing phase yukonite. An understanding of the stability of yukonite is important given indications that it may form in tailings management facilities. In this chapter, the first of two manuscript-based results chapters, stability was investigated under oxic conditions. This was accomplished by first synthesizing yukonite and then subjecting it to long-term stability tests at various pH. In the following chapter, a study will be presented that investigated the stability of yukonite with respect to CO<sub>2</sub> and anoxic conditions, both of which may be encountered in tailings management facilities and could result in dissolution of yukonite and release of arsenic.

This paper is intended for submission to the journal *Geochimica et Cosmochimica Acta*. The current citation information is as follows:

Matthew Bohan, Levente Becze, John Mahoney, and George P. Demopoulos, "The Synthesis, Characterization, and Stability of Yukonite Under Oxic Conditions," *Geochimica et Cosmochimica Acta*, to be submitted.

#### **Abstract**

Recently, processing of complex ores containing high levels of arsenic in conjunction with strengthening environmental regulations has put an increasing burden on hydrometallurgical operations to remove arsenic from processes for disposal in an environmentally stable form. At present, arsenic is removed by coprecipitation of arsenate with ferric iron by lime neutralization. As such the generated tailings are rich in gypsum raising the issue of possible formation of Ca(II)-Fe(III)-As(V) phases resembling the natural mineral yukonite that under certain conditions, may play a role in controlling arsenic pore water concentrations in arsenical waste storage facilities. In this work, an atmospheric precipitation-ageing method for the synthesis of yukonite  $(Ca_2Fe_3(AsO_4)_3(OH)_4\cdot(3+x)H_2O)$  is described along with the study of its stability under oxic conditions over a wide pH range. Under gypsum-saturation conditions, yukonite is determined to be a stable arsenic-bearing phase, with As(V) solubility of 0.6-0.9 mg·L<sup>-1</sup> at pH 7 and 0.6-2.4 mg·L<sup>-1</sup> at pH 8.

## 3.1. Introduction

Arsenic (As) is an impurity element found in many ores, including gold, copper, and uranium [1]. Hydrometallurgical processing of ore to liberate valuable metal leads to dissolved arsenic concentrations in process effluents that require treatment prior to disposal. The most common unit operation to remove arsenic from contaminated process streams is coprecipitation with iron. In this case, it may be necessary to add Fe(III) to the acidic effluent to increase the ratio Fe(III)/As(V)  $\geq$  3 before subsequent lime (CaO) neutralization causes coprecpitation of iron and arsenic [2]–[5]. The resulting solids are a mixture of phases that together are arsenic insoluble, primarily poorly-crystalline ferric arsenate (pcFA), arsenate-adsorbed ferrihydrite, and gypsum (CaSO<sub>4</sub>·2H<sub>2</sub>O) [6]–[9]. Alternatively, arsenic may be immobilized in the form of scorodite (FeAsO<sub>4</sub>·2H<sub>2</sub>O), especially in the case of arsenic-rich and iron-deficient process solutions. Precipitation of scorodite may be achieved byway of a hydrothermal process in an autoclave (T>150°C) [10] or, as developed at McGill University, under atmospheric conditions (T=80-95°C) by supersaturation-controlled precipitation via step-wise neutralization or oxidation [11]–[13].

Ultimately, the precipitates report to a tailings management facility (TMF) for storage. The solids may be reactive and there is a question if they will remain stable in the long-term. In particular, as tailings containing iron and arsenic are often accompanied by gypsum, questions of the role of Ca<sup>2+</sup> ions on arsenic retention and the possibility of the formation of Ca(II)-Fe(III)-As(V) phases have been raised. For instance, calcium ferric arsenate phases such as amorphous Ca-Fe arsenate, arseniosiderite, and yukonite have been identified in tailings at the Ketza River gold mine [14]–[16] and in gold tailings in Nova Scotia [17]–[19]. Several authors have suggested calcium ferric arsenates may be soluble and speculate their decomposition will release arsenic into the environment [15], [16], [18], [20]. Laboratory studies have been conducted to address these concerns. Jia and Demopoulos demonstrated the stabilizing effect of Ca<sup>2+</sup> ions on stability of poorly-crystalline ferric arsenate (Fe(III)/As(V) molar ratio = 2), where neutralization at 22°C with CaO resulted in 25 times lower As solubility than in the case of NaOH. After accelerated ageing for 7 weeks at 75°C, these CaO-neutralized coprecpitates transformed to yukonite [2]. A second study by Bluteau et al. found equilibration of crystalline scorodite in pH 7-9 gypsum-saturated solution at 75°C partially transformed to yukonite [21]. These simulated laboratory findings and its discovery and persistence in actual metallurgical tailings suggest yukonite may play a role in the long-term stability of ferric arsenate coprecpitates in the presence of gypsum.

Yukonite is a rare hydrated calcium iron arsenate mineral first discovered in association with mining activity near Tagish Lake in the Yukon Territory, Canada, as was first reported by Tyrrell and Graham in 1913. These authors described its chemical formula as  $(Ca_3Fe_2)_2(AsO_4)_2(OH)_6\cdot 5H_2O$ , though its composition is variable and consensus has still has not been reached on a theoretical formula [22]. A second occurrence was reported by Dunn at the Sterling Hill Mine in Ogdensburg, New Jersey, United States [23], and later Ross and Post identified a mineral specimen previously known as "asbolite" from Saalfield, Thurgen, Germany, as a third occurrence [24]. Since then, new discoveries have been reported in Redziny, Poland, by Pieczka et al. [25]; at the Ketza River mine in the Yukon Territory, Canada, by Paktunc et al. [14], [15]; at the Nalychevskie hot springs in Kamchatka, Russia, by Nishikawa et al. [26]; and in the Grotta Della Monaca cave in Sant'agata di Esaro, Italy, by Garavelli et al. [27]. Yukonite is identified by its chemical composition and a characteristic X-ray diffraction (XRD) pattern that is broad and diffuse, consistent with a poorly-crystalline material. With the exception of the

occurrence in Nalychveskie hot springs, yukonite is found in areas altered by historical mining activity, most commonly forming as a secondary phase from the oxidation of primary arsenidic and sulfidic minerals in the presence of iron and calcium in a neutral-to-alkaline environment [22], [23], [25], [27], [28].

The solubility of yukonite is not well understood. A lone study by Krause and Ettel measured As solubility of a natural yukonite sample by adjusting to pH 5 and equilibrating for 197 days. Despite a high initial release of As, the final solution equilibrated to 6.3 mg·L<sup>-1</sup> at pH 6.15 [1]. Following the discovery of yukonite in aged simulated tailings, the McGill HydroMET Group has worked to better understand yukonite and its stability. A preliminary report by Becze and Demopoulos investigated the effects of synthesis conditions on the characteristics (e.g. composition, structure, etc.) of the calcium ferric arsenate product, systematically altering initial composition of the synthesis liquor (i.e. Ca/Fe/As molar ratio) and ageing time at 95°C. Of the 9 experiments, 8 were phase identified as yukonite after 13 days, while kolfanite was produced in one instance [29]. Next, Becze et al. reported preliminary results of a yukonite solubility study [30]. Subsequently, Gomez et al. reported an extensive study on the characterization of yukonite, comparing synthetic to natural yukonite and also to arseniosiderite [31], [32].

This paper serves to fill a gap in knowledge of the stability of yukonite, including a summary of recent findings related to: (a) synthesis of yukonite; (b) characterization of synthetic yukonite and comparison to natural, (c) solubility under oxic conditions in gypsum-free and gypsum-saturated solutions. Two distinct phases identified as yukonite were synthesized and used to collect two separate solubility datasets over a range of pH; Study A spanned pH 7-9.5, while Study B pH 3-10.

# 3.2. Experimental

## 3.2.1. Synthesis procedure

Data presented in this paper was collected from experiments that explored various routes for synthesizing yukonite. The flowsheet below (Fig. 3.1.) describes the generalized procedure that will be alluded to throughout.

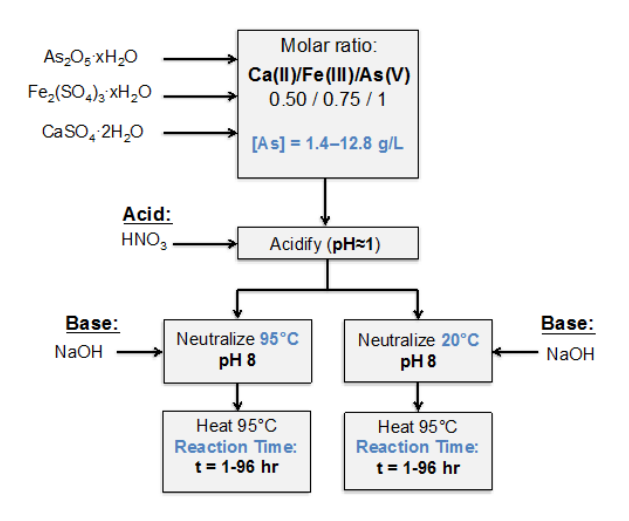


**Fig. 3.1:** Overview of general synthesis scheme. Variables in the synthesis include: initial As concentration (1.4-12.8 g·L<sup>-1</sup>), neutralization temperature (20°C vs. 95°C), and reaction (ageing) time (1-96 h) at 95°C. Material used in solubility studies: Study A (1.4 g·L<sup>-1</sup>, 95°C, 24 h), and Study B (9.0 g·L<sup>-1</sup>, 20°C, 24 h).

First, either arsenic pentoxide (As<sub>2</sub>O<sub>5</sub>·xH<sub>2</sub>O) or disodium hydrogen arsenate (Na<sub>2</sub>HAsO<sub>4</sub>·7H<sub>2</sub>O) was dissolved in ca. 600 mL reverse osmosis (RO) water in a 1 L glass volumetric flask. The solution was placed in an ultrasonic bath to aid dissolution. Once dissolved, appropriate amounts of Fe<sub>2</sub>(SO<sub>4</sub>)<sub>3</sub>·xH<sub>2</sub>O and CaSO<sub>4</sub>·2H<sub>2</sub>O were added to maintain Ca(II)/Fe(III)/As(V) ratio of 0.50/0.75/1 and the flask was diluted to 1 L with RO water before adjusting pH to 1 with nitric acid (HNO<sub>3</sub>) and stirring for 24 h. The contents were transferred to a reaction vessel and fast (15 min) neutralization to pH 8 was performed either at room temperature or elevated temperature (95°C), and subsequent ageing at elevated temperature (95°C) for a length of time (1-96 h). All phases produced using this general scheme were identified as yukonite by XRD. To make communication easier, synthetic material is described as Type 1 (neutralization at 95°C) or Type 2 (neutralization at 20°C) followed by hyphen and a number indicating the initial As(V) concentration of the synthesis liquor. For instance, Type 1-1.4 indicates yukonite synthesized from solution containing 1.4 g/L As(V) by neutralization at 95°C.

To ensure a reproducible synthetic yukonite product, in some cases an Applikon Bioreactor system was employed. The reactor consisted of a 2 L semi-batch jacketed glass reactor, with stainless steel baffles and a stainless steel 45° pitch blade impeller with 5 blades to

provide adequate mixing. Neutralization was achieved by addition of 0.85 M sodium hydroxide (NaOH), the influx rate controlled at ca. 40 mL·min<sup>-1</sup> by use of an external pump. During the neutralization process, relatively high agitation speed of 650 rpm was selected to minimize the formation of localized zones of concentrated NaOH. Upon attaining pH 8, agitation speed was reduced to 500 rpm and pH was maintained by a proportion-integral-derivative (PID) controller for the duration of ageing time. Temperature was maintained at 95±1°C by using a silicone oil bath and recirculator, which pumped hot oil through the jacketed reactor. Temperature was not controlled at 20°C in the case of low-temperature neutralization and the temperature reached approximately 28-30°C as a result of the exothermic neutralization reaction.

Alternatively, synthesis was conducted by heating an Erlenmeyer flask on a hotplate with magnetic stirring at 300 rpm. pH was manually controlled by addition of HNO<sub>3</sub> and NaOH.

#### 3.2.2. Characterization methods

For the purposes of characterization, synthetic yukonite was washed and dried at 50°C for 24 h. Washing procedures varied but followed a common method. In general, a series of repulping stages in RO water was employed, with a minimum of 3 stages. In some instances, repulping stages were iterated with washing stages, where several volumes of RO water were passed through the filtered solids (see 3.2.3. for detailed washing procedures of different types of synthetic yukonite). For phase identification, powder X-ray diffraction patterns were collected at 40 kV and 20 mA with a Cu K $\alpha_1$  source ( $\lambda = 1.506$  Å) Phillips PW1710 diffractometer equipped with a crystal graphite monochromater and scintillation detector. Patterns were measured from 2-100°C 2θ, with a 0.1° step and 3 second acquisition time. Yukonite has traditionally been identified by its characteristic powder X-ray diffraction pattern and chemical composition. Composition was determined by wet chemical digestion, where a precise amount of solid was weighed into a 50 mL polypropylene DigiTUBE and digested for 2 hours in concentrated HNO<sub>3</sub> at 95°C with the aid of a DigiPREP MS digester. Digested solutions were diluted and analyzed for As, Ca, Fe, K, Mg, Na, P, S, and Si with ICP-OES. Each digestion was performed in triplicate. As yukonite is a hydrated mineral, it was necessary to determine the crystallographic water content with a TA Instruments Q500 thermogravimetric analyzer. Particle size distributions were determined with a Horiba Laser Scattering Particle Size Distribution Analyzer LA-920 by dispersing dried samples in isopropanol with ultrasonication. A Micromeritics Tristar

3000 Surface Area Analyzer was used to determine the BET surface area. Morphology was examined with a Philips XL30 FEG scanning electron microscope after ultrasonicating in ethanol for 10 minutes.

## 3.2.3. Stability experiments

Previous experimental work has suggested the solubility of yukonite phases produced in the laboratory depends upon the conditions of synthesis [29]. In addition, procuring accurate solubility data demands material of high purity, and thus adequate washing to remove contaminating phases (e.g. gypsum), physically entrained ions from the synthesis supernatant, and minority fractions of highly soluble particles is of paramount importance. The results of solubility tests are also impacted by the parameters of the experiment, for instance: agitation conditions, pH adjustment schemes, and length of study. Thus, exact details of the preparation of material and the conditions of solubility testing are disclosed here.

Solubility data from Study A was collected from material synthesized in Erlenmeyer flasks affixed with rubber stoppers. Neutralization to pH 8 of a solution containing molar ratios of Ca(II)/Fe(III)/As(V) according to 0.50/0.75/1, where [As(V)] =  $1.4~\rm g\cdot L^{-1}$ , was performed at high-temperature (95°C). As(V) was introduced as Na<sub>2</sub>HAsO<sub>4</sub>·7H<sub>2</sub>O. pH was maintained at 8 by regular addition of HNO<sub>3</sub> and NaOH. Following ageing, the slurry was filtered with a pressure filter at 50 psi to remove the supernatant, which contained ca. 300 mg·L<sup>-1</sup> residual As. After filtering, the solids were extensively washed. Solids were repulped in 1 L of reverse osmosis water for 2 h. The filtrate was removed with a pressure filter (0.02  $\mu$ m membrane) and 3 volumes of RO wash water (1 L) were passed through the filter cake. This process was repeated 8 times, until the final wash water As concentration was below 0.05 mg·L<sup>-1</sup>. The solids (5 g, dry weight) were then equilibrated at pH 7, 8, and 9.5 in both gypsum-free and gypsum-saturated water (200 mL) with a liquid:solid ratio of 40:1. The slurries were continuously magnetically stirred and the pH was regularly adjusted by manual addition of HNO<sub>3</sub> and NaOH. Slurry samples were filtered (0.02  $\mu$ m) and the filtrates analyzed for As, Ca, Fe by ICP-OES.

In contrast, yukonite for Study B was synthesized in an Applikon reactor by room-temperature (20°C) neutralization to pH 8 of a solution containing molar ratios of Ca(II)/Fe(III)/As(V) according to 0.50/0.75/1, where  $[As(V)] = 9.0 \text{ g} \cdot \text{L}^{-1}$ . As(V) was introduced as  $As_2O_5 \cdot xH_2O$ . After neutralization, the slurry was heated to 95°C and aged for 24 hours while

pH was maintained at 8 throughout by addition of nitric acid (HNO<sub>3</sub>) and sodium hydroxide (NaOH), dispensed continuously with a pH controller. Following ageing, the slurry was filtered with a pressure filter at 50 psi (0.22 µm membrane) to remove the supernatant that contained ca. 1400 mg·L<sup>-1</sup> residual As(V). After filtering, the solids were repulped in 2 L of reverse osmosis water for  $\geq 4$  hours for a total of 6 washes, where the As concentration on the final repulp was ca. 4 mg·L<sup>-1</sup>. A final filtering was performed and 5 g (dry weight) of the filter cake was weighed into each of 12 high-density polyethylene 500 mL Nalgene® capped bottles. RO water was added (200 mL) such that the liquid:solid ratio was 40:1. The first 6 bottles, denoted "gypsumfree," were adjusted to the following pH values with HNO<sub>3</sub> and NaOH: 3, 5, 7, 8 and 10; pH 8 was a duplicate. The other six bottles, denoted "gypsum-saturated," were pH adjusted according to the same scheme, with the addition of 5 g·L<sup>-1</sup> CaSO<sub>4</sub>·2H<sub>2</sub>O. The bottles were placed on a Lab Companion SK-71 shaker table in orbital mode operating at 180 min<sup>-1</sup> to provide consistent agitation and maintain a suspension of the solids. pH was adjusted on days 1, 2, 4, and 8 and thereafter were allowed to drift to an equilibrium value for the 132 day duration of the experiment. Sampling and pH measurement was performed under magnetic stirring. Slurry samples were filtered (0.22 µm), and the filtrates were analyzed for As, Ca, Fe, S and Na with a Thermo Scientific iCAP 6000 series ICP-OES.

## 3.3. Results and Discussion

## 3.3.1. Synthesis and Characterization

## 3.3.1.1. Phase identification and structure

The synthesized yukonite was characterized using several tools as its structure (X-ray pattern) and composition are reported to vary in the case of natural mineral specimens from different occurrences. Since Jambor [23] produced X-ray data from Tyrrell and Graham's samples of the original locality (i.e. "type" yukonite), its pattern has been used as a crystallographic fingerprint to identify new occurrences that may differ somewhat in chemical composition from the original samples found at Tagish Lake. There are two diffraction data files on yukonite from the ICDD, which correspond to "type" yukonite (PDF 31-553, Fig. 3.2a.) measured by Jambor and reported by Dunn and yukonite from the same locality as measured and

reported by Ross and Post (PDF 51-1416, replacement of PDF 45-1358, **Fig. 3.2b.**). Both overlaid patterns are normalized to the 32.1° peak.

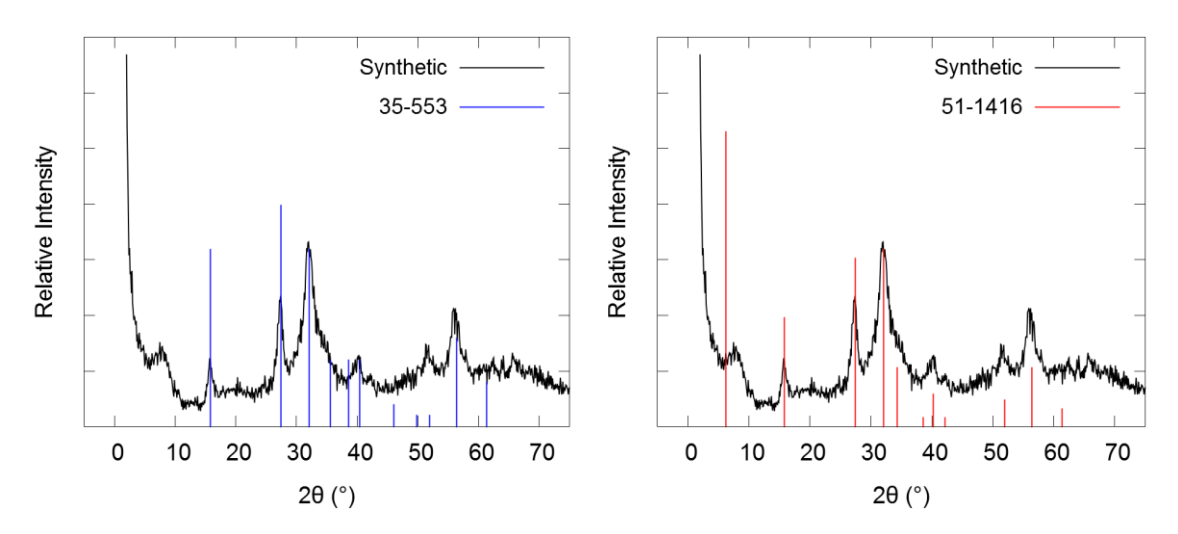


**Fig. 3.2.** ICCD diffraction data files compared with X-ray diffraction pattern obtained for synthetic yukonite. Synthesis conditions: Type 2-9.0 ([As]=9.0 g·L<sup>-1</sup>, 20°C neutralization, 24 h at 95°C ageing).

The two diffraction data files themselves show significant differences. Major peaks (e.g. ~15.8°, 27.4°, 32.1°, 56.4°) show consistency in position but differ in peak height, where the relative peak heights at 27.4° and 32.1° are reversed in the two cases. In comparison to synthetic yukonite, both are consistent in position and show variation relative to peak height. Thus, we conclude semi-quantitatively that the two patterns are in agreement with that of synthetic yukonite (produced in this work) in major peak positions and differ in peak height, a difference that is about the same magnitude as the two references from each other. Qualitatively, synthetic yukonite agrees more closely with PDF 51-1416. Visually, the diffraction pattern of synthetic yukonite closely resembles those presented by Ross and Post, which are weak and diffuse [24].

There is an exception in the case of the low-angle peak that corresponds to the [001] plane [26], [27], which in the case of PDF 51-1416 is the most intense peak and is observed at 6.26° (d-spacing 14.1 Å) and is not present in PDF 35-553. Ross and Post suggested the absence of the low-angle peak in the case of the latter was likely due to instrumental limitations. Additionally, by heating natural yukonite samples at 100°C in air, they showed that the low-angle peak shifts to higher 2θ (lower d-space) in response to mineral dehydration, with the 14.1 Å peak weakening and a new peak at 11.6 Å forming [24]. Moreover, the "asbolite" (the third occurrence of yukonite from Saalfield, Germany) sample studied had a low-angle peak at 15.7 Å,

apparently evidence of yet another hydration state. Therefore, it appears the hydration state of yukonite is dictated by the geochemical conditions under which it forms. In the case of synthetic yukonite, the low-angle peak is observed at 11.4 Å, and is broad and weak as in the case of the sample heated by Ross and Post. We interpret the position of the low-angle peak to indicate synthetic yukonite is a lower hydrate as compared to natural specimens. In fact, analysis by TGA showed that synthetic yukonite contains 14.7% crystallization water, as indicated by loss of mass by 600°C (see **Fig.A-1.** in Appendix). This was less than the 16.8-21.8% range reported of natural yukonite specimens by similar thermogravimetric analysis [26], [31], consistent with a lower hydration state.

The notion that yukonite's structure can expand and contract along its [001] plane to accommodate varying levels of crystallization water is consistent with long-held assertions [22], [24], [27] and recent findings that yukonite is structurally related to arseniosiderite (Ca<sub>2</sub>Fe<sub>3</sub>(AsO<sub>4</sub>)<sub>3</sub>O<sub>2</sub>·2H<sub>2</sub>O) [31]. While the structure of arseniosiderite remains unsolved, the structure of the presumably isomorphous mitridatite (Ca<sub>6</sub>Fe<sub>9</sub>(PO<sub>4</sub>)<sub>9</sub>O<sub>2</sub>·9H<sub>2</sub>O) suggests it is a layered sheet structure [33], [34]. In this view, a nonamer of edge-sharing iron octahedron is coordinated to corner-sharing arsenate tetrahedra in, above, and below the plane. Between these sheets, which are composed of iron and arsenic, are layers of hydrated calcium and molecular water. As pointed out by several [24], [31], yukonite shares nearly identical Bragg angles with arseniosiderite with the exception of the low-angle peak. In the case of arseniosiderite, the lowangle peak occurs at 8.8 Å, where the smaller d-spacing is consistent with less crystallographic water observed than in the case of yukonite (As: $\Sigma [O^2, OH^-, H_2O] \sim 1$ , As: $\Sigma [O^2, OH^-, H_2O] \sim 3$ , respectively). Also in contrast to arseniosiderite, which has sharp, well-defined peaks, yukonite's diffraction pattern has weak and diffuse peaks indicative of a material that is either highly disordered, composed of small crystallites, or both [27]. Therefore, the structure of yukonite is understood to consist of nano-sized domains of disordered arseniosiderite-like crystals, where arseniosiderite itself is microcrystalline. Its lack of long-range order in comparison to arseniosiderite is apparently a result of weaker hydrogen-bonding networks, where its greater water content is not confined to discrete crystallographic sites and is weakly held [31]. In Fig. 3.3., scanning electron micrographs of synthetic yukonite reveal micron-sized particles that are aggregates of small crystallites.

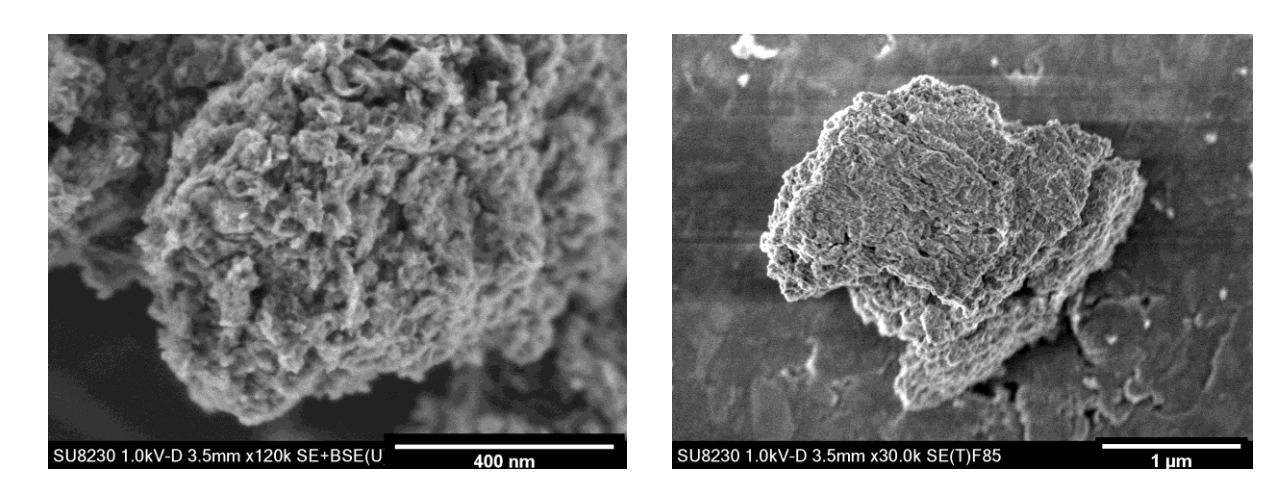


**Fig. 3.3.** Scanning electron micrographs of synthetic yukonite. Synthesis conditions: Type 2-9.0 ([As]=9.0 g·L<sup>-1</sup>, 20°C neutralization, 24 h at 95°C ageing).

## 3.3.1.2. Synthesis Reactions

The synthesis flowchart was presented in **Fig. 3.1.** Formation of yukonite proceeds in two steps: (1) precipitation ferric arsenate (amorphous or crystalline depending on the applied temperature) at low pH, followed by (2) phase transformation to yukonite after high-temperature ageing at high pH.

$$Fe_{(aq)}^{3+} + (AsO_4)_{(aq)}^{3-} + 2H_2O \xrightarrow{fast} FeAsO_4 \cdot 2H_2O_{(s)}$$
 (3.1)

$$3FeAsO_{4} \cdot 2H_{2}O_{(s)} + 2Ca_{(aq)}^{2+} + H_{2}O$$

$$\xrightarrow{95^{\circ}C,pH \ 8,time} Ca_{2}Fe_{3}(AsO_{4})_{3}(OH)_{4} \cdot 3H_{2}O_{(s)} + 4H_{(aq)}^{+}$$
(3.2)

This is evident by observing XRD patterns of solids recovered from slurry samples taken throughout the ageing process at 1 h and 24 h (**Fig. 3.4.**). At 1 h, the diffractogram shows a double-hump feature with local maxima at ~28° and ~58° 20 (these angles indicated by black dotted lines), which is characteristic of poorly-crystalline ferric arsenate, when equilibrated at pH 8 [35], [36]. The tips of small peaks (e.g. 15.6°, 28.4°, 31.4°, denoted with "Y") possibly suggest the phase transformation to yukonite, which is complete by 24 h, and was observed qualitatively by noticing a gradual colour change from milky white to reddish-brown of the synthesis liquor from 4-12 h. It is unclear on a mechanistic level exactly how the transformation occurs; however,

it is assumed that a highly disordered amorphous phase is precipitated that, over time, develops ordered nanodomains characteristic of yukonite.

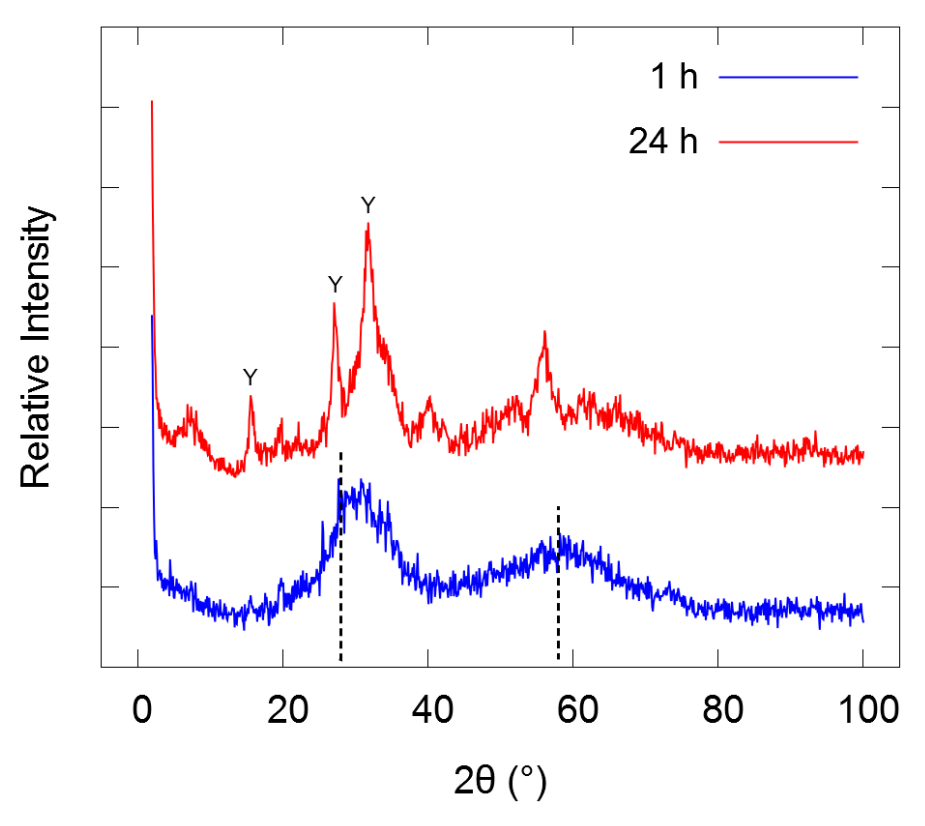


**Fig. 3.4.** Structural evolution of synthetic yukonite. Synthesis conditions: Type 1-9.0 ([As]=9.0 g·L<sup>-1</sup>, 95°C neutralization, 1 h (top) and 24 h (bottom) at 95°C ageing).

## 3.3.1.3. Effect of ageing time

Ageing at high temperature (95°C) after neutralization to pH 8 is necessary to accelerate the kinetics of transformation to yukonite, in which an amorphous phase rearranges into the more ordered yukonite structure. It is likely this reaction will also take place at room temperature but over a longer period of time (i.e. years). The trend illustrated in **Fig. 3.5a.** suggests there is an increase in crystallite size with ageing time. Given the lack of crystallographic information and apparently disordered nature of yukonite, quantification of this effect is difficult as it is unclear whether the effect is due to greater crystallite size or greater crystallinity (i.e. percentage of crystalline material). However, observed increase in peak height and decrease in the full-width-at-half-maximum (FWHM) is taken as a qualitative indication of either greater structural order or

increased crystallite size. The relationship between crystallite size and X-ray line width is defined by the Scherrer equation [37, p. 19], [38]:

$$\tau = \frac{K\lambda}{\beta \cos\theta} \tag{3.3}$$

where  $\tau$  is the mean size of crystalline domains,  $\lambda$  is the X-ray wavelength,  $\beta$  is the line broadening at FWHM (accounting for instrumental broadening), and  $\theta$  is the Bragg angle (e.g. 31.8°). Therefore, a smaller FWHM results in a larger crystallite size. According to diffractograms of samples at 24 h, 48 h, and 72 h displaying FWHM of .984°, 0.492°, and 0.492°, a decrease in FWHM with increasing ageing time suggests particle size has increased. Not surprisingly, there is a concomitant increase in peak height as shown in **Fig. 3.5b.**, a magnified section of the area of **Fig. 3.5a.**, which also reveals the peaks are the result of multiple overlapping reflections. More generally, we infer that the crystalline quality of the samples increases with ageing time. This effect was previously reported [31] and is recreated here separately. Overall, the effect is minor and for this reason our solubility studies are conducted with material synthesized after 24 h out of practicality.

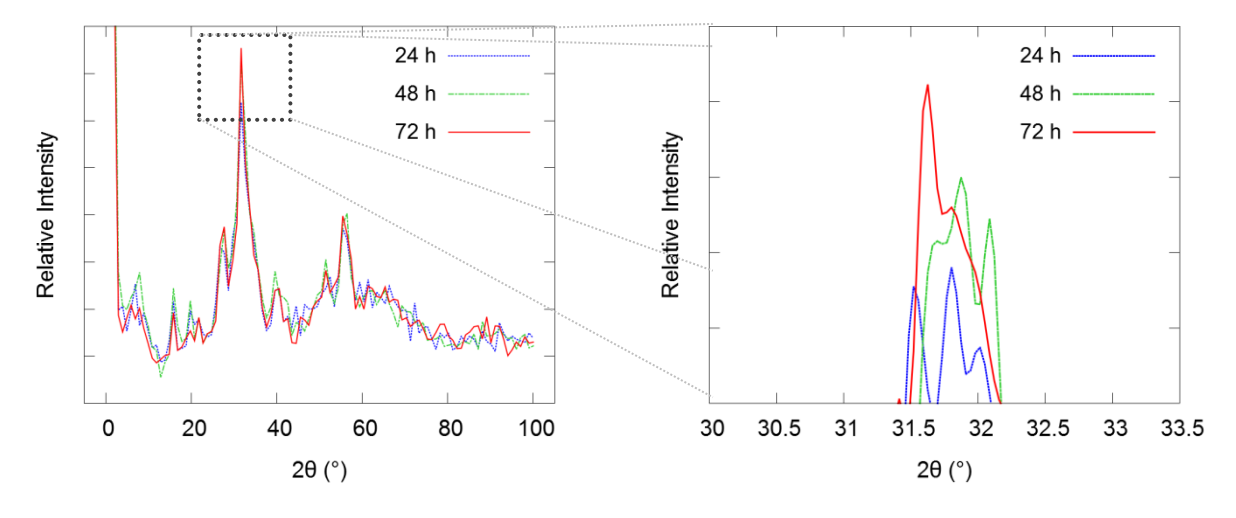


**Fig. 3.5.** (a) Overlay of XRD diffractograms taken at 24 h, 48 h, and 72 h, which show increasing peak height and decreasing FWHM suggesting greater "crystal quality" as a result of longer ageing. (b) A magnification of the dotted area of XRD pattern in (a) showing increased peak height with ageing time.

## 3.3.1.4. Effect of neutralization temperature

Of all synthesis variables tested, neutralization temperature (i.e. 20°C vs. 95°C) had the greatest effect on the synthesis product. The first synthesis method of yukonite neutralized at 95°C; however, ambient temperature neutralization is of interest as it is more representative of industrial tailings preparation and disposal conditions. The first indication of an effect was by visual observation of colour during synthesis (Type 2-9.0: [As]=9.0 g·L<sup>-1</sup>, 20°C neutralization, 24 h at 95°C ageing). In both cases, the slurries prior to neutralization and the final slurries at 24 h were the same colour: milky white (due to presence of gypsum) and dark reddish-brown, respectively. This was not the case for the intermediate time after neutralization and before 24 h, where the low-temperature neutralized slurry first turned light-brown during neutralization (~pH 2) before eventually turning reddish-brown after sufficient ageing, while the high-temperature neutralized slurry first turned a creamy pink. After filtering the synthesis product from the 24 h slurry, it is invariably dark reddish-brown in colour and has a gel-like consistency. Upon drying, it forms brittle aggregates where its dry mass is only ca. 20% of its wet mass after filtration.

The dried material was considerably different in appearance between the two samples of different neutralization temperature. In the case of high-temperature neutralization, "Type 1", the material formed loose aggregates that easily crumbled apart and was yellow-brown in colour. In contrast, low-temperature neutralized material, "Type 2", formed compact, solid aggregates that were dark brown or nearly black in colour. Interestingly, the initial description of type yukonite by Tyrell and Graham described yukonite [22] as "nearly black in colour with a brownish tinge, [occurring] as irregular concretionary masses embedded in a pale yellowish brown earthy material resembling ochre". These authors did not quantitatively analyze the yellow orchreous material but noted it had the same constituents as the dark brown yukonite. Like Tyrrell and Graham, we also observed the coexistence of yellowish and dark brown material in a single sample. A separate synthesis experiment (Type 1-9.0: [As]=9.0 g·L<sup>-1</sup>, 95°C neutralization, 24 h at 95°C ageing) looked at the effect of washing on the synthetic solids. In this case, the dried solids were initially soft and yellow-brown. Over the course of 8 washes (in 1 L reserve osmosis water), the material developed a hard, crazed, dark-brown surface, with the ratio of dark-brown material to yellow-brown material increasing with each consecutive wash and dry cycle. Meanwhile, the composition of both coloured material was found to be nearly identical.

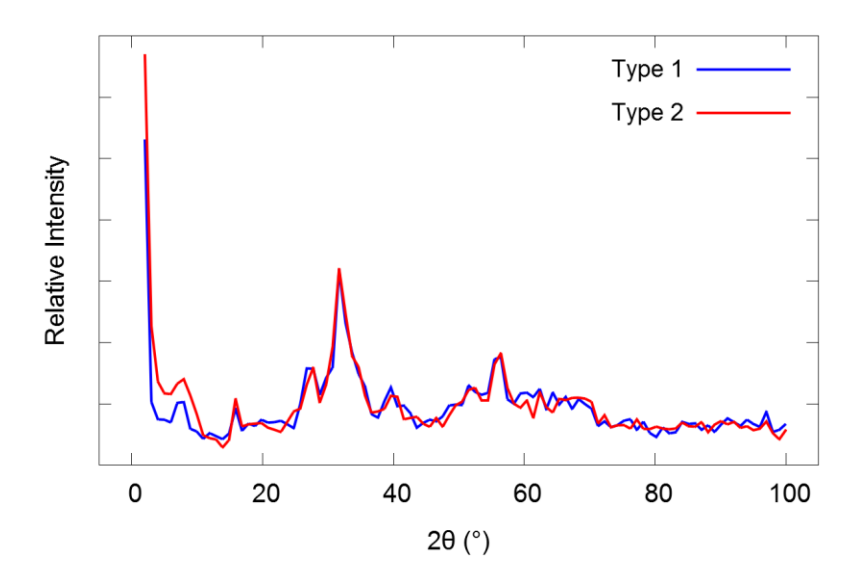


**Fig. 3.6.** Comparison of XRD diffractograms of Type 1 (neutralization T=95°C) and Type 2 (neutralization T=20°C) yukonite (with smoothing).

XRD patterns of Type 1 and Type 2 materials (Fig. 3.6.) showed both phases to be yukonite, with the only discernible difference being the greater intensity of the low-angle peak in the case of Type 2 that, according to the preceding discussion in 3.3.1.1., suggests perhaps a greater order of the planes of crystallization water. In terms of chemical composition, a slight variation (**Table 1**, see 3.3.1.5) was identified; however, considering the wide range in variability of composition of yukonite, Type 1 and Type 2 yukonite have very similar compositions (more on this in 3.3.1.5.). Therefore, it appears on a molecular level the structure of both is quite similar. On a macroscopic level, particle size analysis revealed a significant difference in the particle size distributions (Fig. 3.7.). Type 1, corresponding to the loosely bound yellow-brown material, had an average particle size at 64 µm, while the more compact Type 2 had an average particle size of 103 µm. Mean particle size of Type 1 was skewed lower as a result of a bimodal size distribution, with a large fraction of nanoscale particles. As these are aggregates, the absolute particle size depends upon any actions taken to disperse the aggregates. In this case, particle size analysis was performed with samples that had been dried and were dispersed in isopropanol with the aid of ultrasonification for approximately 1 min. As a result, it is unclear if this method is indicative of the absolute particle size distribution of non-dried yukonite, but it is assumed the relative trend is accurate. This trend was corroborated by measurements of BET surface area, which revealed Type 1 and Type 2 to have surface areas of 40.1 and 5.6 m<sup>2</sup>·g<sup>-1</sup>, respectively.

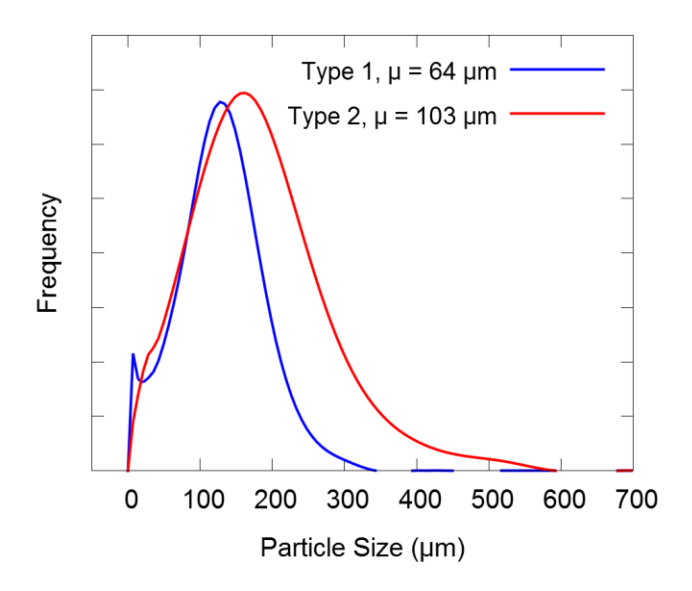


**Fig. 3.7.** Particle size distributions of Type 1 and Type 2 yukonite.

Therefore, we conclude the variation in colour of the materials observed by Tyrrell and Graham in their seminal study of yukonite was a result of different particle size. This is further evidenced by natural yukonite possessing a yellow-brown streak [22], an indication of colour of particles that have been mechanically reduced in size. We conclude smaller aggregates of yukonite appear lighter in colour (yellow-brown) and darker to almost black with increasing particle size.

It is unclear how neutralization temperature changes the reaction mechanism. It is possible that high-temperature neutralization initially favors a crystalline kinetic product at low pH (e.g. scorodite) that must undergo dissolution before forming yukonite, with the result that yukonite crystallite growth is limited. In contrast, the low-temperature neutralized slurry remains amorphous (e.g. poorly-crystalline ferric arsenate) and larger yukonite crystallites are formed at a higher kinetic rate. This is based on results of the previously reported preliminary study that found yukonite formed under many conditions after passing through a scorodite intermediate [29]. In fact, the idea of neutralizing at high temperature came from a previous study that showed high-temperature neutralization of coprecipitates increased the kinetic conversion to scorodite [39].

Another more general explanation considers equilibrium effects. As demonstrated empirically in a previous report, change in the molar ratio of Ca/Fe/As in the initial solution affected the properties of the precipitate. This result is understood theoretically as altering the

distribution coefficient, D, a constant that describes the relationship between the relative proportions of ions (i.e. Ca, Fe, As) between the solution and the precipitate. A simple case of the partition of a primary substance, P, in the presence of an impurity, I, is described by the following equation [40, p. 750]:

$$\frac{I}{P_{ppt.}} = D \frac{I}{P_{soln.}} \tag{3.4}$$

Thus, the ratio of Ca/Fe/As in solution will alter the chemistry of the precipitate, and this explains the results of our experimental study. Temperature alters this equilibrium by changing the distribution constant. For instance, in the case of barium-radium chromates, *D* varies from 8.9 at 0°C to 5.3 at 100°C [40, p. 750]. In contrast to a continuous stirred-tank reactor that maintains constant supersaturation and tends to form uniform particles, the batch process used here inherently forms particles with a composition gradient, a result of the evolution of the supernatant composition during precipitation. Thus, two particles of the same bulk composition may differ in composition at the surface. In this light, it is easy to see why differential temperature during neutralization influences the properties of synthetic yukonite.

## 3.3.1.5. Chemical Composition

The chemical composition of natural yukonite has been a source of bewilderment. Reports of chemical formula have been highly variable. Without a crystallochemical formula — one derived from an understanding of crystal structure — determinations of chemical formula have relied on empirical analyses. As is the case, preparation of chemical formulae with integer stoichiometries is not possible, and the formulae are ultimately normalized in different ways, complicating comparison. To ease comparison, many authors [25]—[27] have compared Ca/Fe/As molar ratios. Analyses are complicated by the presence of impurity phases [27] and also by differing analytical techniques. More importantly, variation appears to result from the nature of yukonite itself, which was described by Garavelli et al. as a hypocrystalline material composed of disordered arseniosiderite-like nanocrystals, embedded in an amorphous matrix of varying composition. This was in agreement with our own assessment, where it was concluded that yukonite can incorporate various amounts of Ca, Fe, As, OH/H<sub>2</sub>O into its structure [31]. In order

to better visualize the variation in composition, Ca/As ratios are plotted against Fe/As ratios of all known analyses of natural yukonite (Fig. 3.8.).

Unfortunately, as other authors have acknowledged [25]–[27], minor ions can also incorporate either interstitially or by direct substitution. For instance, Nishikawa et al. found 15.9 at.% of Si in yukonite from the Nalychevskie hot springs in Russia. These authors were able to show by a strong negative correlation between Si and As that silicate ( $SiO_4^{4-}$ ) was directly substituting for tetrahedral arsenate ( $AsO_4^{3-}$ ) into the crystal structure. This datapoint corresponds to the outlying inverted pink triangle in **Fig. 3.8.**, with Ca/As = 1.05 and Fe/As = 1.46. Pieczka et al. noticed the relatively low amount of Ca in the yukonite from Sterling Hill, New Jersey, was compensated for by inclusion of other bivalent ions (e.g. Mg, Mn, Zn).

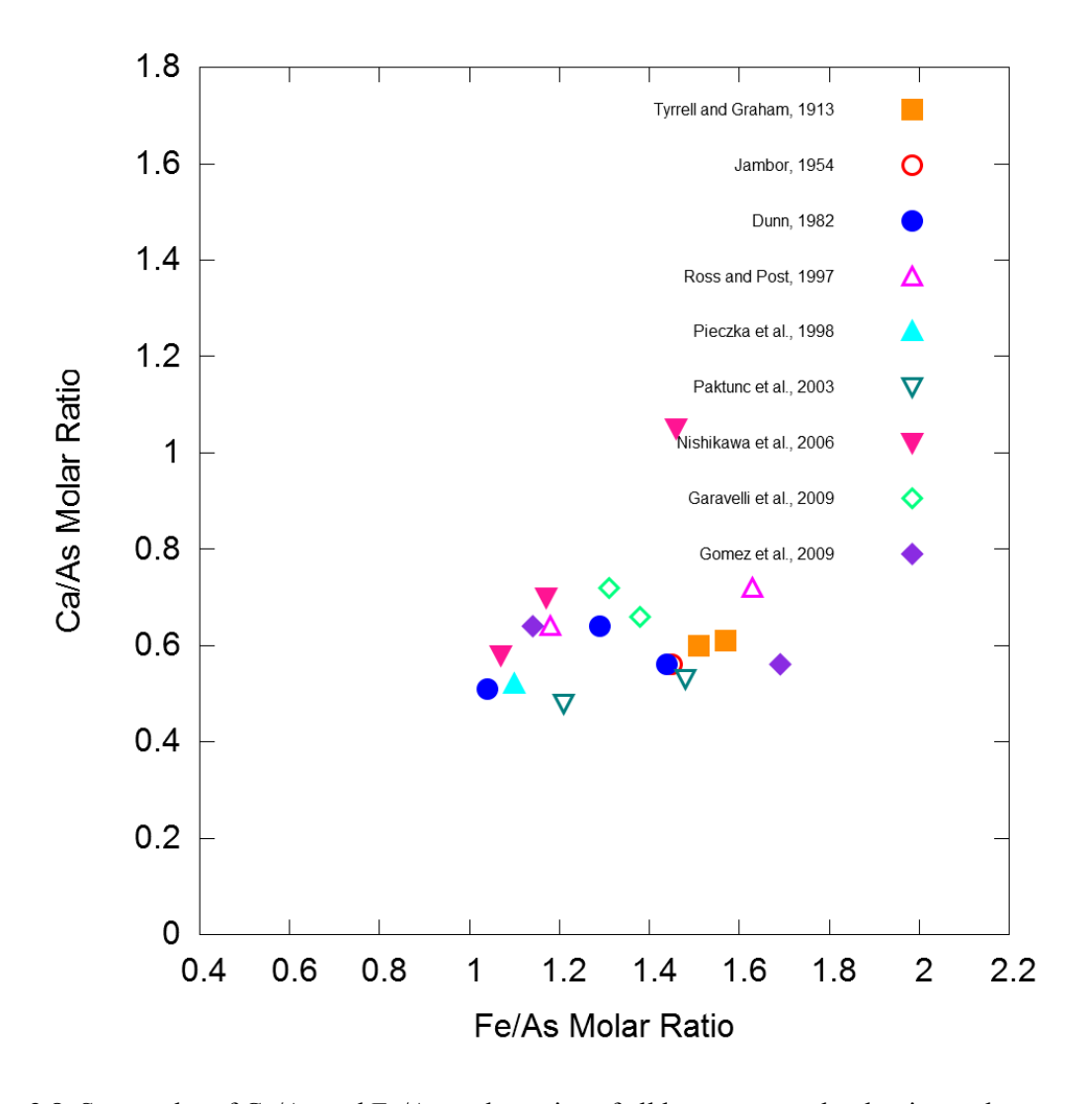


Fig. 3.8. Scatterplot of Ca/As and Fe/As molar ratios of all known natural yukonite analyses.

Table 3.1: Chemical composition of synthetic and natural yukonite samples.

$\mathbf{H_2O}$ (wt.%)	14.67	14.65	14.8	19.9
<b>Si</b> (wt.%)	0.75 ± 0.03	1.12 ± 0.11		
<b>P</b> (wt.%)	0.00 ± 0.002	0.01 ± 0.01		
<b>Mg</b> (wt.%)	0.02 ± 0.002	0.2 ± 0.007		
<b>K</b> (wt.%)	0.02 ± 0.006	0.03 ± 0.02		
Na	0.04 ±	0.23	1.06	$0.02 \pm 0.01$
(wt.%)	0.009	± 0.007	± 0.27	
S	0.15	0.06	0.03	0.03
(wt.%)	± 0.009	± 0.09	± 0.02	± 0.09
<b>Ca</b>	9.86	10.23	8.75	6.90
(wt.%)	± 0.46	± 0.52	± 0.63	± 0.12
<b>Fe</b>	22.02	21.47	26.52	29.12
(wt.%)	± 1.06	± 1.12	± 2.68	± 0.58
AsO <sub>4</sub> (wt.%)	43.91	45.32	40.04	42.79
	± 1.98	± 1.85	± 0.55	± 0.40
<b>As</b>	23.67	24.43	21.60	23.08
(wt.%)	± 1.07	± 1.00	± 0.55	± 0.40
	Type 1ª	Type 2 <sup>b</sup>	Syn. 1°	Tagish Lake <sup>d</sup>

a. Synthesis conditions: [As]=9.0 g/L, 95°C neutralization, 24 h, error reported at 95% confidence

 b. Synthesis conditions: [As]=9.0 g/L, 20°C neutralization, 24 h, error reported at 95% confidence
 c. Synthesis conditions: [As]=1.4 g/L, 95°C neutralization, 24 h, Gomez et al., "Synthetic 1", [31].
 d. National Mineral Collection of Canada, Ref. #064815. Collected 1984 from Venus Mine, Windy Arm, Tagish Lake, Yukon Territory, Canada Gomez et al., [31]. In that case, the Ca/As ratio was 0.53 and the (ΣCa,Mg, Mn, Zn)/As ratio was 0.77, with Mg, Mn, Zn making up 2.6 at.% of the sample. Unfortunately, it is unclear in this case and others what portion of these ions are substituting in place of Ca, Fe, As, and OH, and which are merely incorporated in interstitial spaces and would not affect efforts to elucidate the stoichiometry of yukonite. As a result, it is not possible to arrive at a theoretical formula for yukonite from this data.

Chemical composition, in terms of wt.% of the constituents, natural and synthetic yukonite from this study is summarized in Table 3.1. Wet chemical digestion was selected for analysis to overcome the errors caused by electron beam methods (due to sample dehydration) as described by Dunn and Ross and Post [23], [24], however the compositions previously reported (i.e. "Synthetic 1", Tagish Lake) were determined by electron microprobe. The results indicate Type 1 and Type 2 yukonite prepared in this study have the same formula within measurement error. In comparison to Tagish Lake yukonite, the synthetic yukonite has approximately the same relative amount of As, but less Fe (~7 wt.%) and more Ca (ca. 3 wt.%). Ultimately, the Ca/Fe/As ratios were 0.78/1.18/1 and 0.54/1.67/1 for Type 2 and Tagish Lake, respectively. The synthetic material from the previous stability study (i.e. Synthetic 1) was 0.75/1.65/1. The difficulty in making these comparisons is exemplified in the preceding discussion: foreign ions freely incorporate into yukonite. This phenomenon can be understood by considering Goldschmidt's Rules, which suggest qualitatively that ions of similar charge (ca.  $\pm 1$ ) and similar ionic radius (ca.  $\pm 15\%$ ) will freely substitute into a structure given net electroneutrality is maintained [41]. This leads to discrepancies between natural yukonite, which forms under complex geochemical conditions that includes many soluble ions unique to its locality, and synthetic yukonite, which is produced in relatively pristine laboratory conditions that is relatively free of foreign ions.

Interestingly, even laboratory yukonite is not impervious to foreign occupants. In fact, up to 3.66 wt.% SiO<sub>4</sub><sup>4-</sup> was found in Type 2, and 1.06 wt.% Na was found in "Synthetic 1" [31]. The source of the large incorporation of Na was both the use of Na<sub>2</sub>HAsO<sub>4</sub>·7H<sub>2</sub>O and NaOH in synthesis, while the SiO<sub>4</sub><sup>4-</sup> apparently leached from the glass reactor during the alkaline, high-temperature synthesis, as little was found in analysis of the starting materials. The quantification of SiO<sub>4</sub><sup>4-</sup> in Type 1 and Type 2 yukonites likely explains, at least in part, approximately 10 wt.% of mass not accounted for in the analysis of Synthetic 1 [31]. The chemical analyses of Type 1

and Type 2 had ca. 4 wt.% unaccounted for, which could have been another  $SiO_4^{4-}$  fraction that was not solubilised, as HF was not used in the digestions and some transparent solid material was observed after digestion. While these incorporations may sound insignificant, consider that  $3.66 \text{ wt.}\% SiO_4^{4-}$  substituted for  $AsO_4^{3-}$  changes a  $Ca/(AsO_4^{3-} + SiO_4^{4-})$  ratio from 0.75 to 0.67. With this in mind, we normalized the natural yukonite data from **Fig. 3.8.** and synthetic yukonite (Type 1 and Type 2) in an effort to account for these foreign ions using the following scheme:

$$\frac{Ca^{2+}}{AsO_4^{3-}} = \frac{\Sigma Ca^{2+}, Mg^{2+}, Mn^{2+}, Zn^{2+}}{\Sigma AsO_4^{3-}, PO_4^{3-}, SO_4^{2-}, SiO_4^{4-}}$$
(3.5)

$$\frac{Fe^{3+}}{AsO_4^{3-}} = \frac{\Sigma Fe^{3+}, Al^{3+}}{\Sigma AsO_4^{3-}, PO_4^{3-}, SO_4^{2-}, SiO_4^{4-}}$$
(3.6)

This scheme was selected as it roughly abides by Goldschmidt's Rules and at the suggestion of previous authors [25]–[27], but also because data for these ions was available for most analyses. Na<sup>+</sup> was excluded as it was not commonly analyzed in natural specimens, and note that substantially less was found in Type 1 and Type 2 as opposed to "Synthetic 1". In all, 11 analyses were selected that were considered complete. The results are plotted in **Fig. 3.9.**, where the uncorrected "raw" data is represented by solid shapes and the corrected data is represented by open shapes.

For the natural samples, the mean (std. dev.) ratios for uncorrected and corrected data are 0.68 (0.14) and 1.34 (0.21) and 0.71 (0.10) and 1.22 (0.21), respectively. The ever-so-slight convergence is not statistically significant, but it does show a trend towards lower Fe/As ratios and higher Ca/As ratios. An unexpected result of this analysis was how well the synthetic yukonite samples converged to a molar ratio that approximates the theoretical of arseniosiderite (Table 3.2). In general, this was also the case for natural specimens. This is in agreement with the observation of Garavelli et al., who noted that the (Ca + Fe)/(As+Si+P) ratio for yukonite and arseniosiderite were both 5:3 [27]. While this data treatment is speculative in nature, it is one more piece of evidence that supports the connection between yukonite and arseniosiderite. Based on the formulae proposed by Nishikawa et al. and Garavelli et al., and on the extensive characterization work complementary to this study, we interpret Ca<sub>2</sub>Fe<sub>3</sub>(AsO<sub>4</sub>)<sub>3</sub>(OH)<sub>4</sub>·(3+x)H<sub>2</sub>0

to be the theoretical formula of yukonite, at least until further evidence suggests otherwise. This formula is also consistent with our previously reported "Synthetic 2" formula [31]; however, it is at odds with some empirically determined formulae. Until a more complete understanding of its structure is determined, the true formula of yukonite will remain elusive.

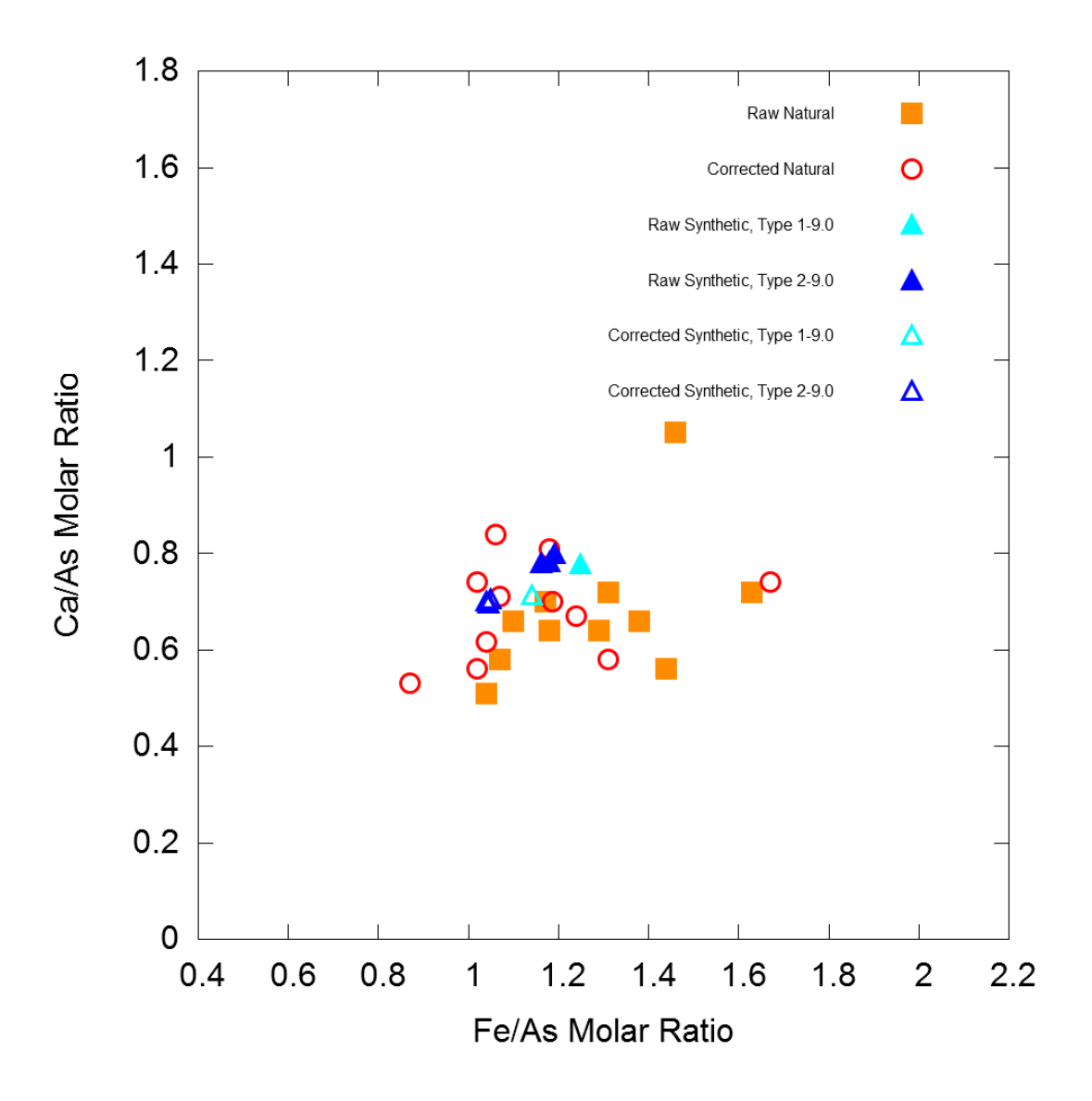


**Fig. 3.9.** Raw and corrected Ca/As and Fe/As molar ratios of select natural and synthetic yukonite analyses.

**Table 3.2:** Ca/Fe/As molar ratios of synthetic yukonite samples in comparison to the theoretical ratios of arseniosiderite, raw and corrected.

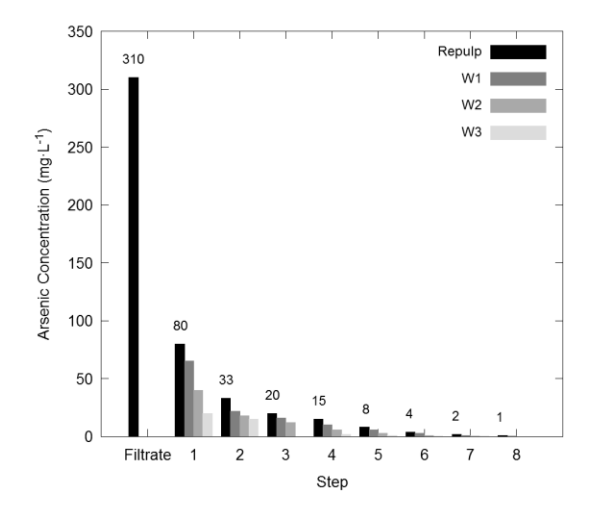
	Ca/Fe/As	Ca/Fe/As
Compound	Molar Ratio	Molar Ratio
	(raw)	(corrected)
Arseniosiderite	0.67/1.00/1	0.67/1.00/1
Type 1	0.78/1.25/1	0.71/1.14/1
Type 2 (a)	0.78/1.18/1	0.69/1.04/1
Type 2 (b)	0.78/1.16/1	0.70/1.05/1
Type 2 (c)	0.80/1.19/1	0.70/1.04/1

#### 3.3.2. Stability

As part of this work, two separate solubility studies were conducted on different synthetic yukonite compounds. In Study A, "Synthetic 1" yukonite was studied at pH 7, 8, 9.5. In Study B, "Type 2" yukonite was studied at pH 3, 5, 7, 8, 10.

#### 3.3.2.1. Pre-treatment of synthetic yukonite

Pre-treatment of the synthetic material was a critical step prior to performing the solubility studies in order to remove any impurity phases. In this case, leftover gypsum  $(CaSO_4 \cdot 2H_2O)$  was a concern, which was selectively solubilized by successive washings in RO water. These water washings also served to remove ions left over in the synthesis liquor, which is



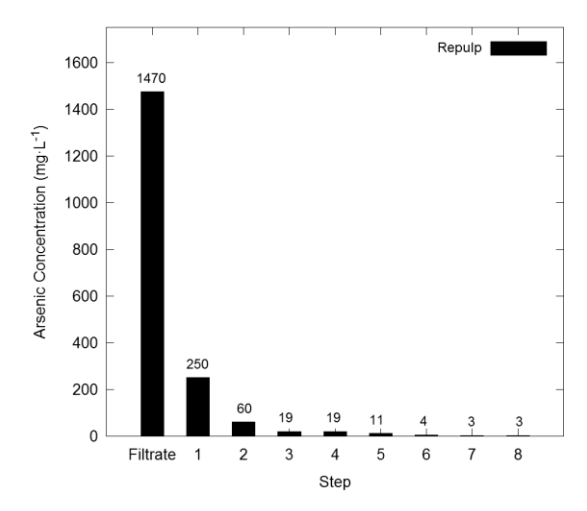


**Fig. 3.10.** Washing procedures for (a) Study A and (b) Study B show As concentration after each step. Solid black bars indicate As in filtrate in mg·L<sup>-1</sup> after repulp. Gray bars (Study A only) indicate As concentration in wash water.

strongly retained by wet yukonite, of which ca. 80% of the mass is water. Finally, washing served to remove minority fractions of highly-soluble material that would not be indicative of true solubility [42].

The results of yukonite pre-treatment for Study A and Study B are shown in **Fig. 10.**, which shows As concentrations after repulping and washing steps. In Study A, the synthesis slurry was filtered, its filtrate containing 310 mg/L As. Each "repulp" (i.e. slurry agitation) of the solids in 1 L of pH 8 (NaOH adjusted) water followed by 3 consecutive volumes of water washes showed a similar trend of high arsenic release after the repulp step with decreasing As release with each wash. In the end, the final repulp contained 1 mg·L<sup>-1</sup> of As and the final wash 0.05 mg·L<sup>-1</sup> As. In contrast, pre-treatment of Study B yukonite was conducted with only repulping in 2 L of reverse osmosis water with no washings. In this case, the supernatant contained 1474 mg·L<sup>-1</sup> excess As. Each repulp showed a decrease in As, with ca. 4 mg·L<sup>-1</sup> As present after 6 stages (8 stages are shown). In both cases, the filtration rate was initially high for the first stage, but for the latter stages was especially slow, taking up to 12 h to complete (ca. 150 mL·h<sup>-1</sup>).

#### 3.3.2.2. *Solubility*

**Table 3.3:** Solubility data for synthetic yukonite under oxic conditions in gypsum-free solution.

Study A	pН			7	7	8	9.5
"Type 1-1.4"	Days			458	458	456	455
	pH (final)			6.91	6.94	7.84	9.17
	As $(mg \cdot L^{-1})$			10.31	11.9	57.2	304
	$Ca (mg \cdot L^{-1})$			0.7	1.6	0.03	0.03
	Fe $(mg \cdot L^{-1})$			n.d.	n.d.	n.d.	0.7
Study B	рН	3	5	7	8	8	10
((T) 0 0 0)							
"Type 2-9.0"	Days	132	132	132	132	132	132
"Type 2-9.0"	Days pH (final)	132 3.37	132 5.45	132 7.23	132 7.63	132 7.56	132 9.66
"1 ype 2-9.0"	•						
"Type 2-9.0"	pH (final)	3.37	5.45	7.23	7.63	7.56	9.66

**Table 3.4:** Solubility data for synthetic yukonite under oxic conditions in gypsum-saturated solution.

Study A-g	pН			7	7	8	9.5
"Type 1-1.4"	Days			490	490	490	490
	pH (final)			7.10	7.20	8.10	9.30
	As $(mg \cdot L^{-1})$			0.9	0.8	2.4	6.2
	$Ca (mg \cdot L^{-1})$			597	588	586	424
	Fe $(mg \cdot L^{-1})$			n.d.	n.d.	n.d.	n.d.
	$S (mg \cdot L^{-1})*$			734	763	887	1014
Study B-g	pН	3	5	7	8	8	10
"Type 2-9.0"	Days	132	132	132	132	132	132
	pH (final)	3.27	5.33	7.02	7.52	7.59	8.84
	As $(mg \cdot L^{-1})$	51.6	3.5	0.6	0.7	0.6	2.2
	$Ca (mg \cdot L^{-1})$	1051	662	600	574	566	540
	Fe (mg·L <sup>-1</sup> )	n.d.	n.d.	n.d.	n.d.	n.d.	n.d.

 $S (mg \cdot L^{-1})$ 

The detailed equilibrium solubility data for yukonite in oxic conditions from both studies are presented in **Table 3.3** and **Table 3.4**. The results of Study A plotted in **Fig. 3.11a.** show the amount of arsenic release, where each of four curves plotted on a logarithmic scale. The curves each represent an individual yukonite sample equilibrated at a particular pH and show measurements of As solubility over 455-458 days at pH 7, 8, 9.5. A duplicate was performed for pH 7. Each curve exhibits similar behavior, with an early increase in As over the first 100 days followed by constant measurements for the duration of the study, evidence that equilibrium with respect to As has been attained. Equilibrium As concentrations increase by about 5 times for each unit increase in pH. The pH was monitored over the course of the experiment (**Fig. 3.11b.**). After each measurement, pH was adjusted with NaOH and HNO3 if necessary to maintain the intended value. Long periods without adjustment showed both the tendency for pH to decrease (ca. days 200-300 days) and increase (ca. days 300-450). A decrease in pH could be attributed to evidence of proton-generating hydrolysis reactions. The two samples at pH 7 were in strong agreement, providing confidence in the reproducibility of the experiment.

<sup>\*</sup>Values considered only approximate

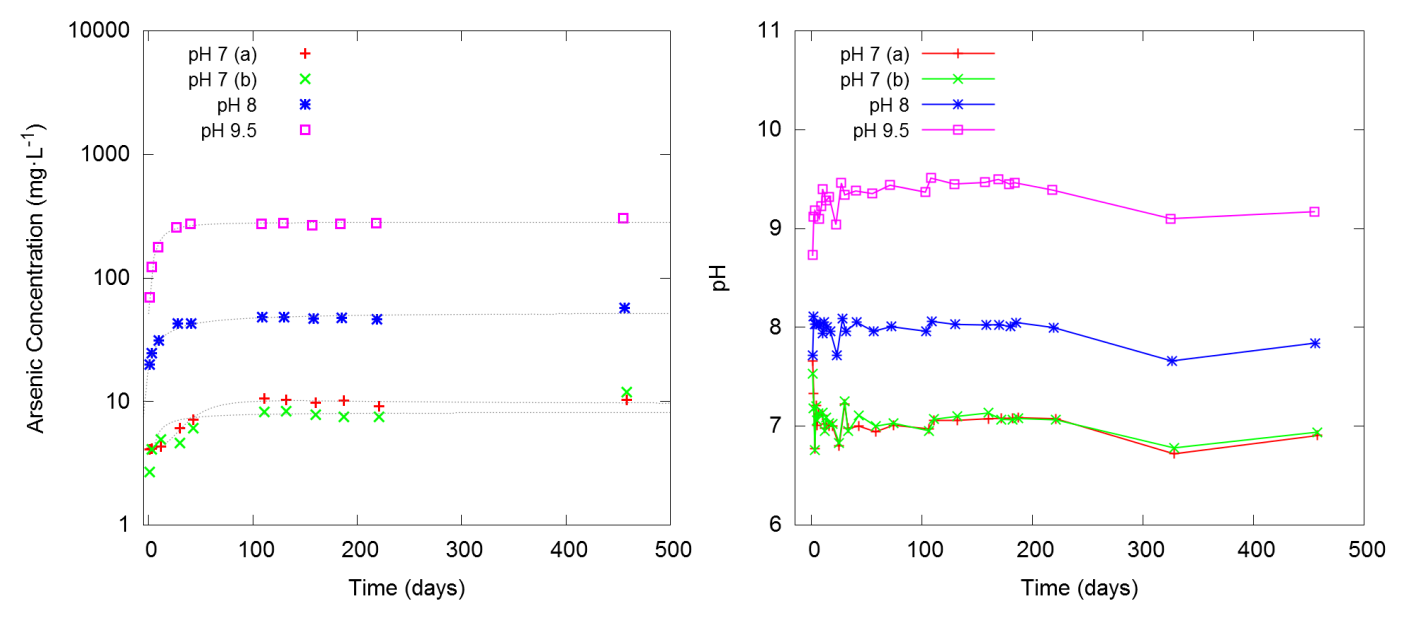


**Fig. 3.11.** Results of Study A ("Synthetic 1"). (a) Arsenic solubility measurements over time of samples at various pH. (b) pH measurements over time.

Similarly, the results of Study B are shown in Fig. 3.12. Like Study A, Study B generally follows a similar behavior of increasing As during the first ~50 days followed by near constant readings for the duration. However, the increase happened much more rapidly in the case of Study B, which is attributed to more aggressive agitation. In addition, the readings after the initial increase were not nearly as constant as in the case of the former. This is justified by the (1) shorter equilibration time and (2) lack of pH adjustment. In contrast to Study A, Study B was not pH adjusted throughout but only on days 1, 2, 4, 8, and was left to drift (Fig. 3.12b.). As a result, As concentrations drift in response to changing pH. In all cases, pH drifted toward circumneutral.

An interesting exception to this trend is the two pH 8 samples, which show the inverse behavior: high initial As followed by a gradual decrease to a stable equilibrium value after ~50 days. This was the result of accidental over-adjustment to pH higher than 8, which in turn had to be acidified with HNO<sub>3</sub>. This occurred in both samples due after selecting NaOH that was too concentrated for the OH sensitive area close to circumneutral pH. The two samples initially diverged due to different magnitude of adjustment error but converged after ~50 days with final equilibrium measurements of 7.3 and 7.5 mg/L As, respectively. A silver lining to this

experimental error was the demonstration that synthetic yukonite can approach equilibrium from both directions: ion-activity products higher and lower than the solubility product.

Overall, Study B confirmed the trend of Study A whereby As concentrations increase in response to increasing pH for pH  $\geq$  7. Additionally, it was shown than for pH  $\leq$  7, As concentrations increase in response to decreasing pH. Therefore, yukonite experiences a solubility minimum at pH  $\sim$  7. This trend is visualized in **Fig. 3.13.**, where equilibrium As

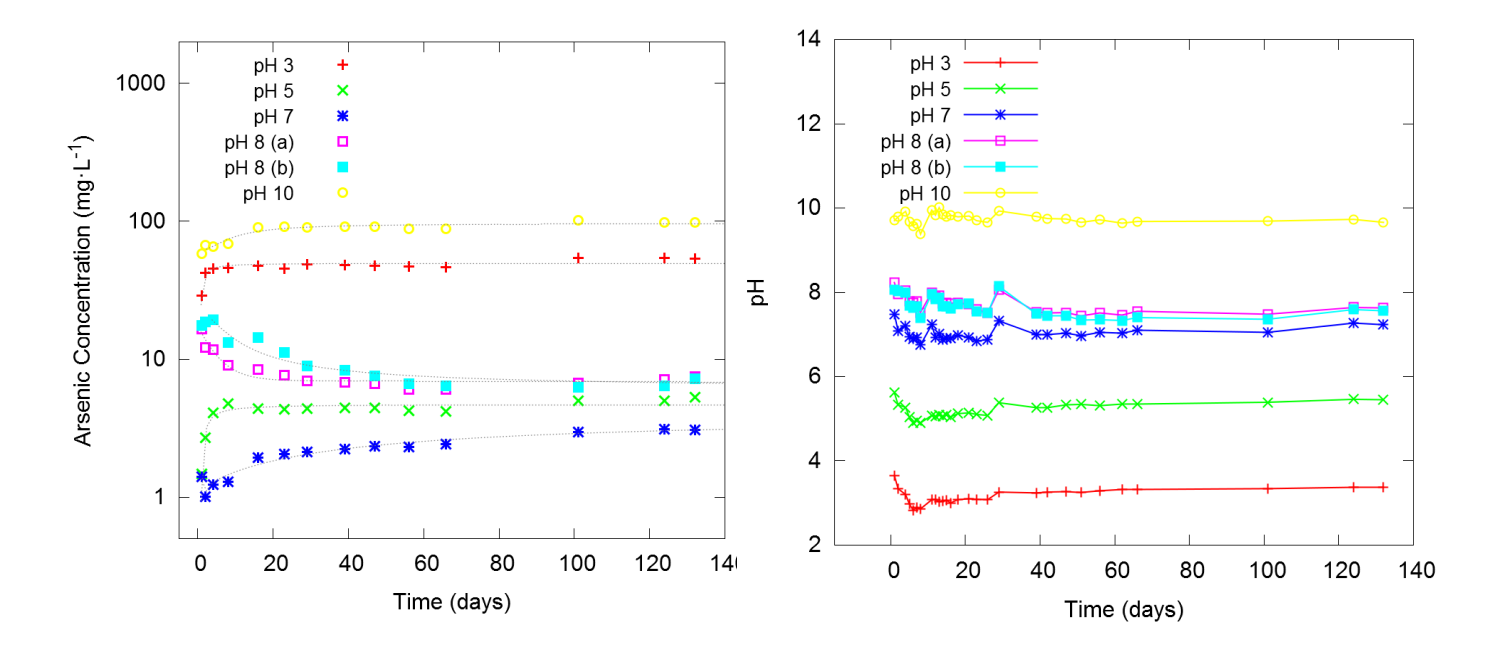


**Fig. 3.12.** Results of Study B ("Type 2"). (a) Arsenic solubility measurements over time of samples at various pH. (b) pH measurements over time.

concentrations are plotted for Study A and Study B. Also plotted is the only known solubility datapoint of natural yukonite sample, of unknown purity, reported by Krause and Ettel, where [As] = 6.3 mg/L at pH 6.15 after 197 days equilibration [1]. Interestingly, the data from Krause and Ettel is remarkably consistent with findings by Nishikawa et al., who found yukonite at the bank of a thermal pool at Nalychevskie hot springs. Chemical analysis revealed the pH 6.3 thermal pool contained 6.4 mg/L As. While the thermal waters were 64°C [26], this is favorable to the view that arsenic can control arsenic pore water concentrations. Moreover, all of the data collected shows consistency.

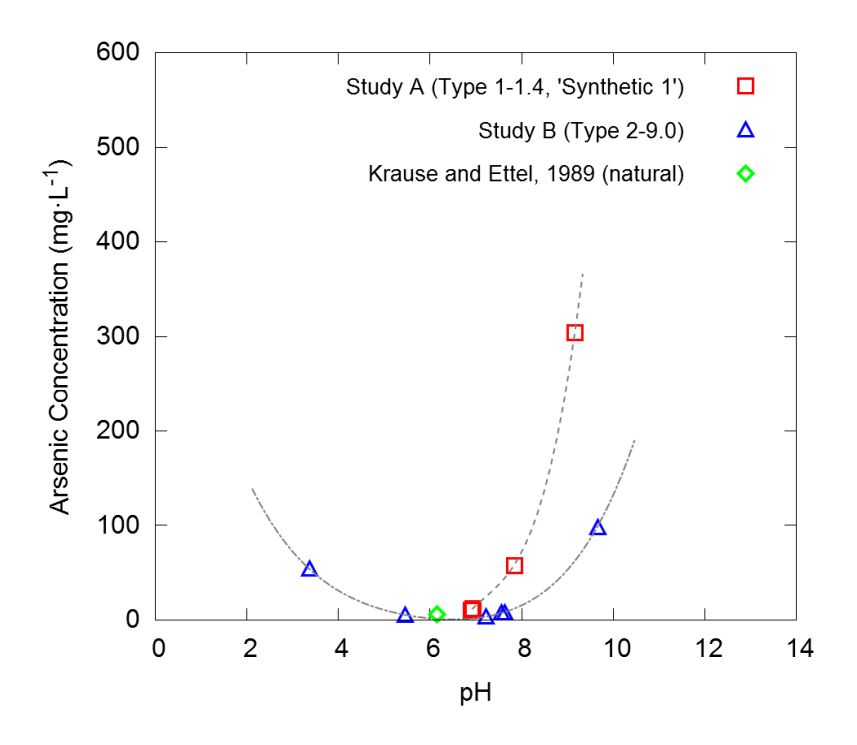


**Fig. 3.13.** Plot of equilibrium As concentrations for Study A and Study B in gypsum-free solution (see Table 3.3.) and natural sample yukonite sample equilibrated for 197 days.

Observation of the same trend in solubility of the two studies raised questions of what caused the discrepancy in absolute values, which led to further characterization (as described in 3.3.1.4.). Change in solubility as a function of particle size is a well-known phenomenon. For instance, it is known in the case of fully crystalline material that solubility varies as a function of crystallite size according to the Gibbs-Thomson equation:

$$C_{eq} = C_{\infty} exp \left[ \frac{2\gamma V_m}{rRT} \right]$$
 (3.7)

where  $C_{eq}$  is solubility of crystalline particles,  $C_{inf}$  is solubility of an infinite size,  $\gamma$  is surface energy,  $V_m$  is molar volume of the crystal, and r is radius of the particle (m) [38]. Thus, increasing crystallite radius decreases the exponential term and results in lower solubility. It is important to stress the difference between particle size and crystallite size. It has been suggested that the crystallite size of yukonite is on the order of 1-15 nm [31], with micron-sized particles forming due to aggregation. While yukonite is not a fully crystalline material, the difference in particle size between Type 1-9.0 and Type 2-9.0 raises the question of possible effects in solubility. A simple solubility experiment was conducted by adjusting samples of Type 1 and

Type 2 yukonite at pH 8 and pH 10 over 157 total days with agitation on a shaker table (60 min<sup>-1</sup>). The results are reported in **Table 3.5.** 

**Table 3.5**. Effect of synthesis conditions on material properties and solubility.

<b>Material Properties</b>	Type 1-9.0	Type 2-9.0	Type 1-1.4
[As] <sub>initial</sub> (g·L <sup>-1</sup> )	9.0	9.0	1.4
$T_{neutralization}$ (°C)	95	20	95
Mean Particle Diameter (µm)	64	103	-
BET Surface Area (m <sup>2</sup> ·g <sup>-1</sup> )	40.1	5.6	-
Solubility			
Time (days)	157	157	158
As Solubility, pH 8 (mg·L <sup>-1</sup> )	39.0	16.6	46.9
As Solubility, pH ca. 10 (mg·L <sup>-1</sup> )	240	129	267

As expected, the smaller particle size and larger BET surface area of Type 1 yukonite resulted in patently higher As solubility than Type 2. At both pH 8 and pH 10, Type 2 solubility was approximately 50% of Type 1. In comparing Type 1-1.4 (which were both neutralized at 95°C), the solubilities were within ca. 10-20%. While not strictly comparable due to differing synthesis conditions (i.e. [As]<sub>initial</sub> = 1.4 g/L) and also by the different methods of solubility testing, this points toward the different absolute solubility between Study A and Study B to be a result of particle size.

## 3.3.2.3. Effect of gypsum-saturation

The solubility of a phase is influenced by the presence of other phases. Sulfate-rich lime neutralized effluents common to the metallurgical industry tend to precipitate  $CaSO_4 \cdot 2H_2O$  (solubility 2 g/L), therefore, the question of the effect of gypsum-saturated solution on yukonite solubility is especially relevant. This is especially true due to the sharing of a common ion, Ca.

To study this effect, experiments were conducted in parallel to Study A and Study B (*from 3.3.2.2.*) with the same method but with an addition of gypsum (5 g/L) to ensure adequate saturation throughout the experiment. These experiments are denoted Study A-g

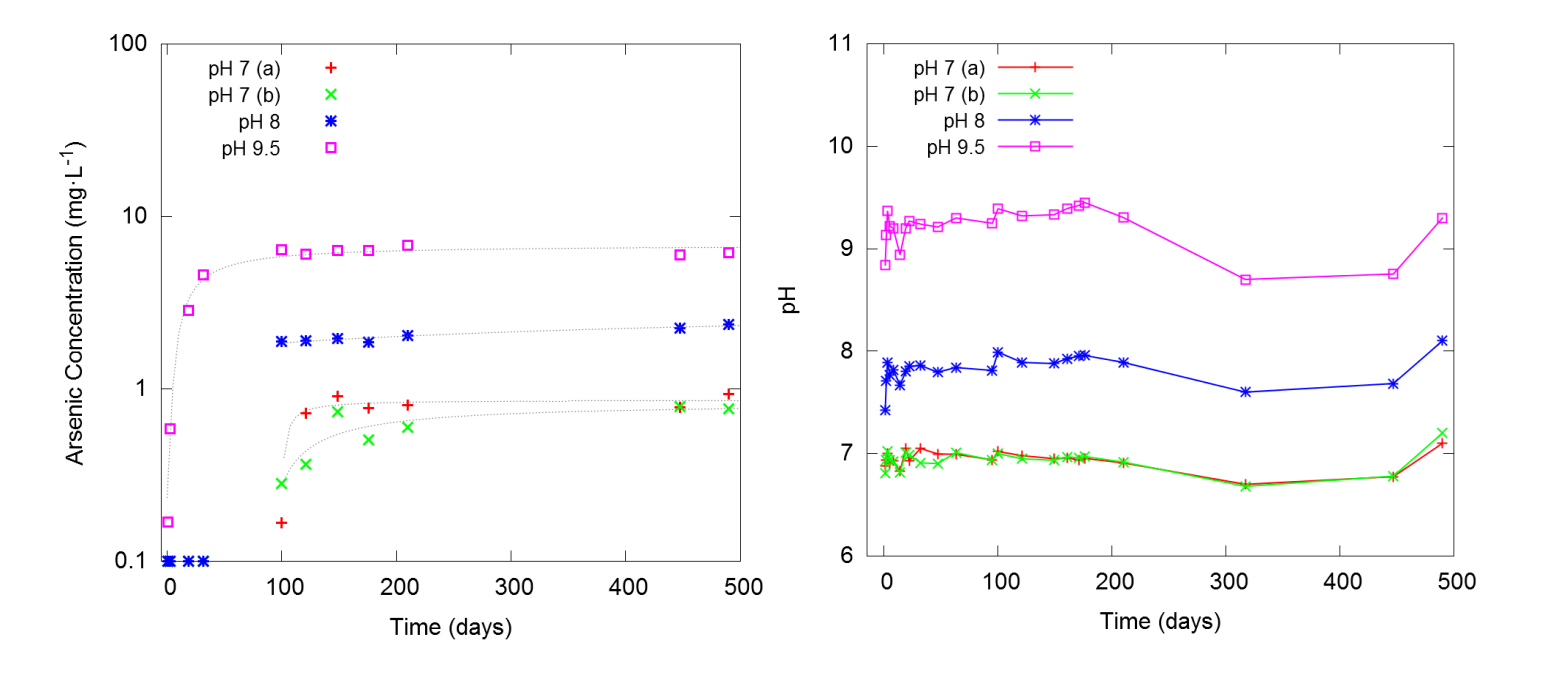


**Fig. 3.14.** Results of Study A-g ("Synthetic 1") with gypsum-saturated solution. (a) Arsenic solubility measurements over time of samples at various pH. (b) pH measurements over time.

and Study B-g. As in Study A, Study A-g showed the trend of increasing solubility with increasing pH for pH  $\geq$  7 (**Fig. 3.14.**). However, in this case, As release was suppressed by  $\sim$ 10, 20, and 50 times at pH 7, 8, 9.5, respectively. In fact, experiments at pH 7 and 8 did not detect any release of As until after 100 days of ageing. Equilibrium As concentrations were below 1 mg/L for pH 7.

The same trend effect was observed in Study B-g (**Fig. 3.15.**) with As concentration reduced by ~5, 10, 50 times for pH 7, 8, 10, respectively, in comparison to Study B. Equilibrium As concentrations were below 1 mg/L for pH 7 and 8. For Study B and Study B-g, equilibrium As concentrations are plotted in **Fig. 3.16.**, which shows the considerable stabilizing effect of gypsum in alkaline conditions. No such effect was observed under acidic conditions, with the gypsum-free and gypsum-saturated samples showing practically identical As concentrations.

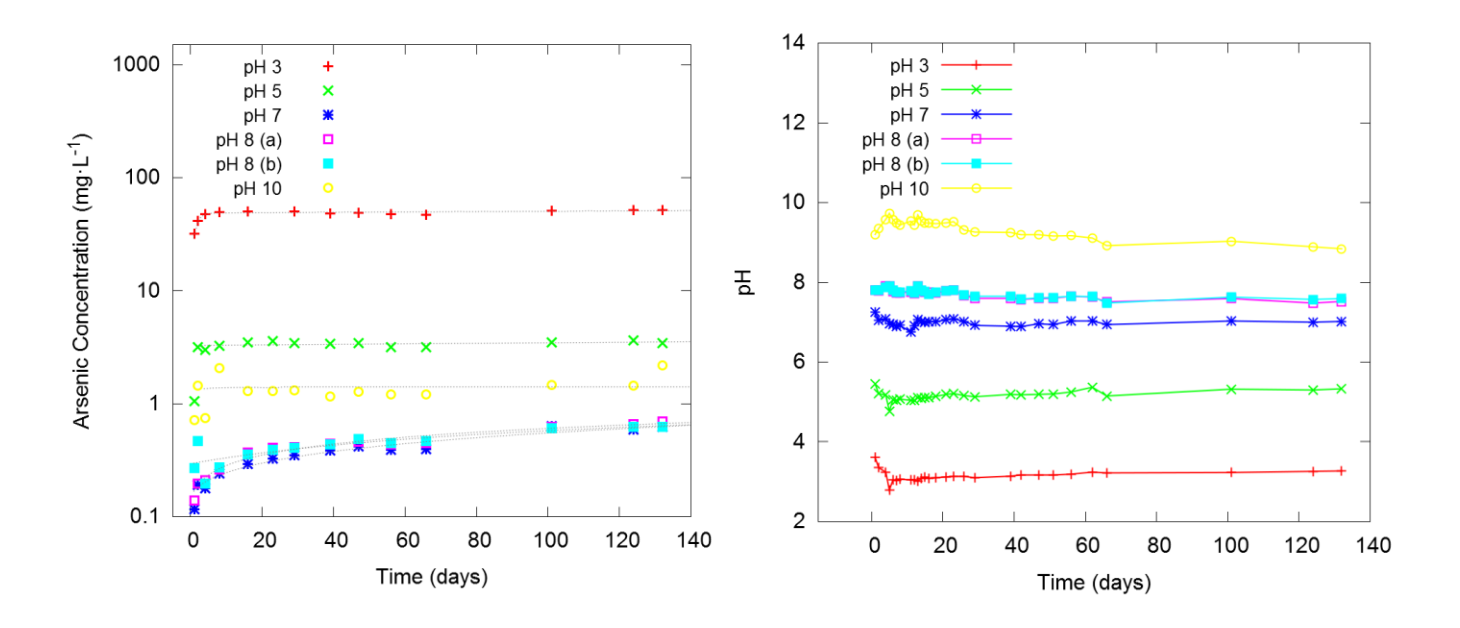


**Fig. 3.15.** Results of Study A-g ("Synthetic 1") with gypsum-saturated solution. (a) Arsenic solubility measurements over time of samples at various pH. (b) pH measurements over time.

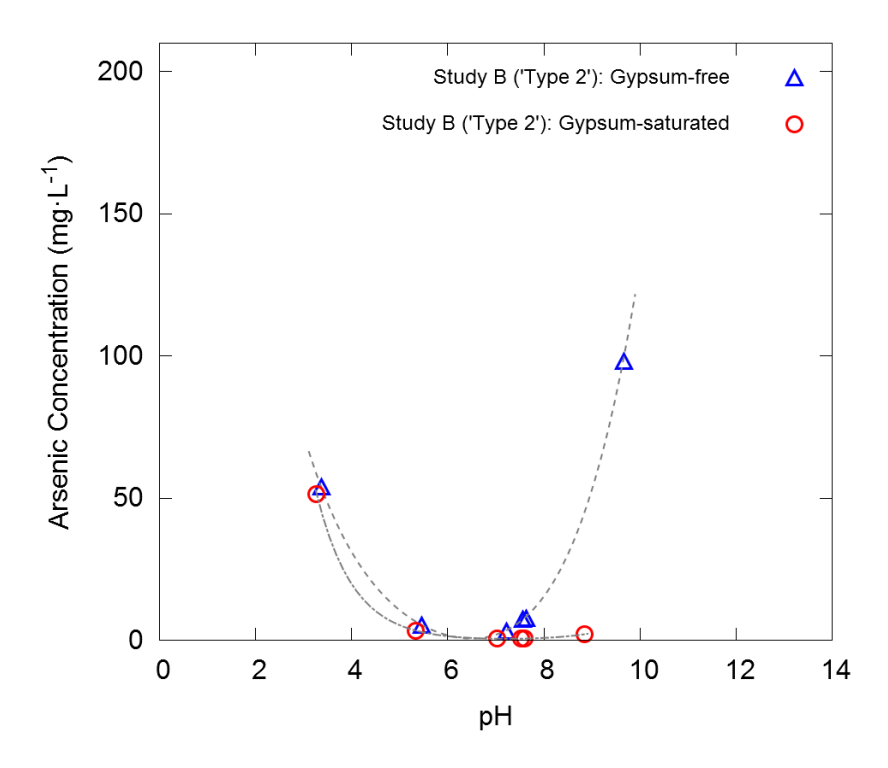


**Fig. 3.16.** Results of Study B and Study B-g. Equilibrium As concentrations after 132 ageing in gypsumfree (triangles) and gypsum-saturated (circles) solutions.

#### 3.3.3. Implications

The results presented in this paper show that yukonite is a phase with potential for arsenic immobilization, justified by findings of low arsenic solubility under neutral-to-alkaline conditions typically encountered in tailings disposal sites. We are tempted to infer that coprecipitated and/or scorodite tailings aged at pH 7-9 in the presence of lime may ultimately form a Ca-Fe-As yukonite-like phase, as demonstrated in previous accelerated ageing experiments [2], [21]. The conversion of ferric arsenates in the presence of lime/gypsum to yukonite would likely be a lengthy process over an untold number of years. However, in the event of its formation, stability data presented in this study suggests yukonite has the potential to serve as an arsenic-stable phase. When intermixed with large fractions of gypsum, as is often the case in hydrometallurgical tailings [3], [4], yukonite possesses low arsenic solubility: 3.5 mg·L<sup>-1</sup> at pH 5, 0.6-0.9 mg·L<sup>-1</sup> at pH 7, 0.6-2.4 mg·L<sup>-1</sup> at pH 8, and 2.2-6.2 mg·L<sup>-1</sup> at pH 9.5-10. Thus, it seems unlikely that pore water concentrations of arsenic would exceed ca. 6 mg·L<sup>-1</sup>. This might not be the case if gypsum present in the tailings mass dissolves over time and pore waters become free of Ca<sup>2+</sup> ions. Even in this case, yukonite shows capacity to immobilize arsenic, exhibiting 5.3 mg·L<sup>-1</sup> at pH 5, 3.1-11.9 mg·L<sup>-1</sup> at pH 7, and 7.3-57.2 mg·L<sup>-1</sup> at pH 8.

Therefore, this new understanding of yukonite is evidence that sweeping claims of instability of Ca-Fe-As phases are unsubstantiated [14], [15]. The majority of such claims point to work by Swash and Monhemius that measured solubility of Ca-Fe-As phases synthesized at various temperatures, pH, and molar ratios with the TCLP test at pH 5 [20]. However, none of these compounds were identified as phases known to occur in nature, such as arseniosiderite and yukonite. A study by Meunier et al. makes an important conclusion that yukonite is relatively soluble under gastric conditions (pH 1.8) based on physiologically based extraction test (PBET) [18]; however, it is crucial to recognize that these results do not necessarily apply to arsenic mobilization under tailings disposal conditions [4], [6]. Finally, relatively high arsenic release found of the tailings from the Ketza River gold mine found by Soprovich [16] and discussed by Paktunc et al. [43] make an assumption that Ca-Fe-As phases are responsible for the release without direct evidence, an assumption that is not valid according to the data presented in this work.

However, it is important to acknowledge the limitations of this data for predictive purposes. For instance, the ageing studies were closed-systems not open to equilibration with

carbon dioxide in the atmosphere (except for a minority of the time during sampling). Therefore, it is not known whether yukonite could be unstable with respect to CO<sub>2</sub>/dissolved inorganic carbon, as has been shown of calcium arsenates [44]. Moreover, the experiments here were conducted under oxygen-rich conditions. While it is not necessarily the case, there are concerns that tailings disposal sites may develop sub-oxic or anoxic conditions, destabilizing the mineral phases responsible for immobilizing arsenic [45]. Therefore, experiments probing the stability of yukonite with respect to CO<sub>2</sub> and also in sub-oxic and anoxic conditions are in progress and will be reported in the near future.

#### 3.4. Conclusions

This study has investigated the synthesis, mineralogical characteristics, and stability-solubility of the mineral phase yukonite in terms of its potential arsenic immobilization role in metallurgical tailings. Review of literature sources and experimental evidence from our laboratory, both past and presented in this paper for the first time, have resulted in several conclusions regarding yukonite:

- 1. Accelerated ageing studies conducted at 75°C indicate ferric-arsenate coprecpitates (Fe(III)/As(V)=2) and scorodite (FeAsO<sub>4</sub>·2H<sub>2</sub>O) in gypsumsaturated waters may phase transform over time to a Ca(II)-Fe(III)-As(V) phase, yukonite, which has already been identified in mine tailings.
- 2. Synthetic yukonite was produced and found by characterization (XRD, chemical analysis) to be consistent with natural yukonite with the theoretical chemical formula Ca<sub>2</sub>Fe<sub>3</sub>(AsO<sub>4</sub>)<sub>3</sub>(OH)<sub>4</sub>·(3+x)H<sub>2</sub>O.
- 3. A pair of stability studies were in agreement that yukonite is a stable arsenic carrier under certain environmental conditions that may occur in mine waste disposal sites. Specifically, yukonite possesses low arsenic solubility under mildly-acid, neutral, and mildly-alkaline conditions. The solubility of yukonite decreases dramatically in the presence of gypsum (< 1 mg·L<sup>-1</sup> for pH 7-8).

Further work is underway to investigate the stability of yukonite with respect to other conditions that may be encountered in hydrometallurgical tailings, including exposure to CO<sub>2</sub> as well as sub-oxic and anoxic conditions.

## Acknowledgements

This work was made possible by NSERC (Natural Sciences and Engineering Research Council) in conjunction with Areva Resources Canada and Cameco Corporation, industrial sponsors through a CRD (Collaborative Research and Development) grant.

#### References

- [1] E. Krause and V. A. Ettel, "Solubilities and stabilities of ferric arsenate compounds," *Hydrometallurgy*, vol. 22, no. 3, pp. 311–337, 1989.
- [2] Y. Jia and G. P. Demopoulos, "Coprecipitation of arsenate with iron(III) in aqueous sulfate media: Effect of time, lime as base and co-ions on arsenic retention," *Water Res.*, vol. 42, no. 3, pp. 661–668, 2008.
- [3] J. Mahoney, M. Slaughter, D. Langmuir, and J. Rowson, "Control of As and Ni releases from a uranium mill tailings neutralization circuit: Solution chemistry, mineralogy and geochemical modeling of laboratory study results," *Appl. Geochem.*, vol. 22, no. 12, pp. 2758–2776, 2007.
- [4] M. A. Gomez, L. Becze, R. I. R. Blyth, J. N. Cutler, and G. P. Demopoulos, "Molecular and structural investigation of yukonite (synthetic & natural) and its relation to arseniosiderite," *Geochim. Cosmochim. Acta*, vol. 74, no. 20, pp. 5835–5851, 2010.
- [5] R. De Klerk, "Investigating the continuous circuit coprecipitation of arsenic(V) with ferric iron in sulphate media," 2008.
- [6] Y. Jia, G. P. Demopoulos, N. Chen, and J. Cutler, "Coprecipitation of As (V) with Fe (III) in sulfate media: solubility and speciation of arsenic," in *Arsenic Metallurgy*, RG Reddy, RN Weizenbach, Eds., TMS, 2005, pp. 137–148.
- [7] B. J. Moldovan and M. J. Hendry, "Characterizing and Quantifying Controls on Arsenic Solubility over a pH Range of 1–11 in a Uranium Mill-Scale Experiment," *Environ. Sci. Technol.*, vol. 39, no. 13, pp. 4913–4920, 2005.
- [8] N. Chen, D. T. Jiang, J. Cutler, T. Kotzer, Y. F. Jia, G. P. Demopoulos, and J. W. Rowson, "Structural characterization of poorly-crystalline scorodite, iron(III)—arsenate coprecipitates and uranium mill neutralized raffinate solids using X-ray absorption fine structure spectroscopy," *Geochim. Cosmochim. Acta*, vol. 73, no. 11, pp. 3260–3276, 2009.
- [9] D. Langmuir, J. Mahoney, and J. Rowson, "Solubility products of amorphous ferric arsenate and crystalline scorodite (FeAsO4 · 2H<sub>2</sub>O) and their application to arsenic

- behavior in buried mine tailings," *Geochim. Cosmochim. Acta*, vol. 70, no. 12, pp. 2942–2956, 2006.
- [10] P. M. Swash and A. J. Monhemius, "Hydrothermal precipitation from aqueous solutions containing iron(III), arsenate and sulphate," in *Hydrometallurgy '94*, Springer Netherlands, 1994, pp. 177–190.
- [11] D. Filippou and G. P. Demopoulos, "Arsenic immobilization by controlled scorodite precipitation," *JOM*, vol. 49, no. 12, pp. 52–55, 1997.
- [12] T. Fujita, R. Taguchi, M. Abumiya, M. Matsumoto, E. Shibata, and T. Nakamura, "Novel atmospheric scorodite synthesis by oxidation of ferrous sulfate solution. Part I," *Hydrometallurgy*, vol. 90, no. 2–4, pp. 92–102, 2008.
- [13] G. P. Demopoulos, "On the preparation and stability of scorodite," in *Arsenic Metallurgy*, RG Reddy, RN Weizenbach, Eds., TMS, 2005, pp. 25–50.
- [14] D. Paktunc, A. Foster, S. Heald, and G. Laflamme, "Speciation and characterization of arsenic in gold ores and cyanidation tailings using X-ray absorption spectroscopy," *Geochim. Cosmochim. Acta*, vol. 68, no. 5, pp. 969–983, 2004.
- [15] D. Paktunc, A. Foster, and G. Laflamme, "Speciation and Characterization of Arsenic in Ketza River Mine Tailings Using X-ray Absorption Spectroscopy," *Environ. Sci. Technol.*, vol. 37, no. 10, pp. 2067–2074, 2003.
- [16] E. A. Soprovich, "Arsenic release from oxide tailings containing scorodite, Fe-Ca arsenates and As-containing goethites," in *Proceedings of the Seventh International Conference on Tailings and Mine Waste'00*, A.A. Balkema, Ed., 2000, pp. 23–26.
- [17] S. R. Walker, M. B. Parsons, H. E. Jamieson, and A. Lanzirotti, "Arsenic Mineralogy of Near-Surface Tailings and Soils: Influences on Arsenic Mobility and Bioaccessibility in the Nova Scotia Gold Mining Districts," *Can. Mineral.*, vol. 47, no. 3, pp. 533–556, 2009.
- [18] L. Meunier, S. R. Walker, J. Wragg, M. B. Parsons, I. Koch, H. E. Jamieson, and K. J. Reimer, "Effects of Soil Composition and Mineralogy on the Bioaccessibility of Arsenic from Tailings and Soil in Gold Mine Districts of Nova Scotia," *Environ. Sci. Technol.*, vol. 44, no. 7, pp. 2667–2674, 2010.
- [19] M. C. Corriveau, H. E. Jamieson, M. B. Parsons, and G. E. M. Hall, "Mineralogical characterization of arsenic in gold mine tailings from three sites in Nova Scotia," *Geochem. Explor. Environ. Anal.*, vol. 11, no. 3, pp. 179–192, 2011.
- [20] P. M. Swash and A. J. Monhemius, "Synthesis, characterization and solubility testing of solids in the Ca-Fe-AsO4 system," *Sudbury '95—Mining Environ. CANMET*, pp. 17–28, 1995.
- [21] M.-C. Bluteau, L. Becze, and G. P. Demopoulos, "The dissolution of scorodite in gypsum-saturated waters: Evidence of Ca–Fe–AsO4 mineral formation and its impact on arsenic retention," *Hydrometallurgy*, vol. 97, no. 3–4, pp. 221–227, 2009.
- [22] J. B. Tyrrell and R. P. D. Graham, "Yukonite, a New Hydrous Arsenate of Iron and Calcium, from Tagish Lake, Yukon Territory, Canada: With a Note on the Associated Symplesite," 1913.
- [23] P. J. Dunn, "New Data for Pitticite and a Second Occurrence of Yukonite at Sterling Hill, New Jersey," *Mineral. Mag.*, vol. 46, no. 339, pp. 261–264, 1982.
- [24] D. R. Ross and J. E. Post, "New data on yukonite," *Powder Diffr.*, vol. 12, no. 02, pp. 113–116, 1997.
- [25] A. Pieczka, B. Golebiowska, and W. Franus, "Yukonite, a rare Ca-Fe arsenate, from Redziny (Sudetes, Poland)," *Eur. J. Mineral.*, vol. 10, no. 6, pp. 1367–1370, 1998.

- [26] O. Nishikawa, V. Okrugin, N. Belkova, I. Saji, K. Shiraki, and K. Tazaki, "Crystal symmetry and chemical composition of yukonite: TEM study of specimens collected from Nalychevskie hot springs, Kamchatka, Russia and from Venus Mine, Yukon Territory, Canada," *Mineral. Mag.*, vol. 70, no. 1, pp. 73–81, 2006.
- [27] A. Garavelli, D. Pinto, F. Vurro, M. Mellini, C. Viti, T. Balić-Žunić, and G. Della Ventura, "Yukonite from the Grotta Della Monaca cave, Sant'agata di Esaro, Italy: characterization and comparison with cotype material from the Daulton mine, Yukon, Canada," *Can. Mineral.*, vol. 47, no. 1, pp. 39–51, 2009.
- [28] R. W. Metsger, C. B. Tennant, and J. L. Rodda, "Geochemistry of the Sterling Hill Zinc Deposit, Sussex County, New Jersey," *Geol. Soc. Am. Bull.*, vol. 69, no. 6, pp. 775–788, 1958.
- [29] L. Becze and G. P. Demopoulos, "Hydrometallurgical synthesis of Ca-Fe-AsO4 compounds," in *Extraction and Processing: Proceedings of Symposium*, Davis, B. & Free, ML, Eds., TMS, 2007, p. 11
- [30] L. Becze, M. A. Gomez, V. Petkov, J. N. Cutler, and G. P. Demopoulos, "The potential arsenic retention role of Ca-Fe(III)-AsO4 compounds in lime neutralized co-precipitation tailings," in *Uranium 2010*, EK Lam, JW Rowson, E Özberk, Eds., CIM, 2010, vol. II., pp 327-333.
- [31] M. A. Gomez, L. Becze, R. I. R. Blyth, J. N. Cutler, and G. P. Demopoulos, "Molecular and structural investigation of yukonite (synthetic & natural) and its relation to arseniosiderite," *Geochim. Cosmochim. Acta*, vol. 74, no. 20, pp. 5835–5851, 2010.
- [32] M. A. Gomez, L. Becze, G. P. Demopoulos, H. Assaaoudi, J. N. Cutler, and R. I. R. Blyth, "Characterization of Ca-Fe (III)-AsO4-SO4 Phases relating to Arsenic Disposal in Hydrometallurgical Operations," *Chem. Mater. Sci. Can. Light Source*, pp. 62–63, 2008.
- [33] P. B. Moore and T. Araki, "Mitridatite: A Remarkable Octahedral Sheet Structure," *Mineral. Mag.*, vol. 41, no. 320, pp. 527–528, 1977.
- [34] P. B. Moore and T. Araki, "Mitridatite, Ca<sub>6</sub>(H<sub>2</sub>O)<sub>6</sub>[Fe<sub>9</sub><sup>3+</sup>O<sub>6</sub>(PO<sub>4</sub>)<sub>9</sub>].3H<sub>2</sub>O. A noteworthy octahedral sheet structure," *Inorg. Chem.*, vol. 16, no. 5, pp. 1096–1106, 1977.
- [35] Y. Jia, L. Xu, Z. Fang, and G. P. Demopoulos, "Observation of Surface Precipitation of Arsenate on Ferrihydrite," *Environ. Sci. Technol.*, vol. 40, no. 10, pp. 3248–3253, 2006.
- [36] J. F. L. Berre, R. Gauvin, and G. P. Demopoulos, "Characterization of Poorly-Crystalline Ferric Arsenate Precipitated from Equimolar Fe(III)-As(V) Solutions in the pH Range 2 to 8," *Metall. Mater. Trans. B*, vol. 38, no. 5, pp. 751–762, 2007.
- [37] R. E. Dinnebier and S. J. L. Billinge, "Chapter 1. Principles of Powder Diffraction," in *Powder Diffraction*, R. E. Dinnebier and S. J. L. Billinge, Eds. Cambridge: Royal Society of Chemistry, 2008, pp. 1–19.
- [38] G. P. Demopoulos, "Aqueous precipitation and crystallization for the production of particulate solids with desired properties," *Hydrometallurgy*, vol. 96, no. 3, pp. 199–214, 2009.
- [39] J. F. Le Berre, R. Gauvin, and G. P. Demopoulos, "A study of the crystallization kinetics of scorodite via the transformation of poorly crystalline ferric arsenate in weakly acidic solution," *Colloids Surf. Physicochem. Eng. Asp.*, vol. 315, no. 1–3, pp. 117–129, 2008.
- [40] J. J. Lingane, "Treatise on Analytical Chemistry. Volume 1 of Part 1, Theory and Practice (Kolthoff, I. M.; Elving, Philip J.; Sandell, Ernest B.; eds.)," *J. Chem. Educ.*, vol. 37, no. 2, p. 108, 1960.
- [41] W. M. White, Geochemistry. John Wiley & Sons, 2013.

- [42] D. Paktunc and K. Bruggeman, "Solubility of nanocrystalline scorodite and amorphous ferric arsenate: Implications for stabilization of arsenic in mine wastes," *Appl. Geochem.*, vol. 25, no. 5, pp. 674–683, 2010.
- [43] A. D. Paktunc, J. Szymanski, R. Lastra, J. H. G. Laflamme, V. Enns, and E. Soprovich, "Assessment of potential arsenic mobilization from the Ketza River mine tailings, Yukon, Canada," *Waste Charact. Treat.*, pp. 49–60, 1998.
- [44] R. G. Robins and K. Tozawa, "Arsenic removal from gold processing waste waters: the potential ineffectiveness of lime," *Can. Min. Metall. Bull.*, vol. 75, no. 840, pp. 171–174, 1982.
- [45] H. McCreadie, D. W. Blowes, C. J. Ptacek, and J. L. Jambor, "Influence of Reduction Reactions and Solid-Phase Composition on Porewater Concentrations of Arsenic," *Environ. Sci. Technol.*, vol. 34, no. 15, pp. 3159–3166, 2000.

# Chapter 4. The Stability of Yukonite—a Calcium Ferric Arsenate—under CO<sub>2</sub>-Rich and Reducing Conditions

The results of this thesis are presented in the form of two manuscripts that together describe the stability of the arsenate-bearing phase yukonite. An understanding of the stability of yukonite is important given indications that it may form in tailings management facilities. In the previous chapter, the stability of yukonite was studied under oxic conditions. Long-term experiments monitored the dissolution of yukonite across a range of pH and it was found to be stable, especially near circumneutral pH and in the presence of gypsum.

In this chapter, the second of two manuscript-based results chapters, stability was investigated with respect to  $CO_2$  and under reducing conditions, which may be encountered in tailings management facilities. The former was accomplished by reaction of synthetic yukonite with  $CO_2$ —in its gaseous form and as NaHCO<sub>3</sub>—while the latter by reaction with chemical-reducing agents Na<sub>2</sub>SO<sub>3</sub> and NaHS.

This paper is intended for submission to the journal *Hydrometallurgy*. The current citation information is as follows:

Matthew Bohan, Thomas Feldmann, and George P. Demopoulos, "The Stability of Yukonite—a Calcium Ferric Arsenate—under CO<sub>2</sub>-Rich and Reducing Conditions," *Hydrometallurgy*, to be submitted.

#### **Abstract**

Recent evidence has suggested the mineral phase "yukonite" (Ca<sub>2</sub>Fe<sub>3</sub>(AsO<sub>4</sub>)<sub>3</sub>(OH)<sub>4</sub>·(3+x)H<sub>2</sub>O) may be important in controlling arsenic pore water concentrations in mineral processing-derived tailings. In this study, yukonite is synthesized and subjected to stability tests to evaluate its reactivity with respect to CO<sub>2</sub> and reducing agents. Its reaction with respect to CO<sub>2</sub> was determined by gas sparging experiments in an Applikon chemical reactor and by equilibration with variable concentration NaHCO<sub>3</sub>. In both cases, yukonite was found to react with partial formation of calcite and release of arsenic in water. Stability with respect to sub-oxic (E<sub>h</sub> ca. 200 mV) and anoxic (E<sub>h</sub> ca. -200 mV) was evaluated by equilibration in Na<sub>2</sub>SO<sub>3</sub> and NaHS solutions, respectively, under a N<sub>2</sub> atmosphere with the latter chemical agent found to severely destabilize yukonite. These findings point to the importance of proper selection of yukonite disposal conditions limiting exposure to carbonate-rich waters without introducing severe chemical-reducing environment.

#### 4.1. Introduction

Arsenic (As) is a toxic impurity found in many ores, including gold, copper, and uranium [1], most often occurring as complex sulfides or arsenide minerals such as arsenopyrite (FeAsS) [2, pp. 1–12], gersdorfite (NiAsS) and niccolite (NiAs) [3, pp. 20–34], or enargite (Cu<sub>2</sub>AsS<sub>4</sub>) and other copper-arsenic minerals [4, pp. 247–298]. Control of arsenic to prevent environmental contamination is a major concern of the mining and metallurgical industry [5], [6]. Pyrometallurgical processing of arseniferous concentrations may lead to volatilization of arsenic as arsenic trioxide (As(III)) flue dusts [7]. Alternatively, hydrometallurgical processing of ores or concentrations to liberate valuable metal leads to dissolved arsenic concentrations (As(III) and As(V)) in process effluents that require treatment prior to disposal [8]. Depending upon the nature of the waste stream, a variety of methods may be used to immobilize arsenic [8]–[10]. In general, the strategy is to transform soluble arsenic species into insoluble compounds. Hence, the issue of controlling release of arsenic in the environment is a question of the solubility and there is a need to fully understand the solubility and stability of candidate arsenic fixation compounds.

A diversity of arsenic compounds are known [11]–[13]. Scorodite (FeAsO<sub>4</sub>·2H<sub>2</sub>O) is perhaps the most well-known stable phase for fixation of arsenic. It can be formed during

hydrothermal (i.e. autoclave, T>150°C) processing of ores [14], or alternatively, in atmospheric supersaturation-controlled precipitation (T=80-95°C) [7], [15]–[18]. Similarly, hydrothermal precipitation of lanthanum and indium arsenates showed <1 mg·L<sup>-1</sup> As arsenic solubility under EPA TCLP-like testing (pH 5, 24 h) [19]. Precipitation of calcium arsenates (e.g. CaHAsO<sub>4</sub>) by lime neutralization was formerly a common technique [20]; however, it is no longer considered appropriate after it was shown by Robins and Tozawa [21] that these compounds are unstable in the long term. Specifically, calcium arsenates react with CO<sub>2</sub> as available in the atmosphere or through equilibration with carbonate minerals to form calcite (CaCO<sub>3</sub>), effectively mobilizing arsenic. In the case of acidic hydrometallurgical effluents, the most common method of arsenic fixation is coprecipitation by addition of iron (Fe(III)/As(V)>3) and subsequent lime (CaO) neutralization. When arsenic concentrations are high, this process results in a mixture of poorly-crystalline ferric arsenate (FeAsO<sub>4</sub>·2H<sub>2</sub>O) and arsenate-adsorbed ferrihydrite (As-FeOOH) [22]. Crucially, calcium from lime and sulfate from the leaching process (either sulfuric acid or oxidation of sulfide) preferentially combine to form significant amounts of gypsum (CaSO<sub>4</sub>·2H<sub>2</sub>O) that admixes with the coprecipitates [23].

A number of studies have investigated the solubility and stability of iron arsenate precipitates over a variable pH range under typically oxidizing conditions encountered in tailings disposal facilities. Krause and Ettel were among the first to study the solubility and stability of ferric arsenates including crystalline scorodite and iron arsenate coprecpitates [10]. The solubility of scorodite has been reviewed and modeled later by Langmuir et al. [24] and its dissolution kinetics experimentally determined by Bluteau and Demopoulos [25]. According to these studies, scorodite exhibits low solubility (<1 mg·L<sup>-1</sup> As) under acidic (pH 3.5-5.5) while solubility of its precursor, poorly-crystalline ferric arsenate, is perhaps 100 times higher under these conditions. Both phases show significant arsenic release with pH rising above 7.5. However, hydrolysis of excess iron to form ferrihydrite increases the stability of iron arsenate coprecpitates as a function of increasing Fe(III)/As(V) ratio, owing to strong surface adsorption of the soluble fraction of arsenate on ferrihydrite [10], [26], [27]. Long-term stability experiments have shown simulated coprecpitated tailings (Fe(III)/As(V)=4) to be stable over 1.5 years at pH 8, releasing <1 mg·L<sup>-1</sup> As [28].

The possible instability of iron arsenate compounds under neutral-to-alkaline conditions has raised questions about the ultimate fate of these phases in tailings facilities, which typically

neutralize to pH > 7 in order to precipitate other problematic elements [22], [27], [29]. There is also the consideration that coprecipitates include a significant amount of gypsum, which introduces the possibility of formation of Ca(II)-Fe(III)-As(V) phases. At pH 7-9, coprecipitates (Fe(III)/As(V)=2) neutralized with lime and subsequently subjected to accelerated ageing (T=75°C) in our laboratory were found to undergo phase transformation to a Ca(II)-Fe(III)-As(V) phase that resembles the natural mineral yukonite (Ca<sub>2</sub>Fe<sub>3</sub>(AsO<sub>4</sub>)<sub>3</sub>(OH)<sub>4</sub>·4H<sub>2</sub>O) [30]. Under similar ageing conditions, scorodite in the presence of gypsum-saturated solution was found to partially transform to yukonite [31]. This information, in addition to several findings of yukonite amongst gold tailings [32]–[35], suggests yukonite may form in tailings where gypsum is present. Together, this evidence highlights the importance in studying the stability of yukonite under a variety of conditions.

Prior efforts by the McGill HydroMET Group have focused on the development of a synthesis method for yukonite and its extensive characterization, with comparison to natural specimens and a related phase arseniosiderite (Ca<sub>2</sub>Fe<sub>3</sub>(AsO<sub>4</sub>)<sub>3</sub>O<sub>2</sub>·3H<sub>2</sub>O) [36]. A subsequent study revealed vukonite to possess low As solubility under oxic conditions in the presence of gypsumsaturated water (0.6-0.9 mg·L<sup>-1</sup> at pH 7 and 0.6-2.4 mg·L<sup>-1</sup> at pH 8) [37]. However, it would be of interest to understand how yukonite may respond to changing conditions when disposed in tailings facilities. For instance, it is unclear if yukonite will suffer the same ill fate as calcium arsenates in the face of CO<sub>2</sub>. Another possible scenario for tailings is the development of oxygen-depleted/reducing conditions. At the Campbell Mine in Balmertown, ON, Canada, reductive dissolution by heterotrophic bacteria was responsible for dissolution of As-rich hematite and maghemite, elevating As porewater concentrations as high as 100 mg/L [38]. This has prompted consideration of the effects of reducing conditions (i.e. low E<sub>h</sub>) on the stability of coprecipitates. A recent laboratory study by Doerfelt [39] found iron(III) arsenate coprecipitates to offer moderate resistance to dissolution upon addition of chemical-reducing agents (i.e. sulphides), with ca. 30 mg/L of arsenic after 24 days' equilibration in a nitrogen atmosphere, corresponding to the dissolution of ca. 1% of total arsenic.

Therefore, the purpose of this paper is to report the stability of yukonite vis-à-vis (a) carbon dioxide, bicarbonate, and carbonate and (b) sub-oxic and anoxic conditions. In the case of the former, a double-pronged approach of CO<sub>2</sub> gas sparging and equilibration with NaHCO<sub>3</sub> is

employed, while chemical-reducing agents (e.g. sulfites, sulfides) are added to achieve reducing conditions.

#### 4.3. Experimental

#### 4.3.1. Synthesis and characterization

Yukonite was synthesized according to a previously developed procedure ("Type 2-9.0") [37]. The synthesis was conducted in an Applikon reactor by room-temperature (20°C) neutralization with 1.25M sodium hydroxide (NaOH) to pH 8 of a solution containing a Ca(II)/Fe(III)/As(V) molar ratio of 0.50/0.75/1, where As(V) concentration was 9.0 g/L. After neutralization, the slurry was heated to 95°C and aged for 24 h while pH was maintained at 8 by addition of nitric acid (HNO<sub>3</sub>) and NaOH, dispensed continuously with a pH controller. Following ageing, the slurry was filtered with a pressure filter at 50 psi (0.22 µm membrane) to remove the supernatant, which contained ca. 1400 mg/L residual As. After filtering, the solids were repulped in 2 L of reverse osmosis water for ≥4 hours for a total of 6 washes, where the filtrate of the final repulp contained ca. 4 mg/L As.

Yukonite was confirmed by powder X-ray diffraction. XRD patterns were collected at 40 kV and 20 mA with a Cu K $\alpha_1$  source ( $\lambda$  = 1.506 Å) Phillips PW1710 diffractometer equipped with a crystal graphite monochromater and scintillation detector. Patterns were measured from 2-100°C 2 $\theta$ , with a 0.1° step and 3 second acquisition time. Chemical composition was determined by wet chemical digestion, where a precise amount of solid was weighed into a 50 mL polypropylene DigiTUBE before digestion for 2 h in concentrated HNO<sub>3</sub> at 95°C with the aid of a DigiPREP MS digester. Digested solutions were diluted and analyzed for As, Ca, Fe, K, Mg, Na, P, S, and Si with ICP-OES. Each digestion was performed in triplicate.

#### 4.3.2. Stability

The CO<sub>2</sub> sparge experiment was conducted in an Applikon reactor. A slurry of filtered synthetic yukonite (1 g dry mass in 1000 mL reverse osmosis water) was heated to 70°C with stirring at 500 rpm. A pH controller maintained pH precisely at pH 8 via addition of 0.2 M sodium hydroxide (NaOH) and 0.2 M nitric acid (HNO<sub>3</sub>). Once at temperature, pure CO<sub>2</sub> (99.8%) was introduced into the reactor via a porous glass sparger. The gas flow rate was

controlled by an Aalborg AFC mass flow controller at 4.4 mL/min, a rate that would introduce 20 times the stoichiometric amount needed to convert all yukonite to calcite (CaCO<sub>3</sub>) over the 48 h experiment. The stoichiometric excess of CO<sub>2</sub> accounted for an assumed capture efficiency < 10%. Samples were taken at regular intervals and analyzed for metal concentrations with a Thermo Scientific iCAP 6000 series ICP-OES and for inorganic carbon with Shimadzo TOC-VCPH total carbon analyzer with combustion detector in (TIC) mode.

The NaHCO<sub>3</sub> equilibration study to determine dissolution reaction order was conducted in 500 mL high-density polyethylene Nalgene® bottles. In each of 6 capped bottles, 200 mL of NaHCO<sub>3</sub> solution was prepared of different molarities: 0 M, 0.0125 M, 0.025 M, 0.125 M, 0.25 M, 2.5 M. After mixing for 24 h on a Lab Companion SK-71 shaker table in orbital mode operating at 180 min<sup>-1</sup> to at ambient temperature (20°C), filtered yukonite (5 g dry weight) was added. This addition corresponded to time zero. Samples were taken at regular intervals and analyzed for metal concentrations with ICP-OES and for inorganic carbon with a total carbon analyzer. Bottles were covered with Parafilm during sampling to minimize degassing of CO<sub>2</sub>.

To determine the effect of temperature on dissolution kinetics in each of 3 Nalgene® bottles 200 mL of 0.125 M NaHCO<sub>3</sub> solution was prepared. Filtered yukonite (5 g dry weight) was added and the samples were equilibrated for 3 days. After the initial equilibration, the samples were maintained at 20°C, 40°C, and 70°C without agitation for 42 days with the aid of an oven and a water bath. Bottles were covered with Parafilm during sampling to minimize degassing of CO<sub>2</sub>.

The anoxic and sub-oxic studies were conducted in parallel over 15 days, with unique samples sealed under inert atmosphere for each sampling day to eliminate the possibility of introducing oxygen during sampling. In each of 12 brown glass 250 mL bottles, 1.0 g of filtered wet yukonite was added. Working in a glovebox under a N<sub>2</sub> atmosphere, 100 mL of NaHS (0.001 M) solution was measured into 6 of the bottles that would correspond to days 3, 6, 9, 12, 15 of the anoxic study, with a duplicate of day 15. This concentration of NaHS corresponds to 25% of S<sup>2-</sup> necessary to fully reduce the Fe(III) to Fe(II) in yukonite, where a 1:1 stoichiometric ratio was avoided to keep the pH from becoming too alkaline [39]. Similarly, 100 mL of Na<sub>2</sub>SO<sub>3</sub> (0.012 M) solution was measured into 5 bottles that would correspond to days 3, 6, 9, 12, and 15 of the sub-oxic study. The selected concentration corresponds to a 3:1 stoichiometric excess of the amount of SO<sub>3</sub><sup>2-</sup> required to reduce the Fe(III) in yukonite to Fe(II). Into a final bottle, 100

mL of reverse osmosis water was dispensed. This sample serves as a control of yukonite solubility under a  $N_2$  atmosphere and was sampled after 15 days. The 12 bottles were placed on a Lab Companion SK-71 shaker table in orbital mode operating at 180 min<sup>-1</sup>. Upon sampling, pH and  $E_h$  measurements were made as well as analysis for metal concentrations with ICP-OES.

#### 4.4. Results and Discussion

This study is comprised of two parts exploring the reactivity of yukonite towards CO<sub>2</sub>/NaHCO<sub>3</sub> (part 1) and towards reducing agents (part 2).

The intention of the first part was to determine experimentally the stability of yukonite with respect to  $CO_2$  in aqueous solutions, i.e., to explore the Ca-Fe-AsO<sub>4</sub>-CO<sub>2</sub>-H<sub>2</sub>O system. Generally speaking, yukonite could react with  $CO_2$  in solution as dissolved inorganic carbon species:  $H_2CO_3*_{(aq)}$ ,  $HCO_3^{-}_{(aq)}$ , or  $CO_3^{-2}$ , where

$$H_2CO_3*_{(aq)} = CO_{2(aq)} + H_2CO_{3(a)}$$
 (4.1)

is the total analytical dissolved carbon dioxide. For a closed system, speciation is a function only of pH and total dissolved carbon concentration [40, p. 150]. Multiple pathways exist for introducing dissolved inorganic carbon (DIC) into solution with different outcomes. For instance, equilibration of CO<sub>2</sub> gas with solution has the effect of lowering solution pH. Alternatively, addition of a carbonate salt will introduce DIC according to the solubility product, which will drive the pH of the solution. Given that the solubility of yukonite is pH dependent, it is possible the mode of introducing CO<sub>2</sub> could influence the results. Therefore, we conducted experiments both by introducing CO<sub>2</sub> by gas sparging and also by equilibration with soluble carbonate salts.

For the second part, the goal was to determine experimentally the stability of yukonite in oxygen-depleted conditions, i.e. low  $E_h$ . For instance, these conditions can form in disposed tailings in the case of microbial activity [38], due to poor oxygen diffusion at depth, or reaction with reduced minerals (e.g. sulfides, arsenides) in the waste. In this experiment, sulfides are used as chemical-reducing agents to simulate these conditions.

#### 4.4.1. Reaction with CO<sub>2</sub>

Below are given the reactions that may take place upon equilibration of CO<sub>2</sub> with yukonite in a water medium:

$$Ca_{2}Fe_{3}(AsO_{4})_{3}(OH)_{4}\cdot 3H_{2}O \rightarrow 2Ca_{(aq)}^{2+} + 3Fe_{(aq)}^{3+} + 3AsO_{4(aq)}^{3-} + 4OH_{(aq)}^{-} + 3H_{2}O \qquad (4.2)$$

$$CO_{2(g)} \to CO_{2(aq)} \tag{4.3}$$

$$CO_{2(aq)} + H_2O \rightarrow H_2CO_{3(aq)}^* + OH^- \leftrightarrow HCO_{3(aq)}^- + OH^- \leftrightarrow CO_{3(aq)}^{2-}$$
 (4.4)

$$Ca_{(aq)}^{2+} + CO_{3(aq)}^{2-} \to CaCO_{3(s)}$$
 (4.5)

The results of the  $CO_2$  sparge experiment plotted in Fig. 4.1. show an additional ca. 30% release of As when sparging pure  $CO_2$  at 4.4 mL·min<sup>-1</sup> through a yukonite slurry (1 g/L), in comparison to a baseline with no gas sparging. Arsenic concentration was monitored as it is the element of concern and also because it dissolves congruently into solution according to the stoichiometry of yukonite, in contrast to iron, which immediately precipitates as ferrihydrite at pH 8.

The method is similar to that of Robins who demonstrated the instability of barium arsenate at pH > 8.3 by comparing an aerated sample with existing solubility data [41]. In this case, pure CO<sub>2</sub> and elevated temperature (70°C) were selected in an effort to increase the rate of any possible effect. In the case where no CO<sub>2</sub> was sparged, the DIC concentration was constant at ca. 10 mg·L<sup>-1</sup>. Sparging with CO<sub>2</sub> caused a nearly linear increase of DIC with time, reaching ca. 215 mg·L<sup>-1</sup> after 48 h. For reference, a tailings pond in Timmins, Ontario, had a maximum of 35 mg·L<sup>-1</sup> DIC [42] while the Greens Creek Mine near Juneau, Alaska, had >240 mg·L<sup>-1</sup> [43]. The solution did not reach equilibrium with respect to CO<sub>2</sub>. Considering the vapour pressure of water at 70°C is ca. 0.3 atm and the reactor was at atmospheric pressure, it is assumed  $P_{CO_2} = 0.7$  atm. In this case (with an absence of yukonite), a simulation with the geochemical modeling software PHREEQC suggests an equilibrium pH of 4.0 and equilibrium DIC of 287 mg/L, illustrated by Equation 4.2 and Equation 4.3, where DIC is the sum of the right side of the latter.

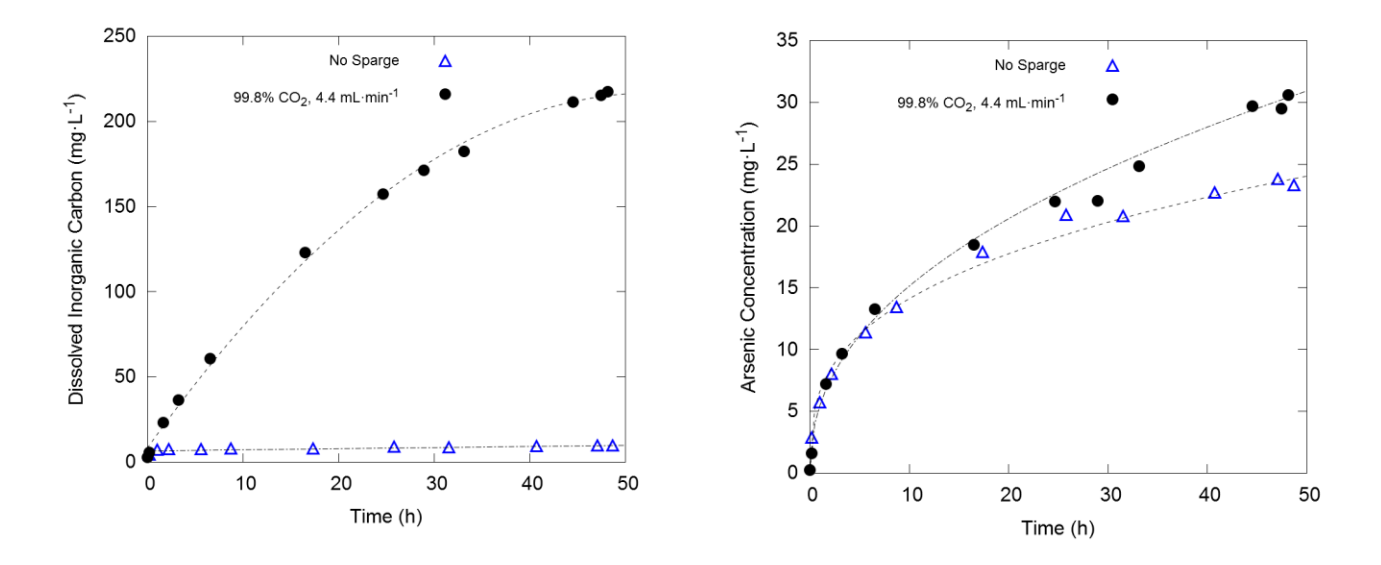


**Fig. 4.1.** Yukonite stability experiment conducted at 70°C by sparging (99.8%) CO<sub>2</sub> (circles) in comparison to no sparging (triangles) in an Applikon reactor for 48 h with pH controlled at 8 with NaOH and HNO<sub>3</sub>. Plots show (a) dissolved inorganic carbon concentration and (b) As concentration with respect to time.

However, in this experiment, pH is controlled at 8. Similar calculations accounting for pH control at 8 suggest equilibrium values of as much as 190 g/L DIC in the absence of precipitation of a solid phase. Therefore, it is assumed in the case of our experiment, equilibrium DIC values are controlled by the solubility product of an insoluble carbonate phase, likely calcite (CaCO<sub>3</sub>) as shown in Equation 4.4.

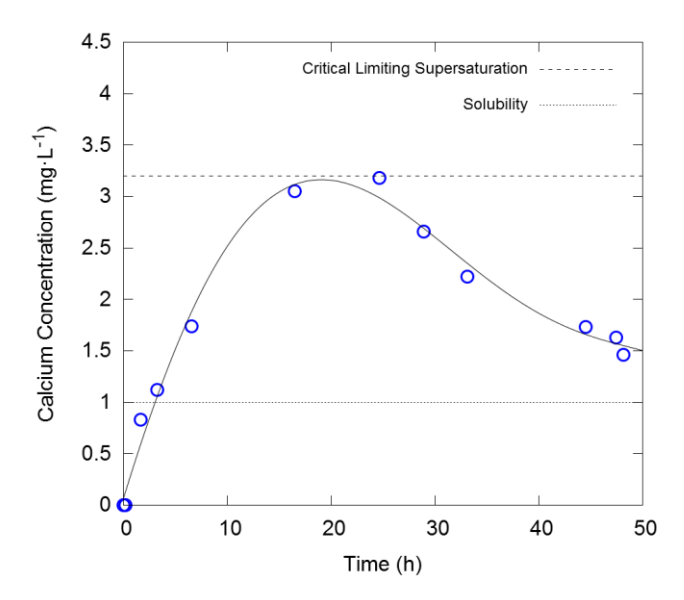


**Fig. 4.2.** Calcium concentration with respect to time for yukonite stability study with sparging of 99.8% CO<sub>2</sub> gas shows a LaMer-like trend. Initial increase in calcium concentration eventually peaks, suggesting nucleation of a calcium phase, and declines, indicating growth of that phase. This is seen as indirect evidence of formation of calcite.

Evidence of calcite formation was difficult to ascertain with XRD due to the small relative mass of calcite that would be formed with respect to the mass of yukonite. However, evidence for precipitation of calcite is seen by observing the concentration of Ca over time (**Fig. 4.2.**). Ca concentration increases starting at t = 0 h and reaches a maximum at t = 20 h, at which point it decreases and appears to begin to plateau sometime after t = 48 h. This trend was also observed by LaMer and Dinegar in the case of nucleation of sulfur hydrols, where it was observed concentration increased until a critical limiting supersaturation was met that initiated nucleation, at which point concentration slowly decreased due to crystal growth until it reached phase solubility [16], [44]. In this instance, we interpret the Ca concentration data to indicate the nucleation and growth of a calcium carbonate phase. Calculation with PHREEQC at t = 48 h showed SI (saturation index) = 0.35 (>0) for calcite, suggesting precipitation was thermodynamically favoured. Precipitation of calcite could also explain the slight negative deviation from linearity of DIC vs. time observed in **Fig. 4.1a**.

Notwithstanding the fact that the experiment involved hot solutions and pure CO<sub>2</sub>, very extreme conditions from a natural tailings disposal environment, the results suggest that yukonite is unstable with respect to CO<sub>2</sub> under these conditions. Another limitation of this experiment is that it is unclear if the additional dissolution in the case of CO<sub>2</sub> sparging was due to thermodynamic instability of yukonite with respect to calcite or due to localized acidity generated by the CO<sub>2</sub> gas. Further work is planned to delve into the thermodynamic modeling of yukonite.

#### 4.4.2. Reaction with NaHCO<sub>3</sub>

Here the reactivity of yukonite towards NaHCO<sub>3</sub> is considered. In addition to reactions (1) and (4) shown earlier, reactions (5) and (6) are relevant.

$$NaHCO_{3(s)} \stackrel{K_{sp}}{\longleftrightarrow} Na^{+}_{(aq)} + HCO^{-}_{3(aq)}$$
 (4.6)

$$HCO_{3(aq)}^{-} + OH_{(aq)}^{-} \leftrightarrow CO_{3(aq)}^{2-}$$
 (4.7)

Equilibration of yukonite with NaHCO<sub>3</sub> solutions of varying concentration showed a clear trend of increasing As concentration with increasing DIC concentration (**Fig. 4.3**.). For all samples, a high initial dissolution rate was followed by a slower but continual dissolution.

NaHCO<sub>3</sub> served as both a source of inorganic carbon and also as a buffer, designed to equilibrate near pH 8. Solution pH was monitored over time (**Fig. 4.3a.**) with all samples abiding by a similar trend of initial pH at or below 8 that increases to 8.5-9 over 60 days. This rules out the possibility that differences in As concentration between samples could be justified by the effect of pH. The

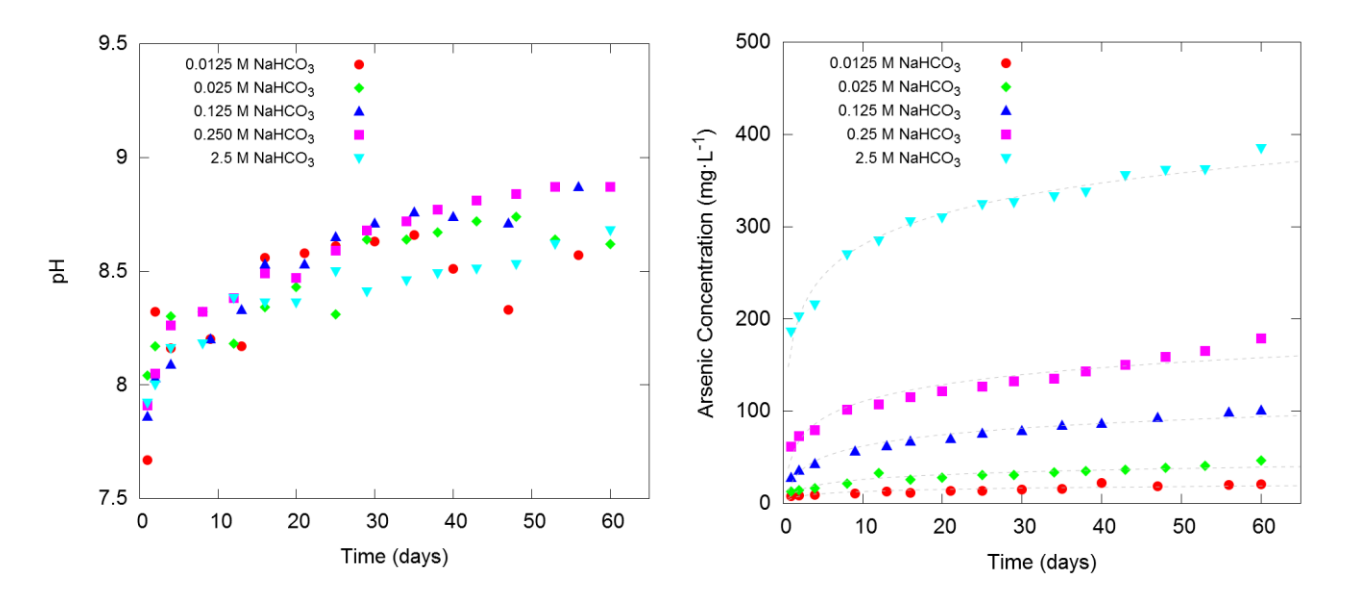


**Fig. 4.3.** Results of equilibrium study with variable NaHCO<sub>3</sub> concentrations showing (a) pH and (b) As concentration over time.

solubility of yukonite is known to have a minimum at ca. pH 7 and increase with alkalinity [37]. According to the effect of pH alone on solubility, the 2.5 M NaHCO<sub>3</sub> sample should have had the lowest As when in fact it had the greatest (385 mg·L<sup>-1</sup>, ca. 7wt.% of total As).

The assertion that DIC influences dissolution rate was confirmed by determining the order of reaction. The method of initial rates [45, p. 82] was selected for its ease of handling reactions that are incomplete. Initial rate was determined for each concentration by finding the slope of samples from t = 0 to t = 1 day (Fig. 4.4a.). For each concentration, the natural logarithm of the initial rate was plotted against the natural logarithm of the DIC measured concentration (Fig. 4b.). This was especially critical given that the 2.5 M sample was above the solubility of NaHCO<sub>3</sub> and therefore the actual DIC concentration was actually only 1.11 M. A linear regression of the plot gives a high correlation coefficient ( $R^2$ =0.991), which provides confidence to accuracy of the slope that indicates a reaction order of 0.700. Direct evidence of CaCO<sub>3</sub> formation by XRD was not found due to the overwhelming presence of NaHCO<sub>3</sub>. However,

indirect evidence of CaCO<sub>3</sub> formation was determined in chemical analysis of the aged solids for the 2.5 M sample, the sample with the greatest amount of yukonite dissolution.

**Table 1:** Tabulation of data used in kinetic study.

[NaHCO <sub>3</sub> ] <sub>0</sub> , (M)	[DIC] <sub>t=1 day</sub> , (M)	*[CO <sub>3</sub> <sup>2-</sup> ] <sub>t=1 day</sub> , (mg·L <sup>-1</sup> )	Initial Rate (M <sup>-1</sup> ·day <sup>-1</sup> )	In(Rate)
0.0125	0.0122	732	1.063E-4	-9.149
0.0250	0.0230	1382	1.718E-4	-8.669
0.125	0.0967	5805	3.754E-4	-7.888
0.250	0.191	11455	8.225E-4	-7.103
2.50	1.11	66840	2.484E-3	-5.998

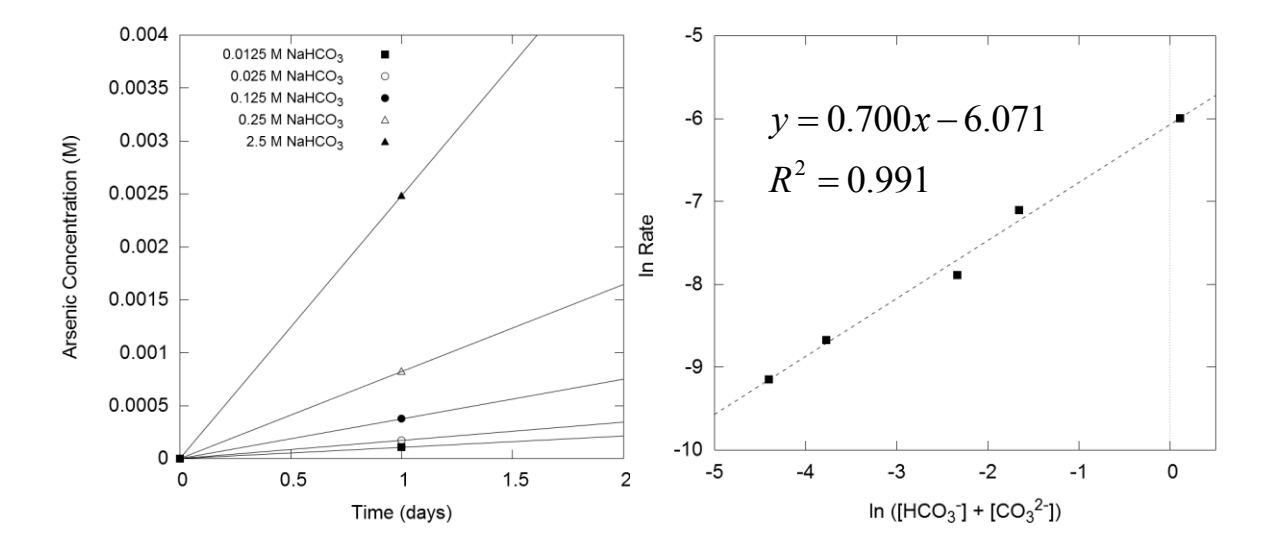


**Fig. 4.4.** (a) Determination of initial reaction rates from various concentration NaHCO<sub>3</sub> solutions at 20°C (b) ln-ln plot of Rate vs. [DIC] to determine the reaction order (slope).

The slurry was first centrifuged and the filtrate removed before drying. The solids formed two clear phases, one yukonite and one carbonate. The carbonate phase revealed a Ca:Fe:As ratio of 6.87:1.19:1, in comparison to the initial yukonite ratio of 0.78:1.16:1. Therefore, the carbonate fraction had become enriched in calcium in a stoichiometric amount that cannot be accounted for by the presence of yukonite. It is assumed that the dissolution of yukonite in CO<sub>2</sub> environments proceeds via two-step sequence involving dissolution (Equation 4.1) and precipitation of CaCO<sub>3</sub>

(Equation 4.4). Therefore, the rate equation can be expressed in the following way, where the rate determined by observation of As concentrations is normalized by the Ca:As stoichiometry of yukonite:

$$Rate = \frac{[As]}{dt} = \frac{[Ca]}{0.78 dt} = \frac{[CO_3]}{0.78 dt}$$
(4.8)

$$Rate = \frac{-k[CO_3]^{0.7}}{0.78} = -0.00296[CO_3]^{0.7}$$
 (4.9)

The previous study was extended in order to study the effect of temperature on the kinetic rate of dissolution of yukonite in the presence of DIC. This was achieved by equilibrating a sample of yukonite in 0.125 M NaHCO<sub>3</sub> at T = 20°C, 40°C, 70°C. The results are shown in **Fig. 4.5.** and **Fig. 4.6.** In this experiment, t = 0 days does not represent a zero value for As concentration, **Fig. 4.5a.**, due to 3 days pre-equilibration at T=20°C. For the subsequent data treatment to be accurate, it was assumed the surface area of solids did not change during the pre-equilibration period. As expected, there was a positive correlation between As concentration and reaction temperature, indicating endothermic dissolution. Evolution of solution pH, **Fig. 4.5b.**, also showed a positive correlation with temperature, suggesting dissolution of yukonite increases alkalinity.

To determine the activation energy ( $E_a$ ) of yukonite dissolution, an Arrhenius plot was constructed (**Fig. 4.6.**) from rates determined from monitoring As concentration. In determining the rate, the initial As concentration at t=0 days was subtracted from the entire dataset and the rate was calculated by taking the slope between the t=0 days and t=2 days datapoints. A strong linear regression ( $R^2$ =0.9987) provides confidence in the slope, from which an activation energy of 69.97 kJ·mol<sup>-1</sup> was calculated, and extrapolation to the y-intercept determined a pre-exponential factor (A) of 92040 day<sup>-1</sup>. The activation energy points to a slow chemically controlled dissolution process. Therefore, the rate dependence on temperature can be described by the following expression:

$$k = 92040 (days^{-1}) e^{69.97 (kJ \cdot mol^{-1})}/_{RT}$$
(4.10)

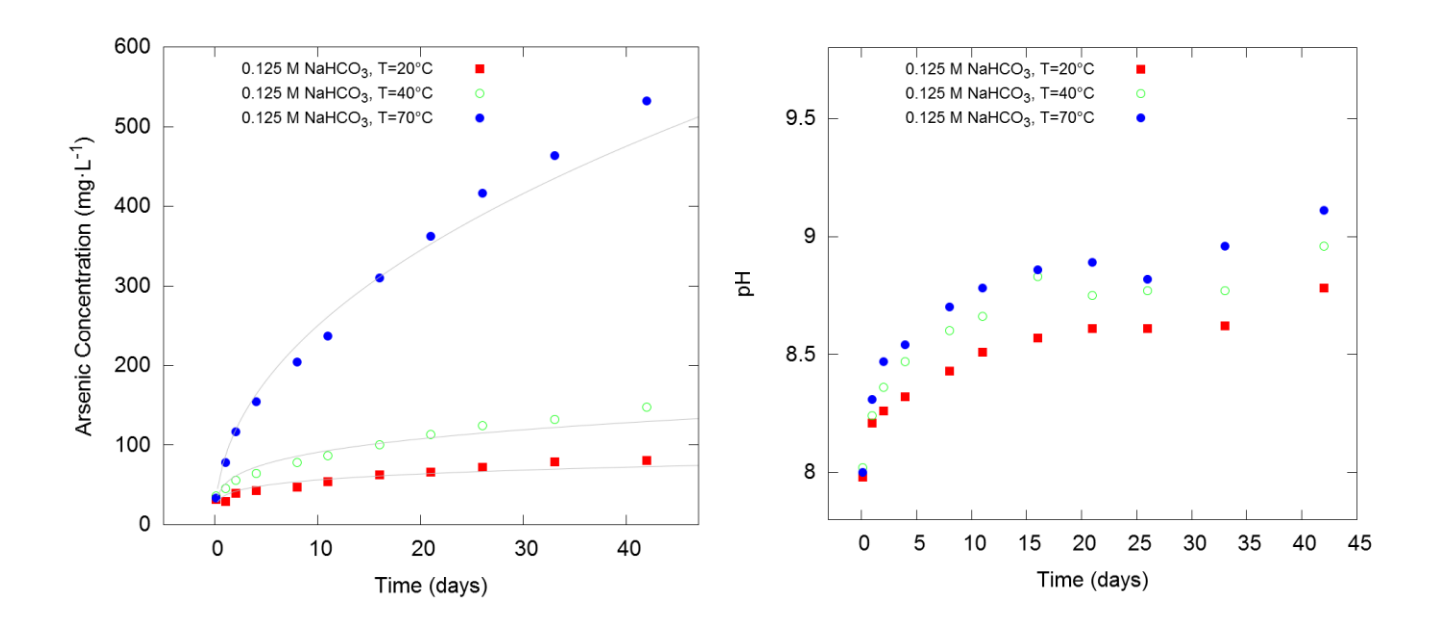


**Fig. 4.5.** Reaction of yukonite with  $0.125 \text{ M NaHCO}_3$  at  $T = 20^{\circ}\text{C}$ ,  $40^{\circ}\text{C}$ ,  $70^{\circ}\text{C}$  show (a) As concentration and (b) pH over time.

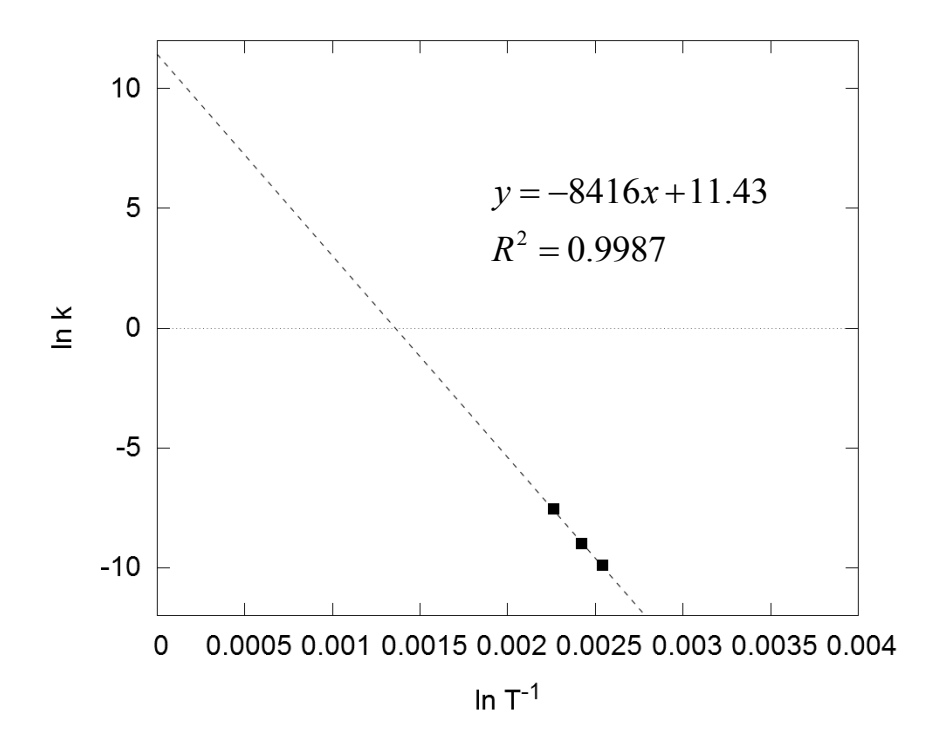


Fig. 4.6. Arrhenius plot for reaction of yukonite in  $0.125 \text{ M NaHCO}_3$  at  $T = 20^{\circ}\text{C}$ ,  $40^{\circ}\text{C}$ ,  $70^{\circ}\text{C}$ .

#### 4.4.3. Stability in Sub-Oxic Conditions: Reaction with Na<sub>2</sub>SO<sub>3</sub>

The results of the sub-oxic stability experiment are presented in Fig. 4.7. Solution  $E_h$  was maintained at ~200 mV throughout the experiment (Fig. 4.7a.) by addition of  $Na_2SO_3$  and subsequent replacement of the atmosphere with nitrogen. In contrast,  $E_h$  of the control sample of distilled water under nitrogen was more oxidizing at 460 mV. At first glance, the As concentration after 15 days in the sulfite solution of 32.4 mg·L<sup>-1</sup> in comparison to 4.6 mg·L<sup>-1</sup> of the control appears to support the case of reductive dissolution of yukonite by  $SO_3^{2-}$ .

$$[As] (mg \cdot L^{-1}) = 0.162(pH)^4 - 3.83(pH)^3 + 37.71(pH)^2 - 180(pH) + 337$$
 (4.11)

However, it is also important to consider the pH also differed between the sulfite and control samples: 9.1 compared to 8.1, respectively. Interpolation of a curve fit with Mathworks MATLAB to solubility data collected under oxic conditions (E<sub>h</sub> ca. 650 mV) after 16 days [37], the solubility of yukonite as a function of pH can be described by Equation 4.10, which is

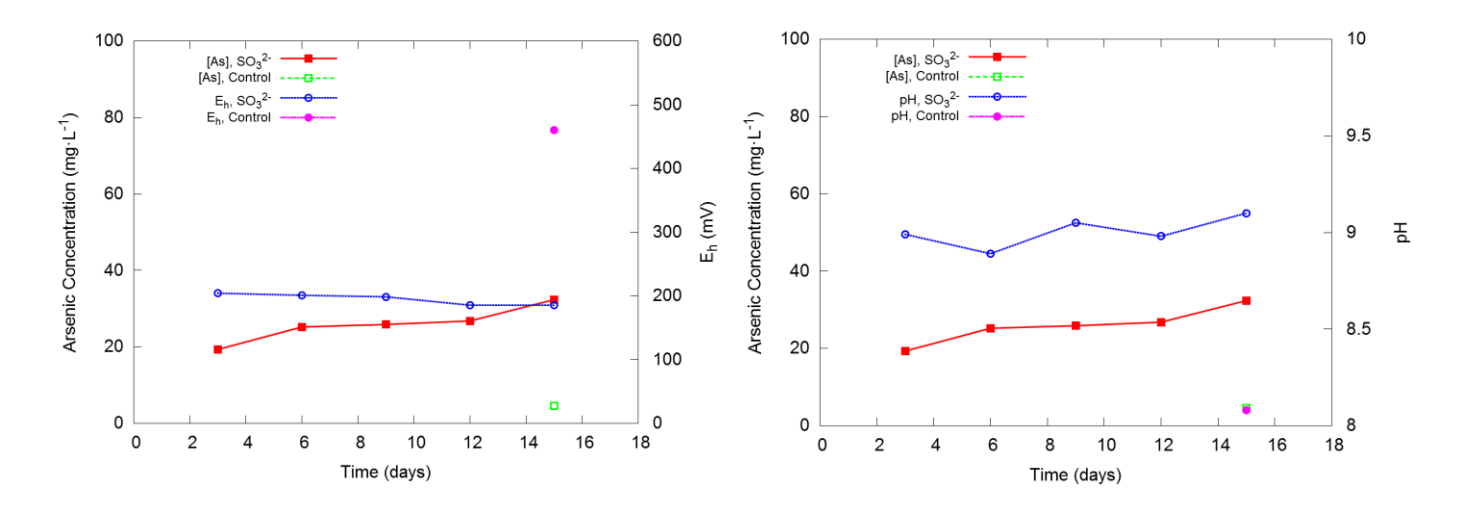


**Fig. 4.7.** Sub-oxic stability study of yukonite by reaction with  $0.012M \text{ Na}_2\text{SO}_3$  under a  $N_2$  atmosphere. As concentration is plotted along with (a)  $E_h$  and (b) pH.

valid for  $3.00 \le pH \le 9.83$ . Both datasets were collected by identical agitation conditions (180 min<sup>-1</sup> on a shaker table). Evaluating this function for pH 9.1 of the day 15  $SO_3^{2-}$  sample, the As concentration under oxic is expected to be ca. 50 mg·L<sup>-1</sup>. This finding, therefore, does not support the idea that reductive dissolution is occurring. Instead, it points towards a pH effect that is responsible for the increased As concentration of the sulfite solution in comparison to the

control, which is consistent with the observation that the solids did not change over the course of the experiment.

Evaluating Equation 4.10 for pH 8.1 predicts an As solubility of 19 mg·L<sup>-1</sup> in the case of the oxic study in comparison to 4.6 mg·L<sup>-1</sup> As for the control of this experiment. Thus, it is tempting to suggest the exclusion of air and its associated CO<sub>2</sub> may be responsible for lower As leaching observed under a N<sub>2</sub> atmosphere. However, it should be noted that neither experiment has likely reached equilibrium with respect to As after 15/16 days. Then, the greater As release in the case of the oxic study is attributed to the use of NaOH and HNO<sub>3</sub> to adjust pH, whereas no pH control was utilized in the case of the control sample.

#### 4.4.4. Stability in Anoxic Conditions: Reaction with NaHS

The results of the anoxic stability experiment presented in **Fig. 4.8.** indicate a 35% increase in As in the presence of S<sup>2-</sup> as opposed to the oxic dataset defined by Equation 4.10. Solution E<sub>h</sub> was maintained at ca. -200 mV through the experiment (**Fig. 4.8b.**) by addition of NaHS, a more strongly reducing potential than in the case of sulfite addition. As concentration was nearly constant over the 15 days, with ca. 200 mg·L<sup>-1</sup>, suggesting partial equilibrium with respect to As may have been attained. The replicate of the day 15 sample was in agreement with the original in terms of As concentration with 205.1 and 203.8 mg·L<sup>-1</sup>, respectively.

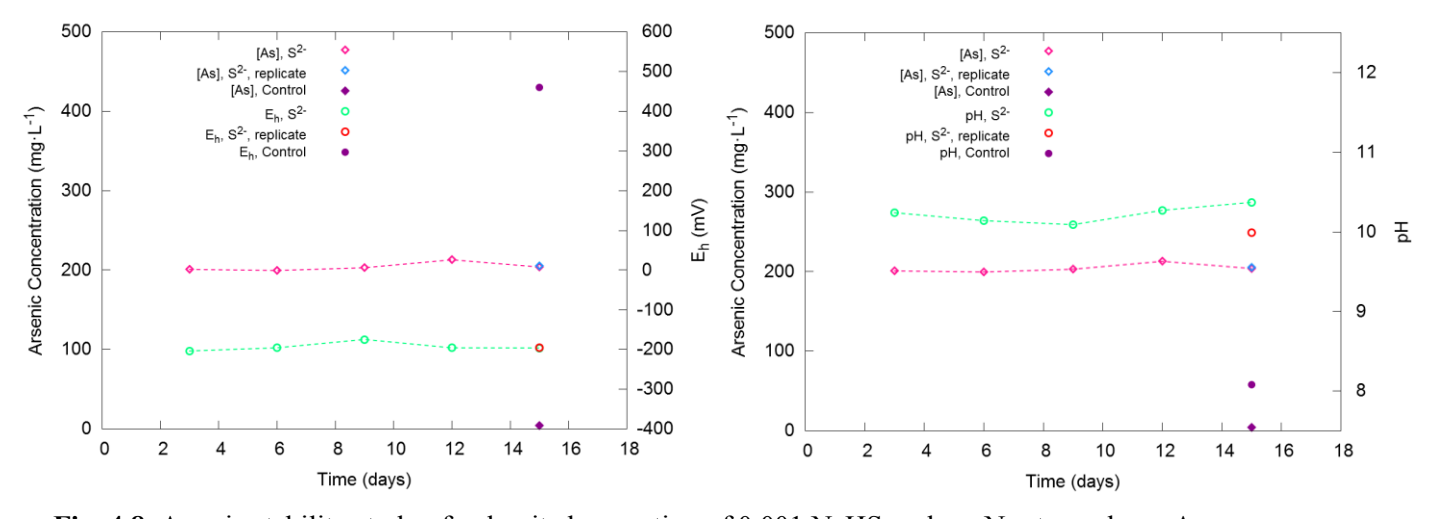


Fig. 4.8. Anoxic stability study of yukonite by reaction of 0.001 NaHS under a  $N_2$  atmosphere. As concentration is plotted along with (a)  $E_h$  and (b) pH.

Solution pH was relatively constant throughout the experiment (**Fig. 4.8b.**), with a value of 10.37 at 15 days. Extrapolation of Equation 4.10 (beyond the datapoint at pH 9.83) suggests the equilibrium solubility of yukonite under oxic conditions may be ca. 130 mg·L<sup>-1</sup> As at pH 10.37. Thus, comparison of the S<sup>2-</sup> sample (200 mg·L<sup>-1</sup> at pH 10.37) to both a control sample (4.6 mg·L<sup>-1</sup> at pH 8.1) and extrapolated oxic dataset (130 mg·L<sup>-1</sup> at pH 10.37) indicates reductive dissolution of yukonite occurs in an anoxic environment (E<sub>h</sub> -200 mV) induced by addition of sulfide. This conclusion is bolstered by observation of the reaction with the naked eye that indicated a phase change had occurred, with the slurry quickly turning from the brownish-red characteristic of yukonite to a dark, mirror-like black with a green filtrate indicative of the presence of Fe(II). Given the strong reducing conditions of the sulfide solution, it is tempting to assume reductive dissolution occurred to form a new sulfide phase, possibly iron (II) sulfide, similar to observations made by Doerfelt [39] in the case of ferric arsenate coprecpitates.

#### 4.4.5. Implications

The results of this work lead to important conclusions about the capacity for yukonite to fix arsenic in metallurgical tailings. It was shown by both gas sparging and equilibration with carbonate salts that the release of arsenic from yukonite is augmented by CO<sub>2</sub>, as in the case of calcium arsenates and barium arsenates [41], [46]. After 60 days equilibration in a slurry of 2.5 M NaHCO<sub>3</sub> (equivalent to 66 g·L<sup>-1</sup> CO<sub>3</sub><sup>2-</sup>), yukonite released 385 mg·L<sup>-1</sup> As. While this is no doubt a significant amount, it corresponds to ca. 7 wt.% of total arsenic in the presence of an excessive level of dissolved inorganic carbon that would not be encountered in a tailings disposal situation. In addition, the presence of lime is known to suppress the solubility of yukonite, which was not present in this study. Therefore, it is assumed the rate of dissolution of vukonite in the presence of CO<sub>2</sub> would be very slow in mineral-derived tailings, which typically have low levels of dissolved inorganic carbon. With respect to oxygen-depleted conditions, yukonite showed resistance to moderate "sub-oxic" reducing potentials (E<sub>h</sub> ca. 200 mV) as produced by reaction with SO<sub>3</sub><sup>2-</sup>, with no apparently additional release of As in comparison to oxic ageing studies. However, exposure to strongly reducing "anoxic" conditions (E<sub>h</sub> ca. -200 mV) showed pronounced As release due to reductive dissolution. Thus, we infer yukonite may control arsenic pore water concentrations under certain conditions in mining/metallurgical tailings. Under oxic

and sub-oxic conditions, and especially in the presence of lime or gypsum, yukonite is less soluble than iron arsenates at neutral and alkaline pH. Although it may be thermodynamically unstable with respect to calcite, the kinetic rate of dissolution is slow. We are reminded of yukonite's many natural occurrences, including in old gold mine tailings [32]–[34], that provide strong evidence of its potential arsenic-regulating role in tailings. However, under highly reducing conditions yukonite appears to play no role in arsenic immobilization, and this should be taken into account in the design of tailings management facilities.

#### 4.5. Conclusions

This study has investigated the reactivity of the mineral phase yukonite towards  $CO_2/NaHCO_3$  and reducing agents  $(SO_3^{2-}/S^{2-})$  in an effort to establish stability boundaries in terms of its arsenic immobilization role in mining/metallurgical tailings. This study complements the results of another parallel study that determined yukonite to be stable in the presence of gypsum over the neutral to mildly-alkaline pH range [37]. From the present study the following conclusions are drawn:

- 1. Sparging 99.8% CO<sub>2</sub> through a slurry of yukonite (1 g/L) at 70°C and pH 8 at 4.4 mL·min<sup>-1</sup> over 48 h showed a 30% increase in As release as compared to no sparging.
- 2. Equilibration with NaHCO<sub>3</sub> of various concentrations revealed yukonite reacts with dissolved inorganic carbon to form calcite according to the following rate equation:  $Rate = -0.00296[CO_3]^{0.7}$  and with an activation energy of 69.97 kJ·mol<sup>-1</sup> that is consistent with a chemically-controlled dissolution reaction.
- 3. Reaction with  $0.012~M~Na_2SO_3~(E_h~ca.~200~mV)$  did not result in increased dissolution of yukonite while yukonite underwent reductive dissolution upon equilibration in 0.01M~NaHS for 15 days.
- 4. These findings point to the importance of proper selection of yukonite disposal conditions limiting exposure to carbonate-rich waters without introducing severe chemical-reducing environment.

# Acknowledgements

This work was made possible by NSERC (Natural Sciences and Engineering Research Council) in conjunction with Areva Resources Canada and Cameco Corporation, industrial sponsors through a CRD (Collaborative Research and Development) grant.

#### References

- [1] R. G. Robins, "The solubility of metal arsenates," *Metall. Trans. B*, vol. 12, no. 1, pp. 103–109, 1981.
- [2] V. G. Papangelakis and G. P. Demopoulos, "Acid Pressure Oxidation of Arsenopyrite: Part I, Reaction Chemistry," *Can. Metall. Q.*, vol. 29, no. 1, pp. 1–12, 1990.
- [3] P. Kondos and G. P. Demopoulos, "Arsenic speciation in oxidative acid leaching systems," *Ellis Horwood Ltd. Sep. Process. Hydrometall.*, pp. 20–34, 1987.
- [4] D. Filippou, P. St-Germain, and T. Grammatikopoulos, "Recovery of Metal Values from Copper—Arsenic Minerals and Other Related Resources," *Miner. Process. Extr. Metall. Rev.*, vol. 28, no. 4, pp. 247–298, 2007.
- [5] P. A. Riveros, J. E. Dutrizac, and P. Spencer, "Arsenic Disposal Practices in the Metallurgical Industry," *Can. Metall. Q.*, vol. 40, no. 4, pp. 395–420, 2001.
- [6] B. Harris, "The Removal of Arsenic from Process Solutions: Theory and Industrial Practice," in *Electrometallurgy and Environmental Hydrometallurgy*, C. Young, A. Alfantazi, C. Anderson, A. James, Davideisinger, and B. Harris, Eds. John Wiley & Sons, Inc., 2003, pp. 1888–1902.
- [7] D. Filippou and G. P. Demopoulos, "Arsenic immobilization by controlled scorodite precipitation," *JOM*, vol. 49, no. 12, pp. 52–55, 1997.
- [8] R. G. Robins, "Arsenic hydrometallurgy," *Arsen. Metall. Fundam. Appl.*, pp. 215–247, 1988.
- [9] M. Leist, R. J. Casey, and D. Caridi, "The management of arsenic wastes: problems and prospects," *J. Hazard. Mater.*, vol. 76, no. 1, pp. 125–138, 2000.
- [10] E. Krause and V. A. Ettel, "Solubilities and stabilities of ferric arsenate compounds," *Hydrometallurgy*, vol. 22, no. 3, pp. 311–337, 1989.
- [11] P. Drahota and M. Filippi, "Secondary arsenic minerals in the environment: A review," *Environ. Int.*, vol. 35, no. 8, pp. 1243–1255, 2009.
- [12] W. R. Cullen and K. J. Reimer, "Arsenic speciation in the environment," *Chem. Rev.*, vol. 89, no. 4, pp. 713–764, 1989.
- [13] D. C. Lynch, "A review of the physical chemistry of arsenic as it pertains to primary metals production," *Arsen. Metall. Fundam. Appl.*, pp. 3–33, 1988.
- [14] M. A. Gomez, L. Becze, J. N. Cutler, and G. P. Demopoulos, "Hydrothermal reaction chemistry and characterization of ferric arsenate phases precipitated from Fe<sub>2</sub>(SO<sub>4)</sub>3–As<sub>2</sub>O<sub>5</sub>–H<sub>2</sub>SO<sub>4</sub> solutions," *Hydrometallurgy*, vol. 107, no. 3–4, pp. 74–90, 2011.
- [15] G. P. Demopoulos, "On the preparation and stability of scorodite," in *Arsenic Metallurgy*, RG Reddy, RN Weizenbach, Eds., TMS, 2005, pp. 25–50.

- [16] G. P. Demopoulos, "Aqueous precipitation and crystallization for the production of particulate solids with desired properties," *Hydrometallurgy*, vol. 96, no. 3, pp. 199–214, 2009.
- [17] T. Fujita, R. Taguchi, M. Abumiya, M. Matsumoto, E. Shibata, and T. Nakamura, "Novel atmospheric scorodite synthesis by oxidation of ferrous sulfate solution. Part I," *Hydrometallurgy*, vol. 90, no. 2–4, pp. 92–102, 2008.
- [18] H. Kubo, M. Abumiya, and M. Matsumoto, *Dowa Mining Scorodite Process*®—application to copper hydrometallurgy, vol. 7. 2010.
- [19] J.-F. Le Berre, R. Gauvin, and G. P. Demopoulos, "Synthesis, Structure, and Stability of Gallium Arsenate Dihydrate, Indium Arsenate Dihydrate, and Lanthanum Arsenate," *Ind. Eng. Chem. Res.*, vol. 46, no. 24, pp. 7875–7882, 2007.
- [20] Y. N. Zhu, X. H. Zhang, Q. L. Xie, D. Q. Wang, and G. W. Cheng, "Solubility and Stability of Calcium Arsenates at 25°C," *Water. Air. Soil Pollut.*, vol. 169, no. 1–4, pp. 221–238, 2006.
- [21] R. G. Robins and K. Tozawa, "Arsenic removal from gold processing waste waters: the potential ineffectiveness of lime," *Can. Min. Metall. Bull.*, vol. 75, no. 840, pp. 171–174, 1982.
- [22] Y. Jia, G. P. Demopoulos, N. Chen, and J. Cutler, "Coprecipitation of As (V) with Fe (III) in sulfate media: solubility and speciation of arsenic," in *Arsenic Metallurgy*, RG Reddy, RN Weizenbach, Eds., TMS, 2005, pp. 137–148.
- [23] P. M. Swash and A. J. Monhemius, "Hydrothermal precipitation from aqueous solutions containing iron(III), arsenate and sulphate," in *Hydrometallurgy '94*, Springer Netherlands, 1994, pp. 177–190.
- [24] D. Langmuir, J. Mahoney, and J. Rowson, "Solubility products of amorphous ferric arsenate and crystalline scorodite (FeAsO4 · 2H2O) and their application to arsenic behavior in buried mine tailings," *Geochim. Cosmochim. Acta*, vol. 70, no. 12, pp. 2942–2956, 2006.
- [25] M.-C. Bluteau and G. P. Demopoulos, "The incongruent dissolution of scorodite Solubility, kinetics and mechanism," *Hydrometallurgy*, vol. 87, no. 3–4, pp. 163–177, 2007.
- [26] R. G. Robins, J. C. Y. Huang, and G. Khoe, "The adsorption of arsenate ion by ferric hydroxide," in *JOURNAL OF METALS*, 1987, vol. 39, pp. A2–A2.
- [27] D. Langmuir, J. Mahoney, A. MacDonald, and J. Rowson, "Predicting arsenic concentrations in the porewaters of buried uranium mill tailings," *Geochim. Cosmochim. Acta*, vol. 63, no. 19–20, pp. 3379–3394, 1999.
- [28] R. De Klerk, "Investigating the continuous circuit coprecipitation of arsenic(V) with ferric iron in sulphate media," 2008.
- [29] B. J. Moldovan, D. T. Jiang, and M. J. Hendry, "Mineralogical characterization of arsenic in uranium mine tailings precipitated from iron-rich hydrometallurgical solutions," *Environ. Sci. Technol.*, vol. 37, no. 5, pp. 873–879, 2003.
- [30] Y. Jia and G. P. Demopoulos, "Coprecipitation of arsenate with iron(III) in aqueous sulfate media: Effect of time, lime as base and co-ions on arsenic retention," *Water Res.*, vol. 42, no. 3, pp. 661–668, 2008.
- [31] M.-C. Bluteau, L. Becze, and G. P. Demopoulos, "The dissolution of scorodite in gypsum-saturated waters: Evidence of Ca–Fe–AsO4 mineral formation and its impact on arsenic retention," *Hydrometallurgy*, vol. 97, no. 3–4, pp. 221–227, 2009.

- [32] D. Paktunc, A. Foster, S. Heald, and G. Laflamme, "Speciation and characterization of arsenic in gold ores and cyanidation tailings using X-ray absorption spectroscopy," *Geochim. Cosmochim. Acta*, vol. 68, no. 5, pp. 969–983, 2004.
- [33] D. Paktunc, A. Foster, and G. Laflamme, "Speciation and Characterization of Arsenic in Ketza River Mine Tailings Using X-ray Absorption Spectroscopy," *Environ. Sci. Technol.*, vol. 37, no. 10, pp. 2067–2074, 2003.
- [34] S. R. Walker, M. B. Parsons, H. E. Jamieson, and A. Lanzirotti, "Arsenic Mineralogy of Near-Surface Tailings and Soils: Influences on Arsenic Mobility and Bioaccessibility in the Nova Scotia Gold Mining Districts," *Can. Mineral.*, vol. 47, no. 3, pp. 533–556, 2009.
- [35] E. A. Soprovich, "Arsenic release from oxide tailings containing scorodite, Fe-Ca arsenates and As-containing goethites," in *Proceedings of the Seventh International Conference on Tailings and Mine Waste'00*, A.A. Balkema, Ed., 2000, pp. 23–26.
- [36] M. A. Gomez, L. Becze, R. I. R. Blyth, J. N. Cutler, and G. P. Demopoulos, "Molecular and structural investigation of yukonite (synthetic & natural) and its relation to arseniosiderite," *Geochim. Cosmochim. Acta*, vol. 74, no. 20, pp. 5835–5851, 2010.
- [37] M. Bohan, L. Becze, J. Mahoney, and G. Demopoulos, "The Synthesis, Characterization, and Stability of Yukonite Under Oxic Conditions," *Geochim. Cosmochim. Acta*, 2014.
- [38] H. McCreadie, D. W. Blowes, C. J. Ptacek, and J. L. Jambor, "Influence of Reduction Reactions and Solid-Phase Composition on Porewater Concentrations of Arsenic," *Environ. Sci. Technol.*, vol. 34, no. 15, pp. 3159–3166, 2000.
- [39] C. Doerfelt, "Investigating the effect of reducing agents on the stability of arsenate-bearing co-precipitates from Fe(ll)/Fe(lll)/Al(lll) solutions," 2014.
- [40] W. Stumm and J. J. Morgan, *Aquatic Chemistry: Chemical Equilibria and Rates in Natural Waters*. John Wiley & Sons, 2012.
- [41] R. G. Robins, "The solubility of barium arsenate: Sherritt's barium arsenate process," *Metall. Mater. Trans. B*, vol. 16, no. 2, pp. 404–406, 1985.
- [42] D. Fortin, J.-P. Rioux, and M. Roy, "Geochemistry of Iron and Sulfur in the Zone of Microbial Sulfate Reduction in Mine Tailings," *Water Air Soil Pollut. Focus*, vol. 2, no. 3, pp. 37–56, 2002.
- [43] M. B. J. Lindsay, D. W. Blowes, P. D. Condon, and C. J. Ptacek, "Managing Pore-Water Quality in Mine Tailings by Inducing Microbial Sulfate Reduction," *Environ. Sci. Technol.*, vol. 43, no. 18, pp. 7086–7091, 2009.
- [44] V. K. LaMer and R. H. Dinegar, "Theory, Production and Mechanism of Formation of Monodispersed Hydrosols," *J. Am. Chem. Soc.*, vol. 72, no. 11, pp. 4847–4854, 1950.
- [45] J. E. House, *Principles of Chemical Kinetics*. Academic Press, 2007.
- [46] R. G. Robins and K. Tozawa, "Arsenic removal from gold processing waste waters: the potential ineffectiveness of lime," *Can. Min. Metall. Bull.*, vol. 75, no. 840, pp. 171–174, 1982.

# **Chapter 5. Global Conclusions**

This thesis has investigated the potential role yukonite may play in arsenic immobilization in certain mining/metallurgical tailings. In Chapter 2, a literature review of the mineralogy of yukonite was presented. In Chapter 3, yukonite was synthesized and subjected to stability tests under oxic conditions. In Chapter 4, the capacity of yukonite to resist reaction with CO<sub>2</sub> and reducing conditions was evaluated. Here, the major conclusions from this body of work are summarized.

Yukonite is a hydrated calcium ferric arsenate mineral of unique mineralogy. Structurally, it is disordered and composed of small (nano-sized) crystallites, leading to variation upon characterization with XRD and in analysis of chemical composition between specimens. The variation stems from the unique geochemical conditions of formation. Of particular interest to this work, yukonite has been found in gold mine tailings in Canada in both Nova Scotia and the Yukon Territory. "Naturally" formed yukonite is found in Fe and As-rich environments with a source of calcium (e.g. limestone) under mildly alkaline conditions. This explains the feasibility of the transformation of iron arsenate coprecipitates, which are neutralized to alkaline pH with lime, to yukonite. In fact, accelerated ageing experiments of both iron arsenate coprecipitates and scorodite have produced yukonite.

To study the propensity of yukonite to fix arsenic in metallurgical tailings, it was first synthesized by means of an atmospheric precipitation process. By neutralization of a solution (Ca/Fe/As molar ratio: 0.5/0.75/1) and subsequent ageing at 95°C for 24 h, yukonite was synthesized that corresponded to natural specimens in terms of XRD pattern and chemical composition. The results of two separate stability experiments were in agreement in finding yukonite to have low arsenic solubility under oxic conditions in a closed system. Specifically, after 132-490 days, As(V) concentration in solution was 5.3 mg·L<sup>-1</sup> at pH 5, 3.1-11.9 mg·L<sup>-1</sup> at pH 7, 7.3-57.2 mg·L<sup>-1</sup> at pH 8, and 98.1-303.8 mg·L<sup>-1</sup> at pH 9.5-10. Moreover, saturation of the experimental solution with gypsum (commonly present in tailings) was found to suppress solubility, with As(V) equal to 3.5 mg·L<sup>-1</sup> at pH 5, 0.6-0.9 mg·L<sup>-1</sup> at pH 7, 0.6-2.4 mg·L<sup>-1</sup> at pH 8, and 2.2-6.2 mg·L<sup>-1</sup> at pH 9.5-10. Together, this information indicates yukonite is a stable arsenic carrier under oxidizing conditions, especially when gypsum is present. However, conditions other than those tested here may be encountered in tailings management facilities.

One concern is that yukonite may be unstable with respect to  $CO_2$ , as in the case of calcium arsenates, which dissolve releasing arsenate and forming calcite in its presence. To test this, a double-pronged experimental approach in one case introduced  $CO_2$  by sparging and in another by equilibration with NaHCO<sub>3</sub> of varying concentration. Both concluded that yukonite does undergo dissolution by reaction with  $CO_2$ . A reaction rate law was derived, and by heating samples to various temperatures ( $T=20^{\circ}C$ ,  $40^{\circ}C$ ,  $70^{\circ}C$ ), the activation energy of reaction was determined to be  $69.97 \text{ kJ} \cdot \text{mol}^{-1}$ . While high arsenic release was observed, this was a result of excessive levels of inorganic carbon not likely found in disposal situations. Therefore, we conclude that reaction of yukonite with  $CO_2$  is a slow, chemically controlled dissolution process. Another possibility is that yukonite may undergo reductive dissolution in tailings facilities where microbial-mediated reduction reactions create reducing potentials. To evaluate this possibility, yukonite was reacted with  $0.012 \text{ M Na}_2SO_3$  and  $0.001 \text{ M Na}_2SO_3$ , no increase in yukonite dissolution was observed. However, reaction with  $S^2$  caused major dissolution and/or phase transformation, indicating yukonite is not stable under strongly reducing conditions.

Overall, it has been demonstrated that yukonite does have potential to fix arsenic under certain environments. It is stable under oxic conditions over a range of pH (5-8) as well as sub-oxic conditions. Care must taken in selecting disposal conditions that are rich in inorganic carbon and strongly reducing conditions, which have been shown in this work to lead to the dissolution of yukonite.

# Appendix

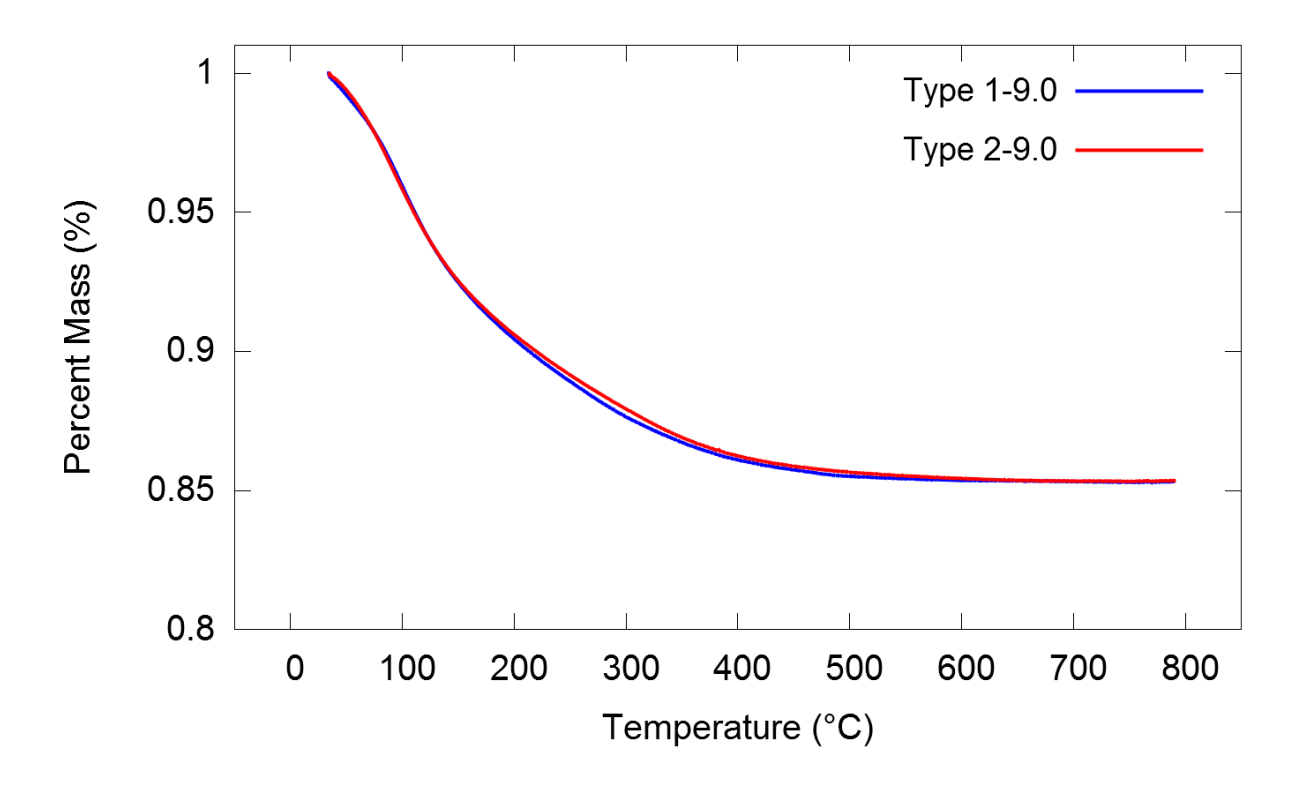


**Fig. A-1**. Thermogravimetric analysis performed with a TA Instruments Q500 instrument at a heating rate of 10°C·min<sup>-1</sup> show nearly identical mass loss over the temperature range (50-800°C) investigated for Type 1-9.0 and Type 2-9.0 synthetic yukonite samples. This mass is assumed to be crystallization water. As measured as mass loss at 600°C, the two samples had 14.67% and 14.65% crystallization water, respectively.